To the Graduate Council:

I am submitting herewith a thesis written by Sicong Zheng entitled "Pixel-level Image Fusion Algorithms for Multi-camera Imaging System." I have examined the final electronic copy of this thesis for form and content and recommend that it be accepted in partial fulfillment of the requirements for the degree of Master of Science, with a major in Computer Engineering.

Mongi A. Abidi, Major Professor

We have read this thesis
and recommend its acceptance:

Seddik M. Djouadi

Andreas F. Koschan

Accepted for the Council:

Carolyn R. Hodges
Vice Provost and Dean of the Graduate School

(Original signatures are on file with official student records.)

Pixel-level Image Fusion Algorithms for Multi-camera Imaging System

A Thesis
Presented for the
Master of Science
Degree
The University of Tennessee, Knoxville

Sicong Zheng
December 2010

Acknowledgements

Before this document starts dwelling on technical details, I would like to express my gratefulness to the supporting pillars of this thesis work. First of all, I would like to thank my parents for raising and supporting. They have always been there for me with all their love and affection whenever I needed them emotionally, financially and every possible situation I imposed upon them.

Dr. Abidi took over as the academic advisor in graduate school, fuelled my quest for knowledge, supporting me technically and financially with the resources in the Imaging, Robotics and Intelligent Systems Lab. Dr. Koschan is expertise that Dr. Abidi introduced me to and I attribute my technical development in the area of focus in this thesis to them. I am also indebted to thank Dr. Djouadi, Dr. Qi, Dr. Cao, Dr. Roberts, Dr. Vander Zanden, Dr. Crilly and Dr. Arazi.

The peers in our lab have been a great learning source in this research journey. I really want to thank friends in the lab, Wei, Jessica (Yao Yi), Hong, Chung-Hao, Sophie, Shafik, Anis, Jacob, Michael, Timothy, Bobby, Dr.Kim, Muharrem, Hari, Zhiyu, Chang, Rangan and several others. It was a pleasure working with you all. Justin Acuff deserves a special mention. Thanks for sharing your system instrumentation expertise in building our imaging prototypes and thanks Justin for meticulously solving one software system issue after another.

Sincere thanks to you all.

Abstract

This thesis work is motivated by the potential and promise of image fusion technologies in the multi sensor image fusion system and applications. With specific focus on pixel level image fusion, the process after the image registration is processed, we develop graphic user interface for multi-sensor image fusion software using Microsoft visual studio and Microsoft Foundation Class library.

In this thesis, we proposed and presented some image fusion algorithms with low computational cost, based upon spatial mixture analysis. The segment weighted average image fusion combines several low spatial resolution data source from different sensors to create high resolution and large size of fused image. This research includes developing a segment-based step, based upon stepwise divide and combine process. In the second stage of the process, the linear interpolation optimization is used to sharpen the image resolution. Implementation of these image fusion algorithms are completed based on the graphic user interface we developed. Multiple sensor image fusion is easily accommodated by the algorithm, and the results are demonstrated at multiple scales. By using quantitative estimation such as mutual information, we obtain the experiment quantifiable results. We also use the image morphing technique to generate fused image sequence, to simulate the results of image fusion.

While deploying our pixel level image fusion algorithm approaches, we observe several challenges from the popular image fusion methods. While high computational cost and complex processing steps of image fusion algorithms provide accurate fused results, they also makes it hard to become deployed in system and applications that require real-time feedback, high flexibility and low computation ability

A list of keywords

Image fusion, pixel-based, multi-sensor, morphing,

Contents

List of Tables

List of Figures

1 Introduction

Image fusion is an important research topic in many related areas such as computer vision, automatic object detection, remote sensing, image processing, robotics, and medical imaging. Multi-sensor image fusion is the process of combining relevant information from several images into one image. The final output image can provide more information than any of the single images as well as reducing the signal-to-noise ratio. The user can collect useful information without gazing at and comparing images from multiple sensors. In Section 1.1, we detail the motivation behind this thesis along with its related research objectives. Next, we formulate these objectives into a problem statement and summarize the solution, provided by this thesis, in Section 1.2 before finally claiming system level and technical contributions for each application in Section 1.3.

1.1 Motivation

The fast development of the technique of sensors, micro-electronics, and communications requires more attention on information fusion. Several situations in image processing require high spatial and high spectral resolution in a single image. For example, the traffic monitoring system, satellite image system, and long range sensor fusion system all use image processing. However, the majority of available equipment is not capable of providing this type of data convincingly. The sensor in the surveillance system can only provide the scenery view in a narrow depth for a particular focus, yet the demanding application of this system requires a clear view with a high depth of the field. Image fusion provides the possibility of combining different sources of information. In this thesis, we state two commonly used image fusion algorithms with manually defined parameters.

The four applications motivating this thesis are (1) Multi-sensor image fusion, (2) Medical image fusion, (3) Surveillance System, and (4) Aerial and Satellite imaging. We discuss the research objectives in each of these applications in the following paragraphs and establish a basis to showcase our research efforts. Figures 1.1 through 1.4 illustrate several of the motivating applications, such as the-state-of-the-art for image fusion and the improvements that we provide as solutions for each of these applications. The particular applications discussed include medical diagnosis, remote sensing, surveillance systems, biometric systems, and image quality assessment.

- ***Multi-sensor image fusion:*** In the field of multisensory image fusion, there are multiple types of systems which require the best image from each available sensor. Fig.1 below depicts various applications of image fusion technology. For example, in the field of aerial and satellite imaging, earth observation systems play an important role in facilitating sustainable development at both the global level as well as at local levels. Aerial photographs, thermal infrared images, radar images, Landsat MSS, and TM images are among those widely used in airborne and satellite

remote sensing data. They provide a high spectral, spatial, and temporal resolution allowing them to be used to monitor and map different phenomena on the earth's surface effectively. It is also important to note that image fusion is used in air traffic control, law enforcement, homeland security, medical diagnosis, robotics (manufacturing, hazardous workplace), and remote sensing (weather forecast based on patterns, environment monitor, mineral resources detection, and buried hazardous waste). Additional systems might need to improve detection with single display and visualization and day/night image enhancement.

- ***Medical image fusion:*** Image Fusion also contains various potential applications for medical data collection and diagnosis. It assists physicians in extracting features that may not be normally visible in images produced by different modalities. For example, a MRI-T1 provides greater detail about anatomical structure, whereas a MRI-T2 provides a greater contrast between the normal and abnormal tissues. Other medical image analyses, an image showing functional and metabolic activity such as a single photon emission computed tomography (SPECT), positron emission tomography (PET), and magnetic resonance spectroscopy (MRS), are often registered to an image which shows anatomical structures such as a magnetic resonance image (MRI), computed tomography (CT), and an ultrasound. Thus to extract more information, medical image fusion is performed in such a manner as to combine these contrasting and complimentary features into one image. Advantages of these applications are to reduce the difficulty in diagnosing disease and reducing storage cost.

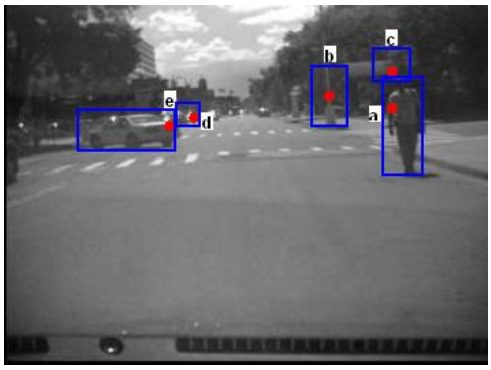

(a) Image Classification

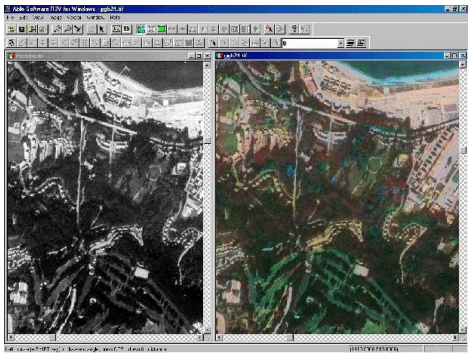

(b) Aerial and Satellite imaging

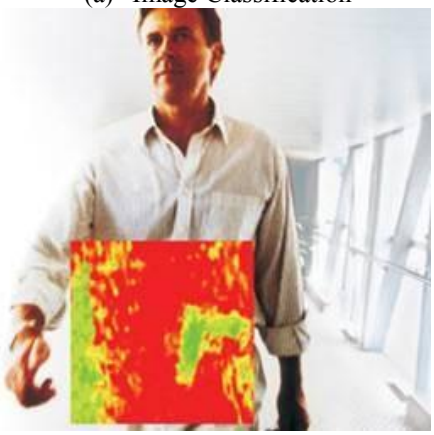

(c) Concealed weapon detection

(d) Robot vision

Figure 1.1: The motivating applications illustrated in this figure are image recognition and classification, aerial and satellite imaging, concealed weapon detection, and robot vision. With a focus on the

environments, a large number of issues arise such as the view, illumination, noise, and resolution clarity. (Original images courtesy of http://www.flir.com/thermography/americas/us/,www.coli.uni-saarland.de/groups/MC/lab.html , http://www.imagefusion.org/)

(a) Battle field monitoring

(b) Multi-focus image fusion

(c) Digital camera application

(d) Medical imaging

Figure 1.2: The motivating applications illustrated in this figure are battle field monitoring from a military field, multi-focus image fusion for pattern recognition, digital camera applications performing recordings, and medical imaging systems such as PET/CT and MRT. (Original Images courtesy of http://www.imagefusion.org/ http://www.imgfsr.com disi.unitn.it/rslab/ www.ablesw.com/3d-doctor/reslice.html)

(a) Original Pan Image (b) Original MS Image (c) Pan-sharpened Image

Figure 1.3. Image fusion of QuickBird images for object extraction. Fusion with one (a) original black and white pan image with high resolution, and (b) original MS color image with low resolution. The result shown (c) is a high resolution, highly accurate color image. (Original Images courtesy of http://www.digitalglobe.com/)

- ***Surveillance System:*** Surveillance and security systems that employ multiple image sensors are still a topic receiving great attention. Previous contributions show that a fused image provides a better representation of the spatial layout of a scene. The use of large surveillance systems with a CCTV camera is widespread in places like banks, super-markets, and streets, where they are used to analyze behavior and accidents. Video surveillance cameras in the form of closed circuit television were first used in 1942 in Germany. They were first installed by Walter Burch, a German engineer of Siemens AG at the Test Standard VII to monitor the cause of any malfunction or problems from V-2 rocket launches. Today, surveillance camera technology is used for different purposes. It can be used for crime prevention, industrial observation, or traffic watch. The FLIR system [FLR] provides a Thermal Imaging Infrared Camera with a fusion feature for the non-invasive monitoring and diagnosing of building conditions. The Geosage generates a DOS-based tool, HightView, for the ultimate image pan-sharpening of high-resolution satellite imagery such as QuickBird, IKONOS, and GeoEys-1.

- ***Aerial and Satellite imaging:*** Pan-sharpening is a technique that produces a high-resolution multispectral image by combining a low-resolution MS image with a high-resolution Pan image. The pan-sharpening technique used in this study is the PANSHARP module (Zhang, 2002) of the PCI Geomantic. The algorithm achieves the maximal spatial detail increase and a minimal color distortion (Zhang, 2002). After the fusion, a pan-sharpened QuickBird image is obtained with a 0.61m resolution and 4 MS bands (NIR/R/G/B). Fig. 1.3 shows a sub-scene of the original QuickBird Pan, MS, and the pan-sharpened images.

1.2 Problem Statement

Initially, image fusion can be defined as a combination of images from different sources (image sensors and cameras) aimed to obtain more informative or a more precise knowledge of the image. In other words, it is

used to generate a result which describes the scene “better” than any single image with respect to relevant properties. In most applications and in image fusion for display purposes in particular, it means the acquisition of perceptually important information.

The main requirement of the fusion process is to identify the most significant features in the input images and to transfer them without loss of detail into the fused image. Depending on different fields of the applications, we have different objectives and goals for using image fusion: 1. Reduce noise, improve Signal-to-Noise-Ratio (SNR) by averaging pixel values over several images; 2. Improve spatial resolution (super resolution); 3. Extend the spatial domain, such as the mosaic algorithm; 4. Extend the image values qualitatively such as registration of the images for different spectral bands to a vector-values (multi-spectral) image; 5. Visualize high dimensional images (multi- and hyper- spectral) as false-color images; 6. Design fusions which are merged from different physical principles such as range image, thermal image, sonar image, Ground Penetrating Radar (GPR), Ultra Sound Sensor (US), and X-ray image.

The object of image fusion is to obtain a better visual understanding of certain phenomena, and to introduce or enhance intelligence and system control functions. Many advantages of multi-sensory data fusion such as improved system performance (improved detection, tracking and identification, improved situation assessment, and awareness), improved robustness (less sensor redundancy and graceful degradation), improved spatial and temporal coverage, shorter response time, and reduced communication and computing, can be achieved. The extent of the visual information contained in the input images that is preserved in the fused image is also a significant measurement of the image fusion performance.

Applications of image fusion might use several utilities and sensors that include the range, thermal sensor, sonar, infrared, Synthetic Aperture radar (SAR), electro-optic imaging sensors Ground Penetrating Radar (GPR), Ultra Sound Sensor (US), and X-ray sensor.

The general multi-sensor image fusion is depicted in Figure 1.4. For simplicity, only three imaging sensors are deployed in this system, which produce three different representation of the same scene. In this figure, a CCD true color image, color-coded range image, and reflectance image captured in the University of Tennessee, Knoxville are shown as an example. The data gathered from multiple sources of acquisition are delivered to preprocessing such as denoising and image registration. This step is used to associate the corresponding pixels to the same physical points on the object. In this method, the input images can be compared pixel by pixel. Image analysis processes the source images by considering criteria such as histogram and principle component to obtain the parameters and to make the decision for image fusion either manually or automatically. Subsequently, the preprocessed data continues to the image fusion process. The post-processing is applied to the fused image. Post-processing includes classification, segmentation, and image enhancement. A performance evaluation could help to achieve quantitative results. The fused image could be evaluated on the basis of predefined metrics according to the application requirement or could be evaluated by the human visual evaluation. At last, the result is generated and displayed to the end user

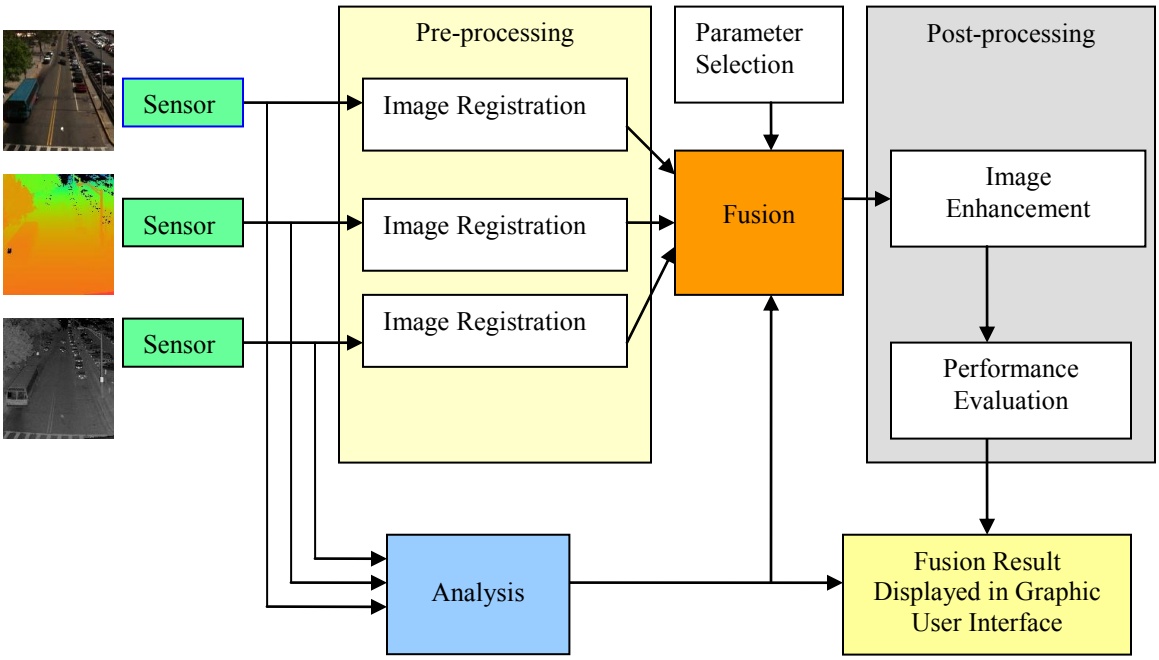

Figure 1.4: Block Scheme of a general multi-sensor image fusion procedure. First, the source images are acquired from sensors. Second, image preprocessing such as denoising and image registration are deployed on the source images. Then, the result is generated from image fusion. Depending on the application, post processing is utilized. (Original image is from the image database of the Imaging, Robotics and Intelligent Systems (IRIS) Laboratory at the University of Tennessee, Knoxville)

After introducing the basic block scheme of image fusion, we come to the mathematic description of image fusion. Considering a general process of image fusion, assume that we have N source images $S=\{S_i, i=1,2,...,N\}$ and M fusion structure $T=\{T_i, i=1,2,...,M\}$. For a certain image fusion algorithm each fusion structure T_i fuse source image S into K_i to generate $F_i=\{F_i^j, j=1,2,...K_i\}$. In this way, the fused image can be expressed as follows:

$$F=\{T_i(\mathrm{s}), i=1,2,...,M\}=\{F_i^j, i=1,2,...,M, j=1,2,...K_i\}$$

The several image fusion topology structures currently in existence vary from each other, as well as producing varying fused images and having different computational costs. Generally, these topologies can be divided into three categories, parallel topology, serial topology, and network topology. As shown in Figure 1.5, parallel, serial, and network topologies are the most basic of these various image fusion algorithms. The arrowhead together with the rectangle sensor shows the related order for image fusion. A parallel topology fusion structure aims at fusing multiple source images in a single step without a predefined order. N input images are processed in the same step. A serial topology fusion structure uses a predefined order to fuse images in a single track. More often than not, the serial topology of an image fusion algorithm is a linear mixing model. A network topology fusion structure is a hierarchical structure where each fusion level has a parallel topology structure. This topology is more complex than the other two topology types; the result from each node $sensor_{i,j}$ is a fused result from its lower level $sensor_{i-1,j}$.

Generally speaking, network topology is the more accurate of the three methods, but the most computationally expensive.

In practice, there are still many constraints for the usage of a high-resolution camera. First, because of the electronic limitations, it is not possible to reduce the size of the camera sensor while keeping a large number of pixels. Large sensors mean lenses which are large sized, heavy, bulky, fragile, and expensive. Even with a novel method that applies multiple small size images to an image stitch algorithm, it is still difficult to extend to real-time applications. Furthermore, when a large sensor runs on batteries, the transmission of a high resolution image between the camera and receiver can drain most of its computing power instead of using this energy for sensing the environment. The size and weight of the batteries also create a camera with a higher cost.

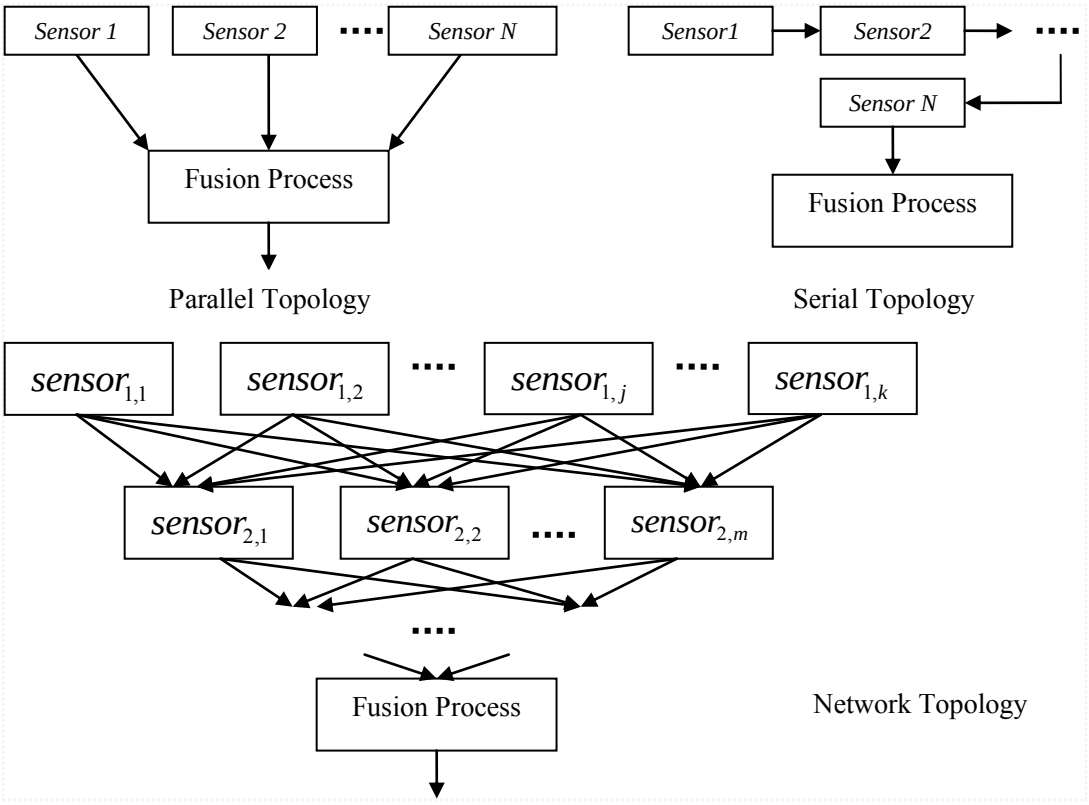

Figure 1.5: Different topologies of image fusion procedure. As shown in the Figure, a parallel topology fusion structure aims at fusing multiple source images in a single step without a predefined order. A serial topology fusion structure uses a predefined order to fuse images in a single track. More often than not, it is a linear mixing model. A network topology fusion structure is a hierarchical structure where each fusion level has a parallel topology structure. This figure was reproduced from (Varshney, 2005).

1.3 Areas of contribution

Motivated towards addressing the needs in the applications mentioned in Section 1.1, our research demonstrates the pixel-level image fusion technology towards a multi-camera imaging system. In making such a claim with this thesis, we list the following contributions addressing key technical issues in ghe image fusion field.

- ***Pixel-based image fusion algorithm:*** The pixel-level image fusion algorithms, including the segment based image fusion and weighted average image fusion, are designed to provide various options for a multi-sensor image fusion algorithm. These algorithms with manual control parameters are deployed to various applications with a wide flexibility. After the data acquisition from a real world scene, preprocessing includes image enhancement and registration, the image fusion is performed to gain a comprehensive information combination with a low computational cost. Although some artificial slice effects will be generated, an appropriate parameter selection will reduce this side-effect and improve the mutual information result. Still, an alternative interpolation process could be added to improve the image fusion result, which is part of the future work for our research.

- ***Image morphing for multi-sensor images:*** Image morphing methods are widely applied to film and television to generate a fluid and breathtaking transformation. However, we tried to seek the intersection between this 2D geometric transformation and the multi-sensor image fusion. We briefly introduce the theory of image morphing, including mesh warping and feature-based image warping, to help with the image fusion algorithm. Such a scheme helps quickly generate the interval transformation status from one sensor image to another in order to approximate the fusion result based on multi-sensor images. Experiment shows that this method can provide valuable information to simulate the image fusion.

- ***Implementation and testing the methods:*** We implement the pixel-level image fusion algorithms using C++ and OpenCV library using Microsoft Visual Studio to generate a graphical user interface with a dynamic parameter control. The graphical user interface plays as a toolbox for our test and the layout is described in the following chapters. We document detailed information about controls including zoom view window, gray scale and pseudo-color window, text, and slide control. We demonstrate our methods used for applications such as thermal image, range image, reflectance image, true color image, and aerial and satellite image. The computational cost and limitations of large image size processing are tested and evaluated for the purpose of various multi-sensor image fusion system applications. Evaluation of these image fusion algorithms is deployed using mutual information via Matlab. Various parameter selections are chosen for our evaluation purposes, and figures between mutual information score and parameter values are drawn to illustrate the trend for parameter selection.

1.4 Document organization

The remainder of this document is arranged as follows:

- **Chapter 2** presents the background of how ideas in the literature help us design a pixel-level image fusion algorithm for a multi-sensor image fusion system and emphasizes the need to handle fast computation in the real world to operate with a large degree of diversity.
- **Chapter 3** designs and implements the generic pixel-level image fusion algorithm for a multi-sensor image fusion system and introduces the theory of an image morphing algorithm to provide various options for a multi-sensor image fusion algorithm. We discuss the entire control parameters targeted to various applications with flexibility.
- **Chapter 4** documents the implementation of the theory derived in Chapter 4 using a graphic user interface for various multi-sensor image fusion applications. We show the process of the image fusion algorithm we designed using an elementary image. We present promising results using examples of thermal image and true color image, aerial and satellite image, range image, reflectance image, and true color image. We show the results from these image fusion and image warping methods by demonstrating comprehensive information from multiple sensors.
- **Chapter 5** showcases the performance of the work presented by deploying the root mean square error and mutual information methods. We test the computation performance in real-world situations directly relating to large image size manipulation.
- **Chapter 6** concludes with the dissertation key points identifying avenues for extending our generic image fusion theory beyond a multi-sensor image fusion system to other applications.

2 Literature Review: Image Fusion

In the previous chapter, we introduced the applications that motivated this thesis and emphasized the need for imaging-based robotic automation solutions. In this chapter, we will briefly discuss the contemporary image fusion methods and elaborate on the state-of-the-art methods with image fusion applications. The study helps us identify the problems of image fusion and its various types of applications. We begin with a survey of image fusion techniques in Section 2.1, and then brief image fusion applications using mobile robots in Section 2.2. Finally, we document the preprocessing of the source images using image registration in Section 2.3.

2.1 Image fusion technologies overview

In this subsection, we discuss image fusion methods and separate them into different categories. We begin by presenting a classification of the different techniques in Figure 2.1. The classification is based on which target object the different methods focus on.

Image fusion algorithms can be categorized into different levels: low, middle, and high; or pixel, feature, and symbolic levels. The pixel-level method works either in the spatial domain or in the transform domain. The prerequisite for such an operation is that the images have been acquired by homogeneous sensors, such that the images reproduce similar or comparable physical properties of the scene. The fusion methods, such as averaging, the Brovey method, principle component analysis (PCA), and IHS based methods fall under the spatial domain approaches. The feature-level algorithms typically segment the image into contiguous regions and fuse the regions together using their properties. The features used may be calculated separately from each image or they may be obtained by the simultaneous processing of all the images. Piella proposed several activity level measures including the absolute value, the median, or the contrast to neighbors measures (Piella, 2003). Finally, she proposed a region-based scheme using a local correlation measurement to perform the fusion of each region (Piella, 2003). Decision-level fusion algorithms combine image descriptions to the fused image, such as in the form of a relational graph (Shapiro, 1982) and (Williams et al., 1999). This is a description of fusion by decision, such as when the classification results are obtained from single images. In this fusion method, inhomogeneous sensors may be used, which allows the generation of decisions that are compatible on a decision level (Beyerer, 2008).

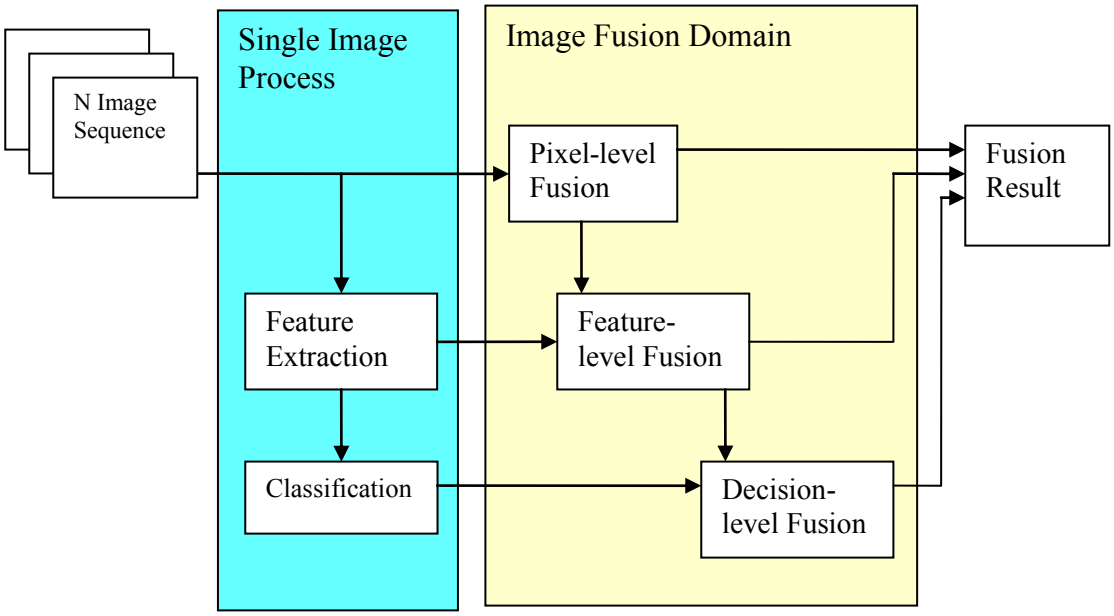

Figure 2.1: Image fusion block scheme of different abstraction levels: pixel-level fusion, feature level fusion, and decision level fusion. The level classification of various popular image fusion methods is based on a computational source. The feature level fusion is generated from feature-extraction for each single image. Decision level fusion is processed based on the classification from feature extraction.

In this part, we cover a portion of the image fusion research from recent years. The theory of image fusion has advanced quickly in the past few years. Currently, image fusion approaches with considerable complexity have been proposed. As previously stated, the fused image usually contains more information about the target or scene than any of the individual images used in the fusion process. The images used for fusion can be taken from multi-modal imaging sensors or from the same imaging sensor at different times. The target or scene in the images can be exactly the same or partially the same, for example, some objects and labels may have disappeared or new objects may be added to the images. Our topic, image fusion, has been investigated by many research groups and a number of algorithms have previously been developed (Scheunders et al., 2001), (Chan et al., 2003), (Rajan et al., 2002), and (Zhang et al., 1999). Although each algorithm has shown promising aspects, there seems to be a lack of universal criteria to measure the quality of the fusion algorithms. In many cases, qualitative criteria, such as visual analysis, are used to assess the resulting fused images.

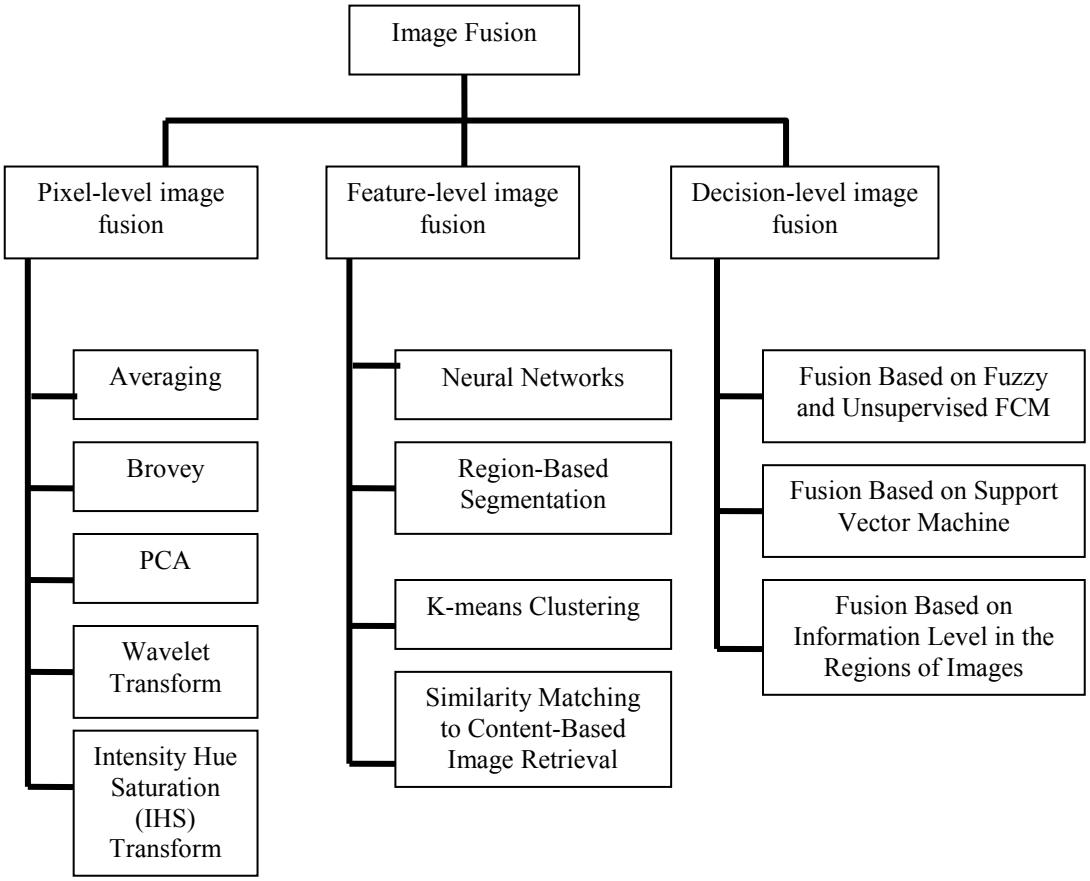

Figure 2.2: The level classification of the various popular image fusion methods is based on the computation source. The bottom branches show the typical image fusion algorithms that fall into each fusion level. The pixel-level method works either in the spatial domain or in the transform domain. Feature-level algorithms typically segment the image into contiguous regions and fuse the regions using their properties. Decision-level fusion algorithms combine image descriptions to fuse.

Over the years, multiple efforts have been made to develop new image fusion techniques. Additionally, efforts have been made to review and assess the image fusion qualities. However, there are still a large number of open issues that need to be resolved in this area. Depending on the specific application and its range of usage, the problems and objectives can vary. For example, when it comes to using the targeted applications on unconstrained outdoor scenes, containing items such as varying terrain, mountainous areas, roads, and buildings, we will generally encounter more background noise caused by environmental and weather factors. The distance to the targets also tends to be greater than indoor scenes, and as a result, the targets usually appear smaller and less clear in the images. Thus, these factors will make image fusion more difficult; however, applications in scenes such as these can also benefit from multisensory image fusion.

2.2 Image fusion technologies

In this section, we will briefly introduce various types of state-of-the-art image fusion technologies. The main principle, and typical advantages and disadvantages are introduced for each approach.

- ***Fusion using Principle Component Analysis (PCA):*** The PCA image fusion method simply uses the pixel values of all source images at each pixel location, adds a weight factor to each pixel value, and takes an average of the weighted pixel values to produce the result for the fused image at the same pixel location. The optimal weighted factors are determined by the PCA technique. The PCA technique is useful for image encoding, image data compression, image enhancement, pattern recognition (especially for object detection), and image fusion. It is a statistical technique that transforms a multivariate data set of inter-correlated variable into a data set of new un-correlated linear combinations of the original variables. It generates a new set of axes which is orthogonal. By using this method, the redundancy of the image data can be decreased. (Pohl et al., 1998)

- ***Fusion using Laplacian pyramid method:*** The IHS fusion converts a color MS image from the RGB space into the IHS color space. Because the intensity (I) band resembles a panchromatic (PAN) image, it is replaced by a high-resolution PAN image in the fusion. A reverse IHS transform is then performed on the PAN, together with the hue (H) and saturation (S) bands, resulting in an IHS fused image. (Aiazzi et al., 2003)

- ***Fusion using Laplacian pyramid method:*** The Laplacian pyramid fusion consists of an iterative process of calculating the Gaussian and Laplacian pyramids of each source image, fusing the Laplacian images at each pyramid level by selecting the pixel with the larger absolute value, combining the fused Laplacian pyramid with the combined pyramid expanded from the lower level, and then expanding the combined pyramids to the upper level. The fusing step above can also be done using a PCA-based weighted averaging technique. (Zeng et al., 2006)

- ***Fusion using gradient pyramid method:*** A gradient pyramid is obtained by applying a set of 4 directional gradient filters (horizontal, vertical, and 2 diagonal) to the Gaussian pyramid at each level. At each level, these 4 directional gradient pyramids are combined together to obtain a combined gradient pyramid that is similar to a Laplacian pyramid. The gradient pyramid fusion is therefore the same as the fusion using the Laplacian pyramid method except replacing the Laplacian pyramid with the combined gradient pyramid. (Zeng et al., 2006) and (Smith et al., 2005)

- ***Fusion using filter-subtract-decimate (FSD) pyramid method:*** The FSD pyramid fusion method is conceptually identical to the Laplacian pyramid fusion method. The only difference is in the step of obtaining the difference images in creating the pyramid. In a Laplacian pyramid, the difference image Lk at level k is obtained by subtracting an image up-sampled and then low-pass filtered from level k+1 from the Gaussian image Gk at level k, while in the FSD pyramid, this difference image is obtained directly from the Gaussian image Gk at level k subtracted by the low-pass filtered image of Gk. It is therefore obvious that the FSD pyramid fusion method is computationally more efficient than the Laplacian pyramid method by skipping an up-sampling step. (Zeng et al., 2006)

- ***Fusion using discrete wavelet transforms (DWT) method***: In the DWT-based fusion method, the source images are first transformed by DWT to their corresponding wavelet coefficient images at each scale level. Corresponding approximation coefficients and detail coefficients of the source

images at each level are then fused, respectively, based on a certain fusion rule. This rule can be a simple addition or averaging, or a PCA-based weighted averaging. The fused approximation and detail coefficients at each level are used in the final reconstruction of a single output fused image by an inverse DWT. (Zeng et al., 2006) and (Wang et al., 2003)

- ***Current trends in super-resolution image reconstruction:*** Super-resolution (SR) reconstruction is a branch of image fusion for bandwidth extrapolation beyond the limits of a traditional electronic image system (Katartzis et al., 2006). Katartzis and Petrou describe the main principles of SR reconstruction and provide an overview of the most representative methodologies in the domain. The general strategy that characterizes super-resolution comprises three major processing steps which are (low resolution) LR image acquisition, image registration/motion compensation, and (high resolution) HR image reconstruction. Katartzis and Petrou also analyze the advantages and limitations of each set of techniques, including frequency domain methods, projection onto convex sets (POCS), Bayesian/variation methods, and interpolation-based approaches. Then they present a promising new approach based on Normalized Convolution and a robust Bayesian estimation, and perform quantitative and qualitative comparisons using real video sequences.

- ***Image fusion through multi-resolution oversampled decompositions:*** Aiazzi, Baronti, and Selva described the methods of multi-resolution analysis in detail and implemented multi-resolution oversampled decompositions for applications of image fusion (Aiazzi et al., 2006). Their work covers component substitution (CS), the fundamental principles of multi-resolution decomposition, orthogonal wavelets method, and bi-orthogonal wavelets method. Additionally, they also cover context-driven multi-resolution data fusion methods such as the undecimated wavelet-based data fusion scheme, pyramid-based fusion scheme, ‗A trous' wavelet data fusion scheme, enhanced spectral distortion minimizing model, and enhanced context based model. Other methods include orthogonal wavelets, the multi-level decomposition of wavelet transforms, and translation-invariant wavelet decomposition of a 2-D image. The performance of each method is evaluated qualitatively and quantitatively.

- ***Multi-sensor and multi-resolution image fusion using the linear mixing model:*** Image fusion of a high spatial resolution (Landsat, Thematic, and Mapper) and a high spectral resolution (Envisat and MERIS) image based on the linear mixing model is presented in this work (Clevers et al., 2007). This is also known as spatial unmixing or unmixing-based data fusion. The value of a pixel is composed of the signals coming from the individual components, and is also called a mixed pixel. An optimization of the number of classes used to classify the high spatial resolution image and the size of the neighborhood, for which the unmixing equations are solved, is presented. Results and evolution are compared. The advantage of the presented technique from Clevers and Zurita-Milla is that the fused images do not include the spectral information of the high spatial resolution image in the final result in any way. The unmixing–based data fusion approach is particularly suitable for fusing MERIS FR time series with one or more TM images since the spectral information of the TM images is not included in the fused image in any way. The multi-temporal data fusion exercise will be of great interest for land cover mapping and monitoring vegetation dynamics at high spatial, spectral, and temporal resolutions.

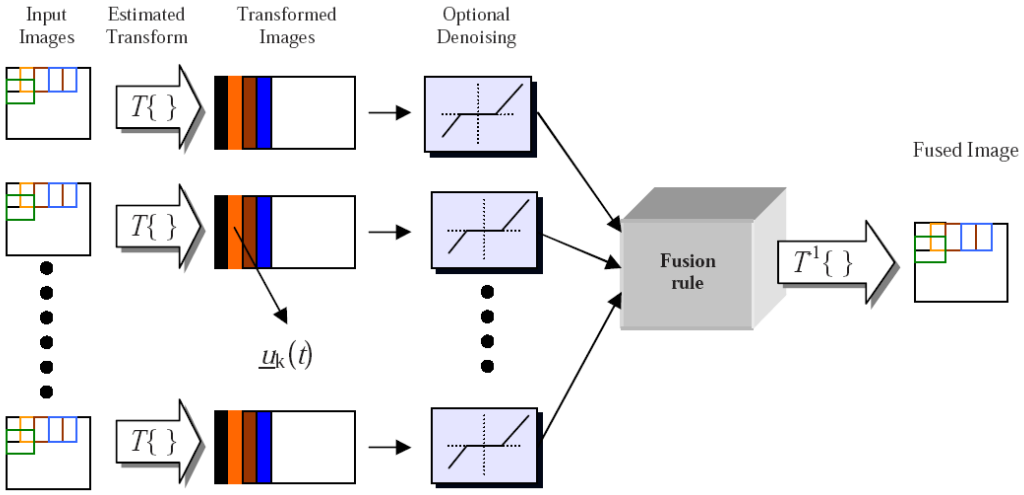

Figure 2.3: The image fusion system using ICA/ Topographical ICA bases, proposed by Mitianoudis et al. Note that the basic different between ICA and topographic ICA bases is the ~~"t~~opography". Topographic bases provide an ordered presentation of the data, compared to the unordered representation of the ICA bases. Images from (Mitianoudis et al., 2006).

- ***Image fusion schemes using ICA bases:*** Mitianoudis and Stathaki demonstrate the efficiency of a transform constructed using Independent Component Analysis (ICA) and Topographic Independent Component Analysis based for image fusion in this study (Mitianoudis et al., 2006). The bases are trained offline using images of similar context to the observed scene. The images are fused in the transform domain using novel pixel-based or region-based rules. An unsupervised adaption ICA-based fusion scheme is also introduced. The proposed schemes feature improved performance when compared to approaches based on the wavelet transform and a slightly increased computational complexity. The authors introduced the use of ICA and topographical ICA based for image fusion applications. These bases seem to construct very efficient tools, which can compliment common techniques used in image fusion, such as the Dual-Tree Wavelet Transform. The proposed method can outperform the wavelet approaches. The Topographical ICA based method offers a more accurate directional selectivity, thus capturing the salient features of the image more accurately.

- ***Statistical modeling for wavelet-domain image fusion:*** This study describes a new methodology for multimodal image fusion based on non-Gaussian statistical modeling of wavelet coefficients of the input images (Achim et al., 2006). The use of families of generalized Gaussian and alpha-stable distributions for modeling image wavelet coefficients is investigated and methods for estimating distribution parameters are proposed. The authors also improved the techniques by incorporating these models into the weighted average image fusion algorithm, tested using visual and infrared light image datasets. The author shows through extensive modeling that typical VI/IR images and their corresponding wavelet coefficients have highly non-Gaussian characteristics that can be accurately described by GGD or SaS statistical models. The modeling results show evidence of those wavelet decomposition coefficients. However, the use of such models has been long hampered by the fact that no convergent second or higher-order moments exist. On the other hand, the less accurate fit offered by GGDs is compensated for by the availability of analytical expressions for their pdfs as well as that of simple parameter estimators (Achim et al., 2006).

- ***Theory and implementation of image fusion methods based on the 'a trous' algorithm:*** Xavier Otazu presented introductory information and detailed explanations of several image fusion methods based on the _a trous' multi-resolution wavelet decomposition algorithm in his work (Otazu, 2005). From the literature regarding the many existing wavelet decomposition schemes, the _a trous' algorithm produces the best results when used for image fusion tasks. The literature mention image fusion algorithms such as energy matching, spatial detail extraction (_a trous' algorithm), and spatial detail injection, as well as offering practical advice and how to implement several image fusion algorithms that use this particular wavelet decomposition. The test results are generated from QuickBird images supplied by Eurimage (www.eurimage.com) with 2.8 meters per pixel. The other image is a panchromatic image with 0.7 meters per pixel. They degraded these two images to 11.2 and 2.8 meters per pixel, respectively. The best test result is from the WiSpeR method, which allows injecting the spatial detail on each multispectral channel in a more accurate way.

- ***Bayesian methods for image fusion:*** In their paper, the authors describe the Bayesian fusion methodology based on a solid mathematical theory, and provide a rich ensemble of methods which allow for an intuitive interpretation of the fusion process (Beyerer et al., 2007). The paper introduces methodologies such as the Bayesian solution of inverse problems in imaging, Bayesian image fusion exemplified for Gaussian distributions, and Bayes estimators. The overall specifications of the fusion task are then obtained by weighting and combining the energy, data, quality, and constraint terms. Several techniques for the exact, and approximate, minimization of global energy are considered: direct minimization, successive optimization, graph cuts, and dynamic programming. The primary disadvantage of the Bayesian fusion methodology is its global perspective on the fusion problem which also causes high computational costs. The high computational costs created by the Bayesian approach can be circumvented by realizing a local Bayesian approach: in essence, as an analogy to the local view of human criminal investigators, fusion agents evaluate and relate clues and evidence in a local manner.

- ***Multidimensional fusion by image fusion:*** The authors demonstrate a framework of capturing information in multiple imaging dimensions using generalized mosaicing (Schechner et al., 2007). They also demonstrate this framework by deriving mosaics having HDR, multispectral, or polar metric outputs. They explicitly mention the background on panoramic focus, the surface of least confusion, best focus, optical implementation, multi-spectral wide field of view imaging, and polarization. Generalized mosaicing is a framework for capturing information in multiple imaging dimensions. Contrary to common optical designs, an SLC that is not flat or normal to the optical axis can be beneficial, as it enables the extraction of depth information when the scene is scanned. This has implications for several aspects of computer vision, such as image-based rendering. It may also be applicable to machine vision systems (e.g., microscopic ones) used for industrialized inspection. In addition to focus, the author demonstrates this framework by deriving mosaics having HDR, multispectral, or polarimetric outputs. Nevertheless, generalized mosaicing permits simultaneous enhancement of multiple dimensions. Furthermore, generalized mosaicing can be used for self-calibration of simultaneous radiometric effects that occur in the camera, including vignetting, automatic gain control (AGC), and radiometric nonlinearity. This is achieved by exploiting the redundancy encapsulated in multiple overlapping frames to retrieve the radiometric parameters.

- ***Fusion of multispectral and panchromatic images as an optimization problem:*** In this study, different approaches to image fusion for pan-sharpening of multispectral images are presented and critically compared (Garzelli et al., 2006). Particular emphasis is devoted to the advantages

resulting from defining pan-sharpening as an optimization problem. Implementation issues are also considered and extensive results in terms of quality of the fused products, both visual and objective, and computational time comparisons are presented for classical, state of the art, and innovative solutions. This study reviews several pan-sharpening methods based on optimization procedures adopting one of two different score indexes as their objective function. A new fast method is also presented which provides near-optimal quality results together with a significant reduction of the computational complexity with respect to genetic or gradient-descent-based algorithms. The experimental results demonstrate that the optimization approach to pan-sharpening outperforms very efficient state-of-the-art solutions. In their paper (Zhang et al., 2004), a new approach for object extraction from a high-resolution satellite image is presented. The new approach introduced by Zhang integrates image fusion, multi-spectral classification, feature extraction, and feature segmentation into the object extraction of high-resolution satellite images. The author utilized both spectral information from multispectral (MS) images and spatial information from panchromatic (Pan) images to improve accuracies. Experiments of road extraction with QuickBird MS and Pan images demonstrate that the proposed approach is effective. As Figure 2.4 illustrates, in order to overcome the shortcoming of classification of low-resolution MS images, the MS and Pan QuickBird images are first fused into a pan-sharpened MS image. An unsupervised classification is then applied to the Pan image to obtain an edge-detected image. In the edge-aided segmentation, the binary edge image from the Pan image is employed to segment the classified road image from the pan-sharpened image. Then, a shape-based segmentation and a segments filtering algorithm are employed to remove non-road objects.

- ***Image fusion using optimization of statistical measurements:*** In this paper, Oudre, Stathaki, and Mitianoudis describe blind fusion methods which mean fusion without a priori knowledge of the ground truth image (Oudre et al., 2007). They use the spatial domain method, Dispersion Minimization Fusion (DMF), and Kurtosis Maximization Fusion (KMF) based techniques to linearly combine the input images with appropriate weights estimated using specific mathematical performance criteria which evaluate in various ways improvements in visual perception. The optimization of the proposed cost functions enables us to obtain a fused image which is less distorted when compared to the input images. In this work we propose to linearly combine the input images with appropriate weights estimated using specific mathematical performance criteria with which to evaluate various ways for improvements in visual perception. More specifically, in order to estimate the weights we propose iterative methods which use cost functions based on two statistical parameters, i.e. dispersion and kurtosis. The optimization of the proposed cost functions enables us to obtain a fused image which is less distorted when compared to the input images.

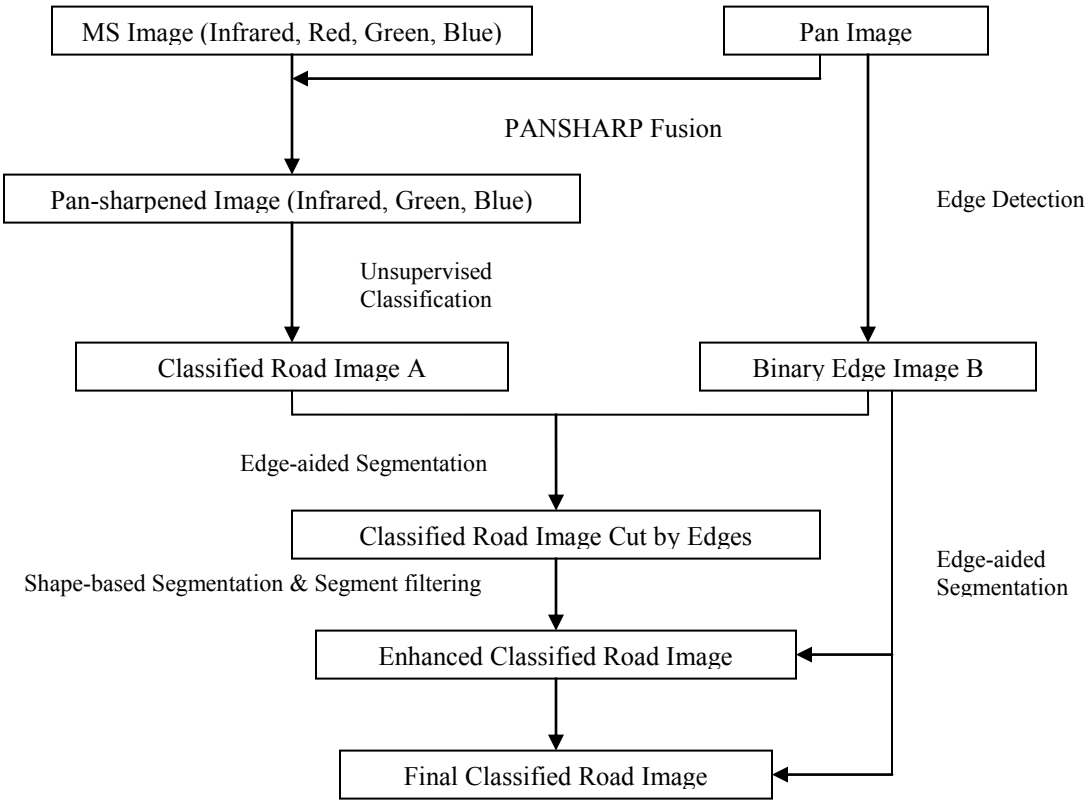

Figure 2.4: The general process of the proposed image fusion, classification, and future extraction integrated approach. The MS and Pan QuickBird images are first fused into a pan-sharpened MS image. An unsupervised classification is then applied to the Pan image to obtain an edge-detected image. In the edge-aided segmentation, the binary edge image from the Pan image is employed to segment the classified road image from the pan-sharpened image. Then, a shape-based segmentation and segments filtering algorithm are employed to remove non-road objects. Images reproduced from (Zhang et al., 2004).

- ***Fusion of edge maps using statistical approaches:*** This work contains the explanation of a new framework which allows for the quantitative fusion of edge maps that arise from both different preselected edge detectors and multiple image realizations (Giannarou et al., 2003). The work is inspired by the problem that despite the enormous amount of literature on edge detection techniques, there is no single one that performs well in every possible image context. Two approaches including the Receiver Operating Characteristics (ROC) analysis and Kappa Statistics are employed in a novel fashion to estimate the accuracy of the above edge maps in order to form the optimum final edge image. The results of applying these two techniques are demonstrated and compared. Both techniques integrate efficiently the preselected set of edge detectors in terms of both the quality of the highlighted features and the elimination of noise and texture. However, the Weighted Kappa Coefficient approach can be considered superior in the sense that the tradeoff

between detection of minor edges and noise reduction can be quantified in advance as part of the problem specifications.

- ***Enhancement of multiple sensor images using joint image fusion and blind restoration***: The authors propose a combined spatial-domain method of fusion and restoration in order to identify the common degraded areas of all input images in all input sensor images, and use a regularized restoration approach to enhance the content in these areas (Mitianoudis et al., 2003). The common assumption for most fusion approaches is the existence of a high-quality reference image signal for all image parts in all input sensor images. In the case that there are common degraded areas in at least one of the input images, the fusion algorithms cannot improve the information provided, but simply convey a combination of this degraded information to the output image. In this study, the authors propose a combined spatial-domain method of fusion image and use a regularized restoration approach to enhance the content in these areas. The approach is tested by multi-focus and multi-modal image sets. More specifically, a combined method of fusion and restoration was proposed as the next step up from the current fusion systems. By definition, fusion systems aim only at transferring the ‗interesting information' from the input sensor images to the fused image, assuming there is a proper reference image signal for all parts of the image. The proposed methodology also exhibits interesting results in the case of multi-modal image sets, producing outputs with distinctively outlined edges when compared to the transform domain methods.

- ***Empirical mode decomposition for simultaneous image enhancement and fusion:*** The authors address image enhancement and restoration via information fusion using inherent fission properties of empirical mode decomposition (EMD) in this work (Looney et al., 2007). Fusion via EMD describes the adaptive decomposition of an image signal into a set of oscillatory modes that act as a set of naturally derived basis functions. Embedded in the modes are the frequency scales of the image data. Given that a variety of humanly observable image features such as object texture or degradation effects such as noise can often be attributed to local variations in specific spatial frequencies, it follows that the behavior of the extracted image modes reflect these features. Simultaneous restoration and enhancement can be achieved by fusion of the ‗relevant' modes. The fusion process can be used to highlight specific image attributes to aid machine vision tasks such as object recognition. With tests on EMD, information fusion, texture analysis, and fusion of multiple image modalities, the authors demonstrate how decomposition via EMD and the subsequent fusion of the extracted components is a powerful tool for the purposes of image enhancement and restoration under the general framework of fusion via fission.

- ***Region-based multi-focus image fusion:*** Li and Yang first describe the principle of region-based image fusion in the spatial domain (Li et al., 2005). Then two region-based fusion methods are introduced. They proposed a spatial domain region-based fusion method using fixed-size blocks. Experimental results from the proposed methods are encouraging. More specifically, in spite of the crudeness of the segmentation methods used, the results obtained from the proposed fusion processes, which consider specific feature information regarding the source images, are excellent in terms of visual perception. The presented algorithm, spatial domain region-based fusion method using fixed-size blocks, is computationally simple and can be applied in real time. It is also valuable in practical applications. More sophisticated approaches proposed use complex segmentation methods. Although the results they obtained from a number of experiments are promising, there are more parameters to be considered as compared to an MR-based type of method, such as the wavelet method. Adaptive methods for choosing those parameters should be researched further. In addition, further investigations are necessary for selecting more effective clarity measures.

- ***Image fusion techniques for non-destructive testing and remote sensing application:*** The authors present several algorithms of fusion based on multi-scale Kalman filtering and computational intelligence methodologies (Morabito et al., 2008). The proposed algorithms are applied to two kinds of problems: a remote sensing segmentation, classification, and object detection application performed on real data available from experiments and a non-destructive testing/evaluation problem of flaw detection using electro-magnetic and ultrasound recordings. In both problems the fusion techniques are shown to achieve a modest superior performance with respect to the single-sensor image modality. The joint use of the eddy current and ultrasonic measurements is suggested because of the poor results that are obtained by processing each single recorded type of signal alone. Therefore, both measurements are jointly processed, and the information used to perform the classification has been extracted at three different levels: pixel, feature, and symbol. The numerical performance of these techniques has been compared by using the probability of detection and probability of false alarm. Experiments performed on real data confirmed the effectiveness of the proposed SL based approach, by maximizing the probability of detection and achieving an acceptable probability of false alarm with respect to the PL and FL fusion techniques.

- ***Concepts of image fusion in remote sensing applications:*** This work focuses on image fusion for remote sensing applications such as multispectral (MS) and panchromatic (PAN) image fusion (Pradham et al., 2006). The Pan sharpening method includes HIS based pan sharpening, and multi-resolution-based pan sharpening, which are explained in detail. Later, the authors implement and compare the results from several multi-resolution analyses (MRA) based methods. The work shows that multi-resolution-based pan sharpening methods are effective for pan sharpening multispectral images while maintaining their spectral integrity. The main multi-resolution-based pan sharpening methods are the additive and substitutive methods. It is seen that the additive method works well only if the Laplacian pyramid is used as the multi-resolution transform. However, the drawback is that it is difficult to implement when the images to be merged do not have a resolution ratio that is not a power of two. On the other hand, the substitutive method is quite flexible and works without modification for any resolution ratio images. The effect of various wavelet bases or filters on the spectral distortion introduced in the pan sharpened images was also studied and recommendations were made as to which wavelet or filter basis to choose, depending on the transform.

- ***Pixel-level image fusion metrics:*** The topic of this study is about the metrics that are designed to quantify the performance of pixel-level image fusion systems (Xydeas et al., 2006). Subjective tests that employ samples of the representative are a reliable and straightforward method for performance evaluation. However, this approach is expensive in terms of time, effort, and utility requirement. As Figure 2.4 illustrates, this process is conducted either by comparing the samples to each other or by performing specific visually oriented tasks. An alternative approach is to employ an objective fusion assessment which takes the form of a computer code, and uses objective evaluation metrics in the development of image fusion systems. Important visual information is considered that relates to ‗edge'-based information and associated image regions. Then the concept is expanded with the involvement of Human Visual System modeling within the metric formulation process. Extensive experimentation is conducted for performance measures. A number of such image fusion measures are therefore developed and their characteristics are examined for accurately predicting fusion system performance as compared to that obtained from subjective tests. Extensive experimentation allows for the detailed analysis, optimization, and understanding of the comparative behavior of these image fusion performance measures. The second approach that takes fully into consideration HVS properties is based on measuring visual differences on a per pixel basis. It was found that pure VC metrics achieve respectable performance, but do not improve upon edge (gradient) –preservation-based algorithms.

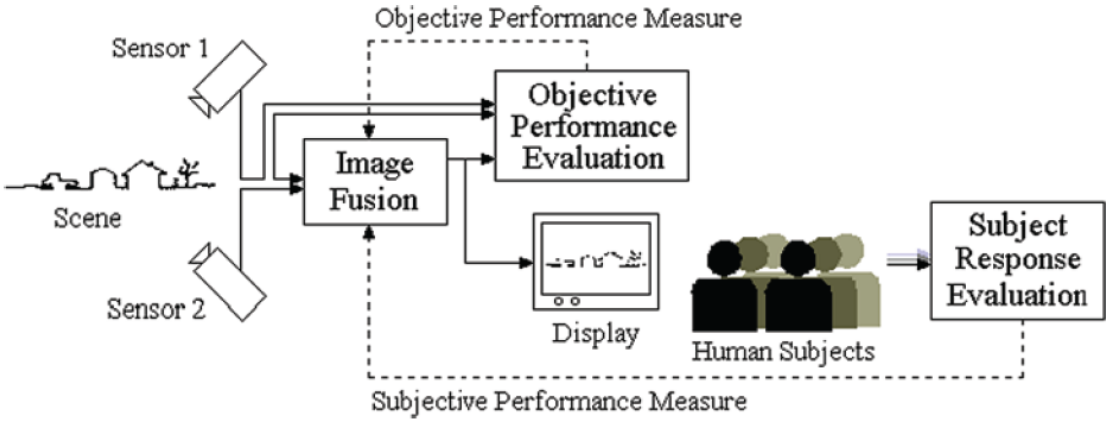

Figure 2.5: The subjective and objective image fusion process evaluation. This process is conducted either by comparing the images to each other or by performing specific visually oriented tasks. Images from (Xydeas et al., 2006).

- ***Objectively adaptive image fusion***: The authors mention the objective fusion evaluation using an edge representation based metric, which transfers input gradient information into the fused image more accurately (Petrovic et al., 2007). They test the objectively optimized, adaptive image fusion approach and show that they can improve the performance and robustness of fusion schemes. This work has shown that an objectively optimized, adaptive image fusion approach can improve the performance and robustness of fusion schemes. By employing the methods used in objective fusion evolution, parameters can be adapted to current input conditions in order to achieve optimal fusion performance. Feedback optimization of fusion parameters was shown to be effective on fusion of image sequences where high dynamics were used to make the process more efficient by optimizing parameters only every N frames or from one frame for the next frame. Finally, a weakness in the objective fusion evaluation of fusion was identified on the example of noisy input data. Noise is a problem of image fusion in general and robust mechanisms for avoiding the situation where noise dominates the fused image are certain to be a topic of research in the future.

- ***Performance evaluation of image fusion techniques:*** This chapter discussed various performance evaluation measures that have been proposed in the field of image fusion and also analyzes the effects of fusion structures on the outcomes of fusion schemes (Wang et al., 2005). Indicative of experiments on applying these measures to evaluate a couple of widely used image fusion techniques are also presented to demonstrate the usage of these measures, as well as to verify correctness and efficiency. The chapter discussed various performance evaluation measures that have been proposed in the field of image fusion and also analyzed the effects of fusion structures on the outcomes of fusion schemes. It is important to stress that there is not a single performance evaluation measure that can be classified as superior. Each measure highlights different features in an image and, therefore, the selection of a particular measure to evaluate an image fusion technique is based on the particular application.

2.2 Morphing techniques

In this work, image morphing is utilized to create a transformation process between the source image and destination image. Image morphing has received much attention in recent years. Morphing has proven to be very useful during this time. There are many applications that use morphing. It is being used frequently to provide a special entertaining effect on television and in the movies, in order to generate the smooth transformation of one digital image into another. One of the most commonly recognized applications may be face morphing. The transformation process will demonstrate the visual appearance and use the transformed intermediate status to simulate the image fusion result. Image morphing between two images begins with choosing control points to establish their correspondence with the pairs of featured objects. The pairs of featured objects are used to compute mapping functions that define the spatial relationship between all points in both images. It is used to interpolate the positions of the features across the morph sequence. Traditional image morphing considers only two input images at a time, the source and target images. Morphing among multiple images involves a series of transformations from one image to another. This limits any morphed image to the features and colors blended from just two input images.

Meng and Liu present a novel approach for image morphing based on the moving least squares method. A sketching interface is proposed for quickly and easily specifying the feature correspondences between the key frame images (Meng et al., 2006). The images are warped and blended using the moving least squares method. Various experimental results show that their approach provides the animator high-level control of the visual effect by providing natural sketching specification, and the ability to generate realistic morphing results.Wolberg surveyed the growth of this field and describes recent advances in image morphing in terms of feature specification, warp generation methods, and transition control (Wolberg, 1998). These areas relate to the ease of use and quality of results. He describes the role of radial basis functions, thin plate splines, energy minimization, and multilevel free-form deformations in advancing the state-of-the-art in image morphing. Recent work on a generalized framework for morphing among multiple images is also described.

A comparison of various techniques for morphing one digital image in to another is made by Oswal and Govindaraju. They compare various morphing techniques such as feature-based image morphing and mesh and thin plate spline based image morphing based on different attributes such as computational time, visual quality of morphs obtained, and complexity involved in the selection of features (Oswal at al., 1998). They demonstrate the pros and cons of various techniques so as to allow the user to make an informed decision to suit their particular needs.

Examples that deploy the morph algorithm in the fields of geospatial data service are available. They are used to describe the transformation between one status and another. The Space Department of NLR has carried out a multi-temporal analysis of change in morphology in the Wadden Sea using imagery from the Landsat satellites. The objective of that morphing study was to establish movements of sandbanks and tidal channels during the period between 1975 and 1987. Below is a figure showing the movements for Pinkegat/Westgat near the Ameland region conducted by the Netherlands Department of Geology and Netherland Institute in Applied Geosciences. Landsat MSS satellite images were selected that were taken at the same low water levels. The darkness of water shows the water level, and the boundary of the sandbanks is moved back between 1980 and 1987.

Pinkegat/Westgat

(a)

Pinkegat/Westgat

(b)

Pinkegat/Westgat

(c)

Pinkegat/Westgat

(d)

Pinkegat/Westgat

(e)

Figure 2.6: The movement of sandbanks and tidal channels during the period between 1975 and 1987 for Pinkegat/Westgat near the Ameland region. (a) 1975, (b) movement between 1975 and 1980, (c) 1980, (d) movement between 1980 and 1987, and (e) 1987. The darkness of the water shows the water level, and the boundary of the sandbanks is moved back between 1980 and 1987.

2.3 Image registration

Image registration is the process of establishing a point-by-point correspondence between multiple images describing the same scene. Most likely, images from the same scene are acquired from different sensors. These images may have relative translation, rotation, scale, misalignment, and other geometric transformations between them. The misalignment of the image is caused by several factors including the geometrics of the sensors, different spatial positions of the sensors, different resolution of the sensors, different temporal capture rates of the sensors, and the inherent misalignment of the sensing elements. Before the image fusion algorithm is applied to the source images, image registration is used to guarantee the correspondence between the pixels in the input images. It is about the proper geometrical alignment of the images so that the corresponding pixels or regions of both images map to the same region being imaged. Registration is necessary in order to be able to compare or integrate the data obtained from different measurements.

There are two general types of differences between the images to be reiterated. One is due to condition changes in acquisition, which cause the images to be spatially misaligned. In the second type, the differences which are not due to spatial misalignment can be attributed to factors such as lighting changes, different types of sensors, similar sensors with different parameters, object movement, or scene changes. Although one can align different sensors together to capture registered images, we are still not able to process the registration after the image acquisition under certain situations.

A significant amount of research has been done in developing various registration algorithms (Rui, et al., 2003), (Antoine, 1998), and (Sadidy et al., 2005). For example, the Block Matching Algorithm (BMA) is applied to find the local correspondence giving rise to the motion vector field and horizontal and vertical shifting and rotation parameters were obtained with a global motion estimation based on these vectors. Another example is that, if the parameter and position of the camera are not changed and only the environment is changed, the resulting images will be spatially registered. The image registration techniques can be generally classified into two categories: the intensity-based methods and feature- based methods. For the intensity-based methods, the images are essentially registered by selecting a number of windows in the high-variance areas of one image, locating the corresponding windows in the other image, and using the window geometric centers or mass center as control points to determine the registration parameters. Feature-based methods extract and match the common features from the source images. Features that are frequently used include edges, corners, and contours.

Although there is a diverse group of images to be registered, and due to various types of degradations, it is impossible to design a universal method suitable for all applications. However, the majority of the registration methods consist of the following four steps (Zitova, 2003). 1) Feature detection: Salient and distinctive objects (closed-boundary regions, edges, contours, line intersections, and corners) are manually or, preferably, automatically detected. For further processing, these features can be represented by their point representatives (centers of gravity, line endings, and distinctive points), which are called control points (CPs) in the literature. 2) Feature matching: In this step, the correspondence between the features detected in the sensed image and those detected in the reference image is established. Various feature descriptors and similarity measures along with spatial relationships among the features are used for that purpose. 3) Transform model estimation: The type and parameters of the so-called mapping functions, aligning the sensed image with the reference image, are estimated. The parameters of the mapping functions are computed by means of the established feature correspondence. 4) Image resampling and transformation: The sensed image is transformed by means of the mapping functions. Image values in non-integer coordinates are computed by the appropriate interpolation technique.

In Fig. 2.7 below, for implementation of registration, the selection of feature points in the image needs to be considered first. The features should be detectable and distinctive to the object. The detected features sets the reference and the sensed images must have enough common elements to be detectable. Occasionally there are situations when the images do not cover exactly the same scene or object occlusion exists. In the next step, the feature matching step, problems can be created when the physically corresponding feature is not similar because of various imaging conditions or the sensitivity of the sensor. In that case, the choice of the feature description and similarity measure has to be considered. The feature descriptors should be invariance to the assumed degradations. In the figures, the corresponding pairs are marked by numbers from 1 to 6. After the feature matching step, the mapping function should be chosen according to the reliability of the feature correspondence estimation and error estimation. In the end, the appropriate type of resampling technique depends on the tradeoff between the interpolation accuracy and computational cost.

Although there are many proposed methods, in this paper, we try to use a simple segmentation based image fusion method to represent the comprehensive information from multiple (2 or 3) sources. The segment fusion methods we provide allow the user to manually construct parameters to fuse the images at different levels. This feature provides the flexibility and modifiability to fuse the information with different features based on importance and perspective. Finally, our method‘s performance on different test image sizes and computer configurations is evaluated.

At the same time, the weighted average fusion method is also supplied for comparison. Similar to what the current image fusion application employs, the weighted average fusion is a pixel-based method. The obvious advantage of pixel-based image fusion is that the images used contain the original information. Additionally, the algorithm is easy and fast to implement and does not require a variety of image sizes. However, the drawback is that the weighted average fusion is very sensitive to mis-registration and noise. It may not suitable for some applications due to its low robustness.

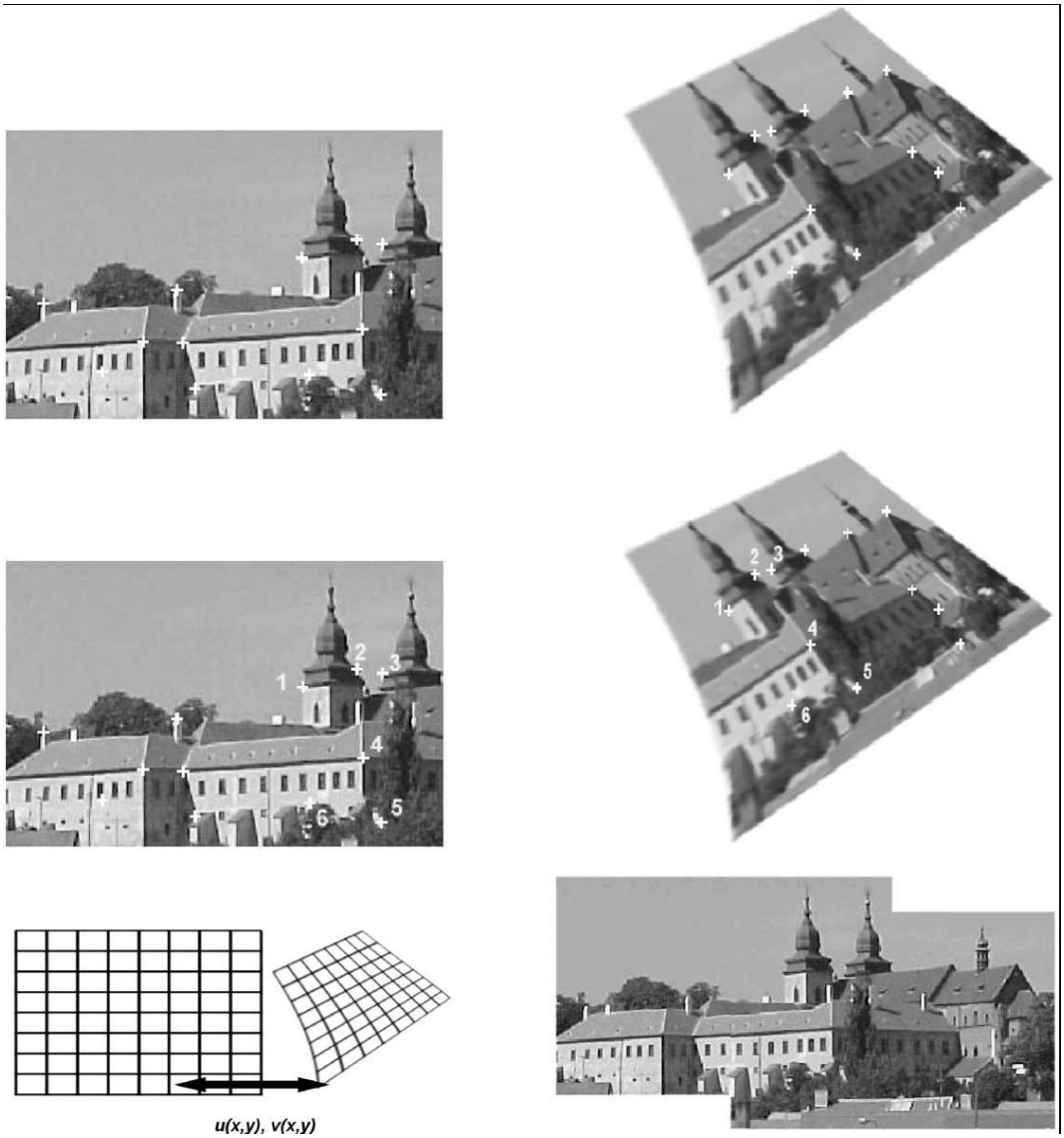

Figure 2.7: Four steps of image registration: top row—feature detection (corners were used as the features in this case). Middle row—feature matching by invariant descriptors (the corresponding pairs are marked by numbers). Bottom left—transforms model estimation exploiting the established correspondence. Bottom Right—image resampling and transformation uses the appropriate interpolation technique. Images originally from (Zitova, 2003).

3 Technical Approach: Image Fusion and Image Morphing

In the previous chapter, we stated that the challenges of the image fusion algorithm are how to best represent all the information effectively in the fused image. Based on different applications, there are, respectively, varying demands on computation time, complexity, environment constraint, and information quality. Since it is known that the image fusion algorithm's performance is application dependent, we will focus our approach, especially on multi-sensor applications, and then compare their performance. In this part, we propose to linearly combine the input images with their appropriate weight estimated using specific mathematical performance criteria. These two interactive methods help users to define the weight and pattern for the fused image.

3.1 Segmentation-based Image Fusion Approach

In image fusion applications such as a multi-sensor image fusion system for pilot and scene monitoring, there are always conditions that can cause the various images to be generated from different perspectives, or sensors. We introduce these methods to generate the fused image with a low computational cost.

In the segmentation-based image fusion algorithm, the task addressed in the frame is to fuse images derived from both registered and correlated digital images. The source image is decomposed into a mound of slice, which shows the respective source information in the pixels. Then these slices are aligned in the order of the source images in order to provide a combined virtual view of the information. With the various widths of these slices, the combination of the source images can provide different weights and definitions for the end user. Since the RGB components of each input image are assigned separately, all sources images have to be aligned or registered before being fused.

Let us consider a generic N-sensor system (N>2) with several sensors and each sensor generates a frame of the image $f_i(x,y)$ (i=1,...,N). We assume that $f_1(x,y)$, $f_2(x,y)$, $f_3(x,y)$,…, $f_N(x,y)$, denote the N images with height (x_s) and width (y_s) capturing the same scene loaded for image fusion, and the $g(x,y)$ represent the output image. A vector of properties M(x, y) is a list of primitives which describe the "state" of a part of the property at the coordinate (x, y).

$$M(x,y) \equiv \{f_1(x,y), f_2(x,y), \ldots f_n(x,y)\} \qquad (3.1)$$

The first step of segment fusion is to segment the input image into pieces and map them to the output image:

$$g(m,n) = \begin{cases} f_1(\mathrm{x},\mathrm{y}) & if\ \mathrm{n} \in [NL, NL+k_1] \\ f_2(\mathrm{x},\mathrm{y}) & if\ \mathrm{n} \in [NL+k_1, (N+1)L-k_3] \\ f_3(\mathrm{x},\mathrm{y}) & if\ \mathrm{n} \in [NL+k_1+k_2, (N+1)L] \end{cases} \qquad (3.2)$$

For $0 < \mathrm{m} < (k_1+k_2+k_3)\,x_s$, $0 < \mathrm{n} < (k_1+k_2+k_3)\,y_s$, and N = 0, 1, 2, 3…

Where $L = k_1+k_2+k_3$, and integer k_1, k_2, k_3 = 1,2,3,…. The k_1, k_2, k_3 represent the horizontal slice width for each of the 3 source images, and are the parameters defined by the end user beforehand. It is used to control the "slicing width", or the width of appearance for each source input in the segment and combined pattern. This slicing process is used to piece each slice from each input image together in order to show the integrated information.

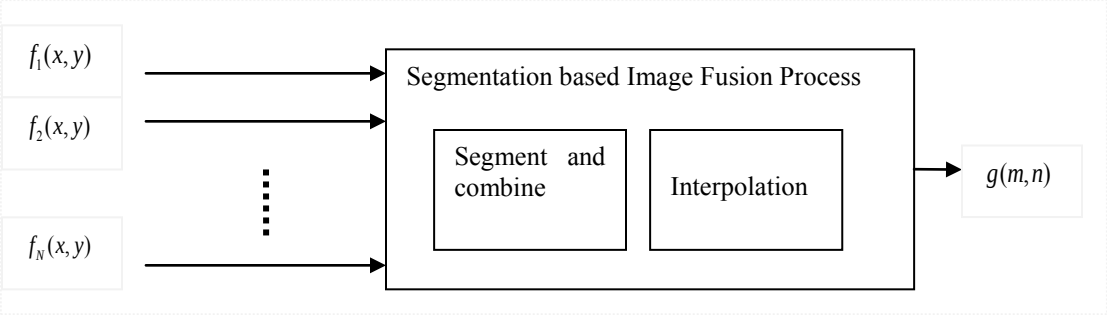

Figure 3.1 Segmentation based on the Image Fusion Process: This image fusion algorithm is targeted to a multi-sensor image fusion system where N ($N \geq 2$) sensors are employed. Within this approach, a segment and combine process, and an interpolation process, is integrated.

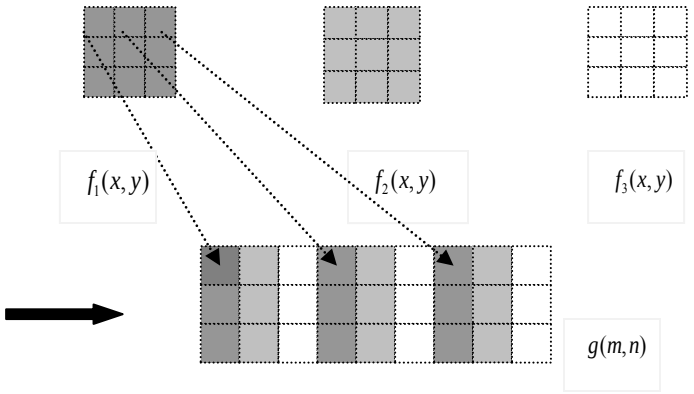

Figure 3.2 Segmentation based on the Image Fusion Process: Segment and combine step. The three 3x3 pixel grids represent the input source images. Each image is segmented into slices and combined together in order, with each width controlled by the parameters. The pixels with a different intensity represent the corresponding source image where the pixels originate. The results from this step are stretched in a horizontal direction.

Now we have shown the case of 3 source images. As the sensor application develops, additional types of sensors will be deployed in the future. For the case of *N* source images, this fusion method's complexity will not increase dramatically while still providing unfading information. In fact, since the computation time has a linear relation with the output image size, the computation time will have a quadratic relationship with N ($O(N^2)$). The segment based method can be applied as:

$$g(i,j)=\begin{cases} f_1(x,y) & if\ \ j\in[NL, NL+k_1] \\ f_2(x,y) & if\ \ j\in[NL+k_1, NL+k_1+k_2] \\ \vdots & \vdots \\ f_n(x,y) & if\ \ j\in[(N+1)L-k_n,(N+1)L] \end{cases} \tag{3.3}$$

where $L=\sum_{i=1}^{n} k_i$, The k_i (i=1, 2…n) are the parameters defined beforehand and we use integer values in our implementation.

After the process of the segment and combine steps, we will use interpolation to further process the image. The goal of image interpolation is to produce an acceptable image at different resolutions from a single low-resolution image. It can be described as filling in the pixels between the images. The interpolation problem is also known by many names, depending on the specific application: image resizing, image down-sampling, resolution enhancement, and super-resolution. The term super-resolution generally refers to producing a high-resolution image from multiple images such as from a video sequence.

The segmentation-and-combination step always stretches the image in a horizontal direction because there are always multiple source images. The distortion resulting from the stretch is undesirable in most applications. In order to keep the same aspect ratio without distorting the image, for each vacant pixel, the image fusion algorithm processes the linear interpolation in the vertical direction, which is generated from the upper and lower pixels. The actual RGB values in an integer value vary between 0 and 255. In that case, the calculation value of each pixel will be transformed into an integer value. Alternatively, one can use methods such as the nearest neighbor interpolation, cubic interpolation, B-spline interpolation, polynomial interpolation, and Lagrange interpolation to determine the pixel values between the samples. Generally, the linear interpolation, along with nearest neighbor interpolation, is the most common interpolation scheme in commercial software. Other linear interpolation filters such as quadratic zoom, the B-spline method, and zero-padding differ in their choice of how to determine the weighted average of nearby pixels. However, due to shortcomings in either accuracy or computational efficiency in the other methods, we deploy the linear interpolation in this work.

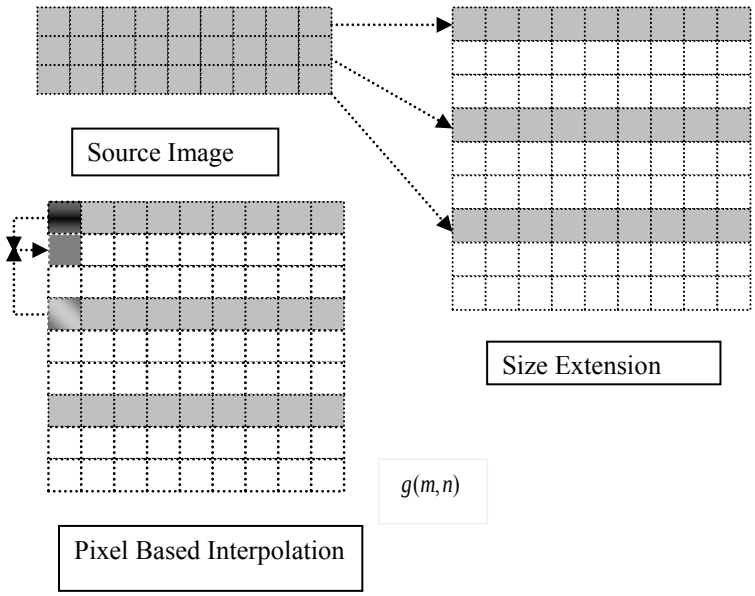

Figure 3.3 Segmentation-based Image Fusion Process: 2. Interpolation Step. This step is processed along the vertical direction. Interpolation is pixel-wise based on pixels above and below. The interpolation step is used to keep the output image in the same ratio aspect as the input image.

Linear interpolation (sometimes known as lerp) is one of the curving fitting approaches using linear polynomials. It is a first degree method that passes a straight line through every two consecutive pixels.

Let us continue with our interpolation implementation. For each pixel in the interval (x_i, x_{i+1}), the value of $g(m,n)$ can be derived geometrically from the straight line between the nearby points $f(x_{i+1}, n)$ and $f(x_i, n)$:

$$g(m,n) = \left| f(x_i,n) + (m - x_i)\frac{f(x_{i+1},n) - f(x_i,n)}{x_{i+1} - x_i} \right| \qquad (3.4)$$

If $x_i < m < x_{i+1}$, and i = 1, 2, 3….m, which is an integer value range in [1,m] $x_i = x_{i+1} + L$.

Of course, the advantage of this linear interpolation process is that it is quick and easy, that is to say, the output image produces smoother interpolatory points at a moderate cost. It will not be distorted in the aspect ratio and is not computationally expensive. The disadvantage is that the method is not very precise and the interpolatory point is not differentiable at the point (m,n). Thus, for an even better performance, a more complicated approach such as spline interpolation or a higher degree polynomial interpolation is needed. After the interpolation process, the resulting image size will increase from $x_s \times y_s$ to $(\sum_{i=1}^{n} k_i x_s) \times (\sum_{i=1}^{n} k_i y_s)$. That is $(\sum_{i=1}^{n} k_i)^2$ times larger than the original image size. An appropriate value k should be defined to avoid using excessive computer memory.

Although the segmentation and combination step might provide discontinuities or a blurring effect on the edges and texture of the images, from the perspective of a large image view, these effects will only

sacrifice a minimal amount of the visual effect and still fuse the large image size at a low computational cost.

3.2 Weighted Average Fusion

We have thus far discussed the philosophical inspiration used to proceed towards implementing the segment-based image fusion algorithm. One of the important reasons to achieve visualization of the comprehensive information using statistical image fusion is the representation of the object towards the goal of extracting information from multiple sources. There are several arguments in the literature with regards to the application of these theories in real world situations (Maskell, 2008).

Another commonly used algorithm is the weighted average (WA) image fusion method. It is one of the most direct and basic methods. A weighted average method multiplies each pixel value by an arbitrary "weight" and divides it by the sum of the weights, which is one in the weighted arithmetic mean case. Additionally, each weight should range between zero and one. Even years after its inception, the weighted average method proposed remains one of the most effective, yet simple and easy to implement image fusion algorithms. It is also a pixel-based fusion rule and produces the output image with the same size pixels as the input image.

In our implementation, we will use the weighted average method as the fusion function because it can maximize the information gain from each sensor individually without damage from information corruption.

The parameter k_i is set up in the beginning by the end user. For the values of the R, G, and B components, the formula is computed respectively. For the situation of *N* source images, the fusion process can be indicated as following:

$$g(x,y) = \left\lfloor \frac{\sum_{i=1}^{N} k_i * f_i(x,y)}{\sum_{i=1}^{N} k_i} \right\rfloor \qquad (3.5)$$

For $0 < x < x_s$, $0 < y < y_s$ which denote $f(x,y)$ locate within the size of image. $0 < k_i < 1$, $\sum_{i=1}^{N} k_i = 1$.

where $f_i(x,y)$ is the RGB component value of the input image, $g(x,y)$ is the RGB component value of the output image at coordinate x and y, and $\lfloor\ \rfloor$ is the ceil function, which is used to round up the value so that the integrated value is assigned to $g(x,y)$. The parameter k_i denotes the weight of the i^{th} source image regarding the fused output image. In other words, it shows how much information is included in the i^{th} source image regarding $g(x,y)$. By introducing the dependency relationship between the coefficients $0 < k_i < 1$, $\sum_{i=1}^{N} k_i = 1$, the value of the output is normalized to a range in the meaningful scope. In our implementation of this algorithm, the parameter k_i can be defined by the user. In general, for higher values of k_i (i = 0,1,2…*N*), the component $k_i \times f_i(x,y) / \sum_{i=1}^{N} k_i$ will tend to have a higher value. This property influences the fusion results significantly. It is intuitive to choose the higher value for k_i in order to stress the importance of one particular image $f_i(x,y)$, and it should be more obvious to recognize

the i^{th} source image in the applications. The weights can be used to account for the differences in accuracy between sensors, and a moving average can be used to fuse together a sequence of measurements from a single sensor so that the more recent measurements are given a greater weight. By means of adopting redundant information provided by each source images, the weighted average fusion method can improve detection reliability. Meanwhile, when it applies to multi-frame image fusion, it can increase the SNR (signal-to-noise ratio). In fact, the averaging image fusion is a type of smoothing process which not only reduces the image noise but also weakens the image contrast. The edges and outlines of the images are blurred to some extent.

The pixel level weighted averaging algorithm is a straightforward approach to image fusion. There are several different methods that fall into this category. Two representative methods are the principle component analysis (PCA) method and adaptive weighted averaging (AWA) method. In the PCA method, the weighting for each source image is obtained from the eigenvector corresponding to the largest Eigen value of the covariance matrix from a certain source image. In the AWA method, based on the local variance of the pixel intensity nearby, the algorithm chooses large weight parameters in the region where the pixel value has a high variance value based on its neighboring pixels.

3.3 Segment Weighted Average Fusion

In this section, segment weighted average fusion (SWAF) is also included in order to provide a high degree of control to the image fusion. It is a similar method to segmented fusion. As one can notice, the previous method has a limitation regarding the image contrast. To overcome this limitation of the segment fusion, we propose the SWAF fusion scheme. Our motivation is to produce better results by generally controlling the fusion. Although the SWAF is not developed as an automatic method, it is still a straightforward spatial way for the end user to determine the optimal weighting and width coefficients, with respect to visual effect and accuracy. SWAF is a combination of the two previously discussed methods, segmented based image fusion and weighted averaging method, using n parameter k_i ($k_1 k_2 k_3 ... k_n$) to control the fusion in terms of the pixel aspect, and using alpha α and beta β to control the weighting in terms of intensity aspect. As we have stated in the methods above, the $f_1(x,y)$, $f_2(x,y)$, and $f_3(x,y)$,…, $f_n(x,y)$ denote the n source images with the same height (x_s) and width (y_s), which are loaded for SWAF image fusion. The symbol $g(x,y)$ represents the output image pixel value at coordinate (x, y). For image intensity shifting purposes, the weight coefficients α , β , γ here represent the constraints of the image 1, image 2, and image 3 components respectively. Whereas the coefficients are linked by the dependency relationship:

$$\alpha + \beta + \gamma = 1 \qquad (3.6)$$

Based on the equation above, the weight coefficients can be rewritten as α , β , $1-\alpha-\beta$.

$$g(m,n)=\begin{cases}\dfrac{\alpha}{\max}[f_1(x_i,n)+(m-x_i)\dfrac{f_1(x_{i+1},n)-f_1(x_i,n)}{x_{i+1}-x_i})], & \forall \quad n\in\left[(N-1)L,(N-1)L+k_1\right]\\ \dfrac{\beta}{\max}[f_2(x_i,n)+(m-x_i)\dfrac{f_2(x_{i+1},n)-f_2(x_i,n)}{x_{i+1}-x_i})], & \forall \quad n\in\left[(N-1)L+k_1,NL-k_3\right]\\ \dfrac{1-\alpha-\beta}{\max}[f_3(x_i,n)+(m-x_i)\dfrac{f_3(x_{i+1},n)-f_3(x_i,n)}{x_{i+1}-x_i})], & \forall \quad n\in\left[(N-1)L+k_1+k_2,NL\right]\end{cases} \tag{3.7}$$

For $\{(m,n)\,|\,m\in(0,(k_1+k_2+k_3)x_s),n\in(0,(k_1+k_2+k_3)y_s)\}$, where $N=1,2,3...$, the weight coefficients $0<\alpha<1, 0<\beta<1, 0<\alpha+\beta<1$, $\max=\max\{\alpha,\beta,1-\alpha-\beta\}$ which is the maximum value of parameter α , β , $1-\alpha-\beta$ or γ .

The normalization of $g(m,n)$ is obtained by dividing its expression by the maximum value of the coefficients. By using this normalization process, one of the three ratios will be 1, which means that it will normalize the value to the identical value of $f(x,y)$, and reduce the other two values. The aspect ratio α /max, β /max, $(1-\alpha-\beta)$/max controls the intensity value of the three input components and k_1 , k_2 , k_3 are the times each slice is taken from input image. By doing this slice reiteration, different weights and strengths for each individual component will show up when the user zooms out to see a full view of the resulting image. If $\alpha=\beta=\gamma$, then the individual component will retain the same intensity value as the original, otherwise there are two components that are decreased by the ratio, and only the maximum value keeps the same intensity value.

As we have designed our method to target multi-sensor image fusion applications, we will not limit the algorithm to 3 source images for fusion. Instead, we will extend the SWAF algorithm to a generic method for *N* source images. For the case of *N* source images, the same computational principle can be used. Consequently, several of the constraints and mathematical formula expressed below are identical or similar to the ones in the case of the 3 source images. Let us assume $w_i \quad i\in[1,n]$ is the weight for i^{th} part of the slice image. Where $0<w_i<1$ for $i\in[1,n]$, also, they should always follow the constraint $\sum_{i=1}^{n}w_i=1$, $\max=\max\{w_1,w_2,\cdots w_n\}$ which is the maximum value of all the parameters w_i . The segment weighted average fusion can be described as follows:

$$g(m,n)=\frac{w_i}{\max}\,f_i(x,y)\ \ if\ n\in[NL+\sum_{i=1}^{i-1}k_i,NL+\sum_{i=1}^{i}k_i] \tag{3.8}$$

In other words, the expanded formula can be represented in the following way:

$$g(m,n)=\begin{cases}\dfrac{w_1}{\max}[f_1(x_i,n)+(m-x_i)\dfrac{f_1(x_{i+1},n)-f_1(x_i,n)}{x_{i+1}-x_i})] & if \quad n\in[NL,NL+k_1]\\ \dfrac{w_2}{\max}[f_2(x_i,n)+(m-x_i)\dfrac{f_2(x_{i+1},n)-f_2(x_i,n)}{x_{i+1}-x_i})] & if \quad n\in[NL+k_1,NL+k_1+k_2]\\ \vdots\\ \dfrac{w_i}{\max}[f_i(x_i,n)+(m-x_i)\dfrac{f_i(x_{i+1},n)-f_i(x_i,n)}{x_{i+1}-x_i})] & if \quad n\in[NL+\sum_{i=1}^{i-1}k_i,NL+\sum_{i=1}^{i}k_i]\end{cases}$$

(3.9)

For $0 < m < (k_1 + k_2 + k_3)x_s$, $0 < n < (k_1 + k_2 + k_3)y_s$, where N = 1, 2, 3…..

Segmented Weighted Average fusion divides each source image into pieces of the slice with a width of 1, and then determines the intensity value of the pixels from each slice by w_i /max, and repeatedly aligns those slice together k_i times with order from $f_1(x, y)$ to $f_n(x, y)$ then back again. The mathematical development shows that, as formulated, if $w_1 = w_2 = ... = w_n$, the intensity value of the individual source image will keep the same intensity value as the original $f_i(x, y)$, otherwise, while the maximum w term increases with w_i /max =1, the other source intensity value will be reduced by the scale w_i /max accordingly. Consequently, the intensity value of those pixels will turn out darker when compared with the original ones.

The advantages of this segmented weighted average fusion method includes a higher degree of control over the fusion, manipulation of intensity for each sensor image, and maintains the true color of the interested max intensity value. With the help of a controller, the user can quickly receive visual feedback about the results of this algorithm. As is usually the case in a pilot system or Geography Graphic Information System (GIS), the user can manipulate the fusion view window by shifting the weight w_i and parameter k_1, k_2, k_3 to control the visualized sensor information.

The drawback of segmented weighted average fusion includes: no performance measure in the SWA process exists to judge and control performance quality; a processing parameter of SWA is manually selected based on different application situation, so the method is not fully automated; and SWA will enlarge the size of resulting image from $x_s \times y_s$ to $(\sum_{i=1}^{n} k_i x_s) \times (\sum_{i=1}^{n} k_i y_s)$, so it will increase computational complexity and memory requirement. We will illustrate the results and evaluate the performance in more detail in a later chapter.

3.4 Image morphing

In addition to the methods we described above, we use another approach, image morphing, to approximate the fusion results based on multiple sensor images. It is also described as image warping with color interpolation. In this section, we will briefly introduce the theory of image morphing, and then test the algorithm in a later chapter. Morphing is an image processing technique to generate a warp that distorts the first image towards the second image. The results of the processing show that the first image is gradually faded away and the second image starts to be revealed, distorted from the first image.

There are many breathtaking examples in film and television of this fluid transformation. Morphing has been used in these areas as a computer graphic technique for decades. It applies 2D geometric transformations to the images to retain geometric alignment between their features, while color interpolation blends their colors. Beside the applications that have traditionally been associated with visual effects for entertainment, we would like create the image between two transition statuses, statues range from different perspectives of view, different angles of view, and different sensors of views. Morphing, also known as metamorphosis is an image processing technique used for the metamorphosis of one image to another. In this part of the dissertation, we would like to introduce the morphing transform algorithm with a particular focus on applying the mesh warping technique to still images from multi-sensor images.

Image morphing has currently received much attention. It has proven to be a powerful tool for visual effects in film and television, enabling the transformation of one digital image into another. In this work, we use a morphing scheme which would combine cross-dissolving with warping methods to calculate the pixel value. The morphing process consists of a warping stage before cross-dissolving based on the control points so that the two images have the same shape. We also use the phanta morph 4 to test and evaluate the results from the image morphing.

In general, morphing algorithms consist of two processes: warping and combination or cross fading. Let us consider a transition that consists of *N* frames in length between source image $f_s(x, y)$ and destination image $f_d(x, y)$, assuming that the image we applied morphing to is the source image, and the image we want to eventually generate is the destination image. Thus, the intensity of a pixel at (x, y) in frame n is indicated as:

$$g(x, y, n) = (\frac{N-n}{N-1}) f_s(x, y) + (\frac{n-1}{N-1}) f_d(x, y) \qquad (3.10)$$

However, this linear combination operation generally will not provide a smooth, organic transformation. With a source image which is considerably different from the destination image in terms of shape or size, the morphing result will be abrupt. In this case, the linear combination operation is usually used for a simple transformation between two similar statuses. We still need other techniques for complicated applications.

3.4.1 Mesh warping

In order to create a morphed image with a satisfyingly smooth effect which is still feasible, we use a mesh warping algorithm. In this technique, the features are identified by a series of control points.

Mesh warping is a two-pass algorithm that accepts a source image and two 2-D arrays of coordinates S and D. The source and target images are broken up into small regions, and then mesh warping maps the small regions from one image to the other. As shown in the figure below, the S coordinates are the control pixels in the source image. The D coordinates specify the location in the destination image to which the S coordinates map. For simplicity, we used the grid image to demonstrate the visual effects of mesh warping. It is applied with every cross point used as a control point. That is, in total, 30 control points. The intermediate image is generated based on the source image (a) and the destination image (b) and is really just a middle status transformed from one status to another. The final image is the source image warped by means of meshing S and D. The 2-D arrays in which the control points are stored impose a rectangular topology on the mesh. The only constraint is that the meshes defined by both arrays be topologically equivalent, i.e. no folding or discontinuities. Therefore the entries in D are coordinates that may wander as far from S as necessary, as long as they do not cause self-intersection.

The first pass is responsible for re-sampling each row independently. An intermediate array of points I, whose x coordinates are the same as those in D and whose y coordinates are the same as those in S, is created. Vertical splines are generated to fit each column of data in S and I. The data for each span (region) in a row is interpolated to create intermediate image I.

The second pass is responsible for re-sampling each column independently. Horizontal splines are generated to fit each row of data in arrays I and D. The data for each span (region) in a column is

interpolated from the intermediate image I to create the destination image D. The collection of vertical splines fitted through S and I in the first pass, along with the horizontal splines fitted through I and D in the second pass, are demonstrated. Below are the figures that illustrate the mesh warping.

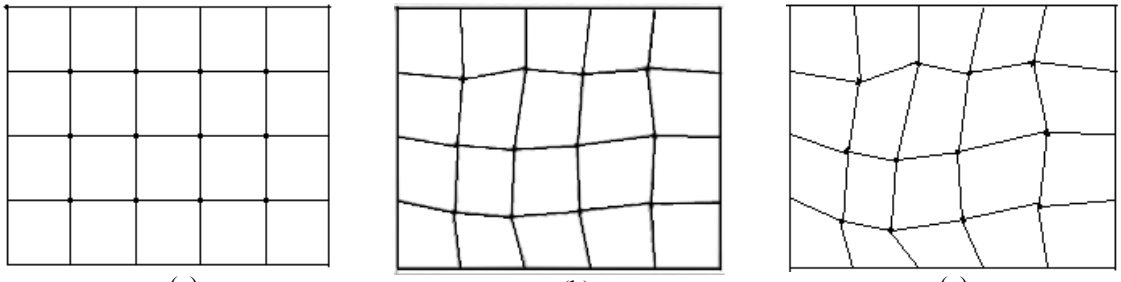

(a) (b) (c)

Figure 3.4 Mesh warping process: Generate the intermediate pixels based on the source and destination images. The grid image is used here to illustrate the idea of morphing with control points on every cross point on the image. (a) Source image. (b) Intermediate image. (c) Destination image.

Figure 3.5 Feature based image warping process: one defined relative to the source image, the other defined relative to the destination image. X is the pixel co-ordinate in the destination image and X' is the corresponding pixel co-ordinate in the source image, PQ is a line segment in the destination image, and P'Q' is the corresponding line segment in the source image. This is reproduced from (T.Beier, S.Neely 1992).

From the figure above, the mesh warping generates the pixels based on the source and destination images, the grid image is used to illustrate the idea of morphing with control points on every cross point on the image. The intermediate grid shows the transformation status between the two images. For this mesh warping, we select 6x5 control points, sometimes called the mesh node, as shown in Fig. 3.4. This mesh warping method needs the users to specify features by selecting the control points, which might be a time consuming process. The control points associated with the target features on the image may have an arbitrary structure. Generally speaking, the more control points that are applied, the more time it will need to process the warping and the smoother the visual transformation result will be. We will demonstrate the performance evaluation results in a later chapter.

3.4.2 Feature based image warping

Feature based image warping is used with a higher level of control over the process. The corresponding feature lines in the source and destination images are predefined for the morphing process. After that, this approach uses the lines to correlate features in the source image to features in the destination image. The relationship is based on the surrounding weight, which are the fields of influence surrounding the feature lines selected. The pixel in the destination image is estimated from corresponding pixels in the source image. Above is the figure that illustrates the mechanism of feature based image warping, a pair of lines here, one is defined relative to the source image, the other one is defined relative to the destination image, shows a mapping from one image to the other image. X is the pixel co-ordinate in the destination image and X' is the corresponding pixel co-ordinate in the source image, PQ is a line segment in the destination image and P'Q' is the corresponding line segment in the source image.

To perform the algorithm, the following parameters are calculated (T.Beier, S.Neely 1992):

$$u = \frac{(X - P) \cdot (Q - P)}{\|Q - P\|} \tag{3.11}$$

$$v = \frac{(X - P) \cdot Perpendicular(Q - P)}{\|Q - P\|} \tag{3.12}$$

$$X' = P' + u \cdot (Q' - P') + \frac{v \cdot Perpendicular(Q' - P')}{\|Q' - P'\|} \tag{3.13}$$

where X is the pixel co-ordinate in the destination image and X' is the corresponding pixel co-ordinate in the source image, PQ is a line segment in the destination image and P'Q' is the corresponding line segment in the source image. The perpendicular () returns the vector perpendicular to the input vector. Still, the perpendicular vector is the same length as the input vector. The value u is the position along the line, and v is the distance from the line. The value u goes from 0 to 1 as the pixel moves from P to Q, and is less than 0 or greater than 1 when outside that range. The value for v is the perpendicular distance in pixels from the line.

The algorithm can be described as follows:

```
WarpImage(SourceImage, L'[...], L[...])
begin
   for each destination pixel X do
      XSum = (0,0)
      WeightSum = 0
      for each line L[i] in destination do
         X'[i] = X transformed by (L[i], L'[i])
         weight[i] = weight assigned to X'[i]
         Xsum = Xsum + X'[i] × weight[i]
         WeightSum += weight[i]
      end
      X' = XSum/WeightSum
      DestinaitonImage(X) = SourceImage(X')
   end
   return Destination
end
```

Figure **3.6** Feature based image warping algorithm pseudo code. It is used to compute the corresponding pixel position of the source image to the destination image. This figure was reproduced from (Varshney, 2005).

From this approach, we find out that the algorithm transforms each pixel coordinate by a rotation, translation, and/or a scale. Through this, it transforms the entire image. These figures and description are used to show the case of a single feature line for simplicity. Usually, multiple feature lines are needed for most morphing applications.

After describing the case of a single feature line, we will briefly show the case of multiple pairs of lines for a complex transformation. For this approach, a weighting of the coordinate transformations for each line is performed. A position X_i' is calculated for each pair of lines. The displacement $D_i = X_i' - X$ is the difference between the pixel location in the source and destination images, and a weighted average of those displacements is calculated. The weight is determined by the distance from X to the line, and the average displacement is added to the current pixel location X to determine the position X' to the sample in the source image. The single line case falls out as a special case of the multiple line case, assuming the weight never goes to zero within in the image. The weight assigned to each line should be strongest when the pixel is exactly on the line and weaker the further the pixel is from the line. The equation for the weight is:

$$weight = \left(\frac{length^p}{(a + dist)} \right)^b \qquad (1.14)$$

Where *length* is the length of a line, *dist* is the distance from the pixel to the line, and a, b, and p are constants that can be used to change the relative effect of the lines. The displacement of a point in the source image is then actually a weighted sum of the mappings due to each line pair, with the weight related

to distance and line length. The parameter a is used to specify where the pixels on the line will go. With a larger value a, it will generate a smoother warping with less precise control. The variable b determines how the relative strength of the different lines falls off with distances (T.Beier and S.Neely 1992). If it is large, then every pixel will be affected only by the line nearest it. If it is zero, then every pixel will be affected by all lines equally, in other words, all lines have the same weight. The weight assigned to each line should be highest when the pixel is exactly on the line and should be lower when the pixel is further from the line.

Compared with mesh warping, the feature-based image warping is more computationally expensive. However, it provides a higher degree of speed and control for the user to manipulate the transformation. Because it is global, all line segments need to be referenced for every pixel (T.Beier, S.Neely 1992). Additionally, the feature-based approach needs to select the control points to manipulate the transformation as compared with the mesh warping technique. Every control point has the same impact as the others.

Thus far, we have introduced mesh warping and feature based image morphing. Having explained these theories in this chapter, we next demonstrate the theory of implementing several approaches in a multi-sensor image fusion system.

4 Image Fusion Implementation and Experimental Result

The previous section described the theoretical formulation of segment fusion and weighted average fusion. In this section, simple examples are implemented using segment-based fusion (SF) and weighted average fusion (WAF) for better illustration. In this chapter, we will demonstrate the implementation of the discussed image fusion algorithms in Chapter 3. We begin in Section 4.1 by describing the graphical user interface in terms of functionality and usage. Then, we demonstrate the results of these algorithms using elementary images in Section 4.2. Additionally, we present real world deployment results in Section 4.3 regarding multi-sensor image fusion and experiments including thermal and color image fusion, aerial and satellite image fusion, multi-sensor image fusion based on LMS-Z210 system, and morphing using urban images.

4.1 Graphical user interface

A Graphic User Interface (GUI) is a program interface item that allows people to interact with the programs in more ways than just typing commands. It offers graphical icons, and a visual indicator, as opposed to text-based interfaces, typed command labels, or text navigation, to fully represent the information and actions available to users. The GUI is introduced in reaction to the steep learning curve of command-line interfaces. When comparing command-line interfaces, a GUI is used to enhance the efficiency and ease of user. Well-designed graphical user interfaces can free the user from understanding intricate theories, learning complex command languages, and implementing complicated algorithms. In other words, user-friendliness and usefulness for the user can help to achieve the transparency necessary to understand the program.

For evaluation purposes, the implementation of these algorithms is completed using C++ together with an open source library, the OpenCV library. We develop the Graphical User Interface in Microsoft Visual Studio 2005 with a Microsoft Foundation Classes (MFC) console application in a Windows XP environment. The GUI provides zoom in and out control to analyze detail about the output image, information dialog to examine the pixel value and to coordinate the gray-scale view and color coding view to provide an alternative perspective. Besides the basic functions of loading and saving images, the GUI also provides an interactive initial parameter setting which allows the user to assign the values of k_1, k_2, k_3, and their respective weights. Finally, the function to show computation progress and runtime is added for additional performance evaluations.

Fig.2.1 shows the graphic user interface window boxes which illustrate a sample of input images. A user can import the image, using the formats JPEG, BMP, PNG, and TIFF, from the load image button on the

upper left corner of GUI. Using the slide bar in the middle, a user can initialize the k_1, k_2, k_3 parameters for Segmentation-based and Segment Weighted Average image fusion. Considering the potential large size of the loaded image, a wide range [1, 1,024] of parameter for k is provided for flexibility purposes.

The Image Fusion GUI is intended to perform fusion of two or three source images using the methods studied in this research in a user friendly environment. First, all the images can be selected by clicking the Load Image button on the upper left corner. A dialog screen will appear to allow the user to select the source image, as shown in Fig.4.2, which can be any of the file formats in Table 4.1.

From the above figure, we can see that our GUI support the most commonly used image formats. They are built in to the support images from the various types of sensors for multi-sensor image fusion. As usually used in computing, the JPEG format is a commonly used method of lossy compression for photographic images. The degree of compression can be adjusted, allowing an acceptable tradeoff between image quality and storage size. Nearly every digital camera can save images in the JPEG format, which supports 8 bits per color (red, green, and blue) for a 24-bit total, producing relatively small files. TIFF is a flexible file format that normally saves 8 bits or 16 bits per color (red, green, and blue) for 24-bit and 48-bit totals, respectively, for TIFF and the TIF filename extensions. It is used to contain handling images and data within a single file, which include the header tags (size, definition, image-data arrangement, applied image compression, time and data, shutter speed, exposure, name of camera, and color information). GIF is limited to an 8-bit palette, or 256 colors, which makes the GIF format suitable for storing graphics with relatively few colors such as simple diagrams, shapes, logos, and cartoon style images. The GIF format supports animation and is still widely used to provide image animation effects. BMP, also known as bitmap, is used to store bitmap especially on Microsoft Windows and OS/2 operation systems. While BMP files are usually large and uncompressed, it has the advantages of simplicity and wide acceptance in Windows programs. PPM and PGM image file formats were originally designed to be easily exchanged between platforms. When using the binary formats, PGM uses 8 bits per pixel, and PPM uses 24 bits per pixel with 8 pixels for each red, green, and blue channel.

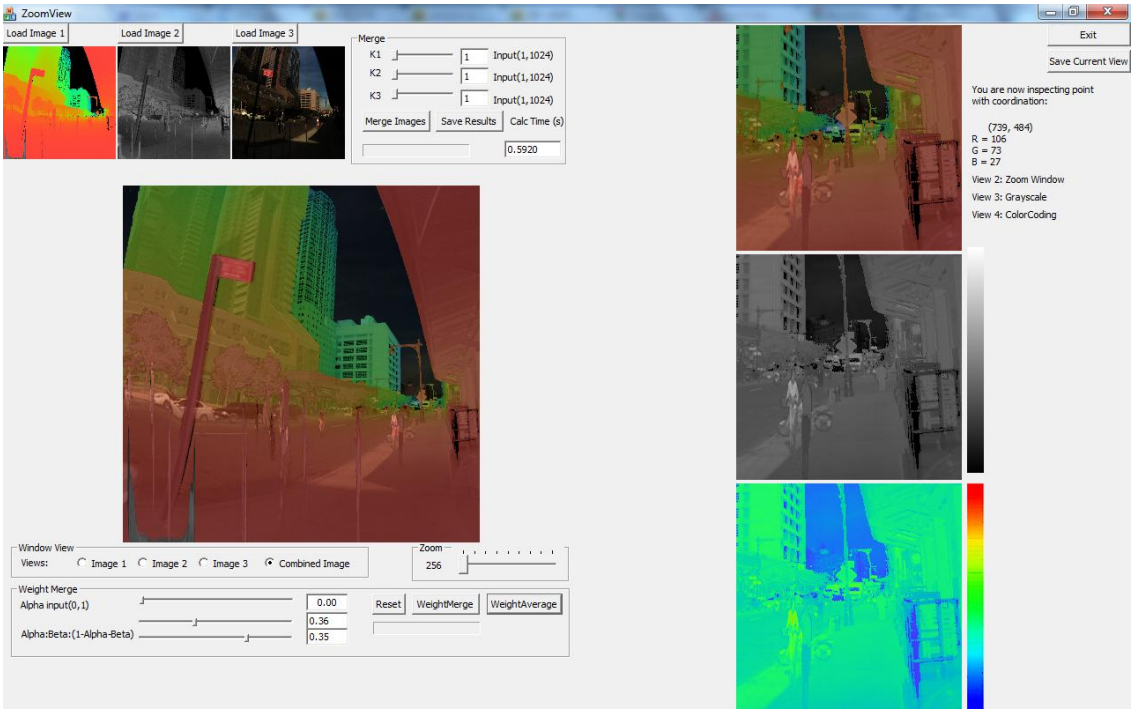

(a) Overall layout

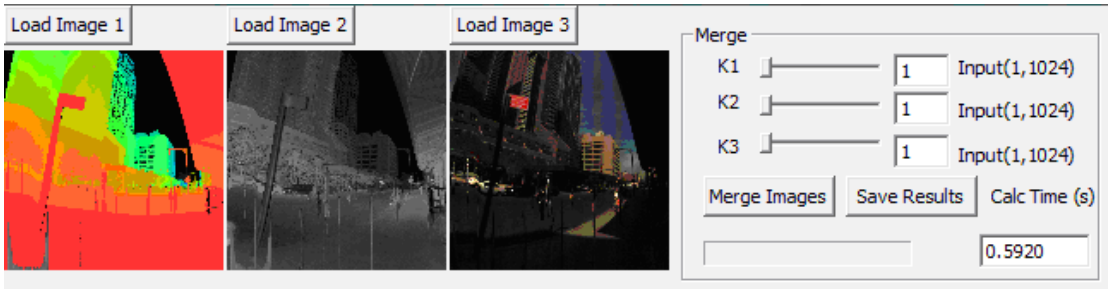

(b) Image loader and segment fusion function group

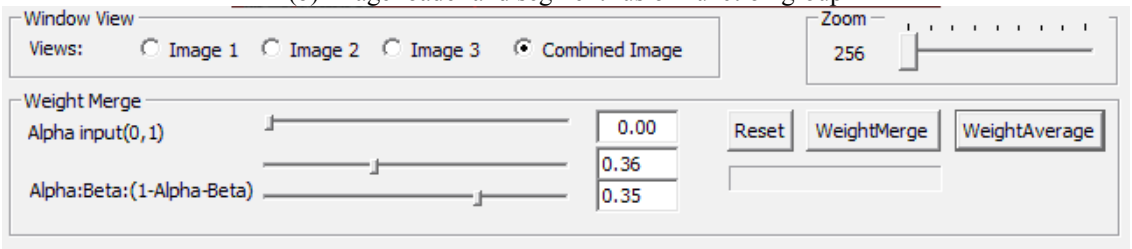

(c) window view function, zoom function and, segment weight average function group

Figure 4.1 Screenshot of the Pixel-Based Image Fusion Graphical User Interface. The left layout is used for the basic image fusion function, and the right layout is used for visual evaluation. (a) Overall layout, (b) Image loader and segment fusion function group, (c) window view function, zoom function and segment weight average function group

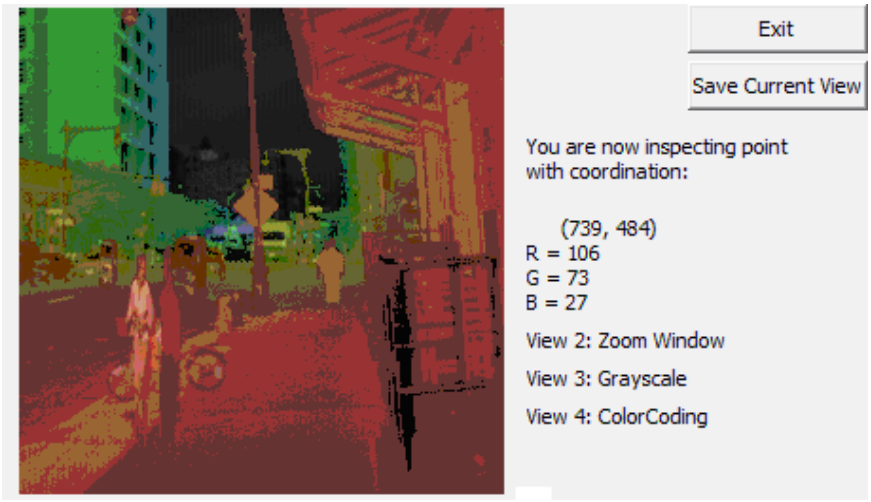

(d) zoom in information window group

Figure 4.1 (continued) Screenshot of the Pixel-Based Image Fusion Graphical User Interface. The left layout is used for the basic image fusion function, and the right layout is used for visual evaluation. (a) Overall layout, (b) Image loader and segment fusion function group, (c) window view function, zoom function and segment weight average function group, and (d) zoom in the information window group.

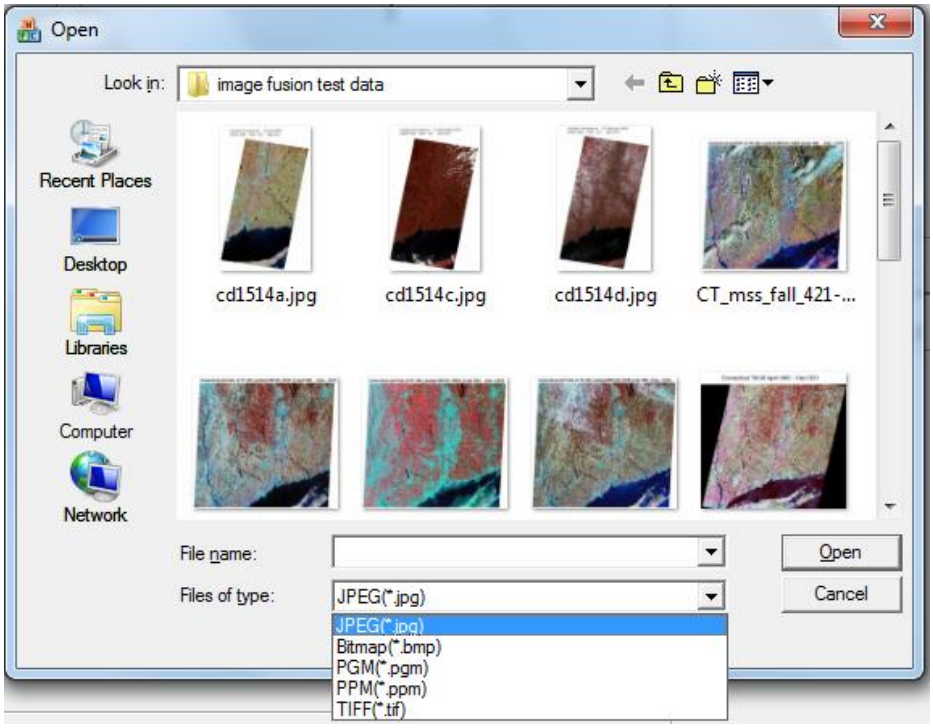

Figure 4.2 Screenshot of the Pixel-Based Image Fusion Graphical User Interface, with Load Image Dialog; by selecting the files in the type section, we can upload various image formats to the Graphical User Interface.

Table 4.1 File format type and respective information that can be loaded into the graphical user interface. Formats include JPEG, TIFF, GIF, Bitmap, PGM, and PPM.

File Extension	Abbreviation	Full Name	Compression
„jpg' or „jpeg'	JPEG	Joint Photographic Experts Group	Loss
„tif' or „tiff'	TIFF	Tagged Image File Format	Lossless/ Loss
„gif'	GIF	Graphics Interchange Format	Lossless
„bmp' or 'dib'	Bitmap	Window Bitmap image	Lossless
„pgm'	PGM	Portable Gray Map	Lossless
„ppm'	PPM	Portable Pixel Map	Lossless

After loading the images into the GUI, we can setup the parameters by using either the control edit box or slide bar. A two image fusion can be set up by loading only two images at the first two dialogs and setting $k_1 = 1,\ k_2 = 1,\ k_3 = 0$, while a three image fusion can be achieved by loading all three dialogs and setting k_1, k_2, k_3 as none-zero values. Notice that these three input parameters can be an integer and range from 0 to 1,024 to control the slice width for image fusion.

By clicking the "Merge Images" button, we can apply segment-based image fusion on the selected images. The progress bar nearby will display the time for the computational progress. When the computation is complete, the text box "Calc Time" on the right shows the computation time in seconds. Meanwhile, the resulting image is displayed in the left center window. We can also switch the view of the left center window by selecting the corresponding radio button on the bottom of the window from image 1, image 2, image 3, or the combined image. When one of the radio buttons is selected, the other round buttons in the group are empty; this is described as a mutually exclusive feature. The button "Save Results" is available whenever you want to save a fused image. The JPEG and BMP image formats support the save function.

For the functionality of weighted image fusion, we can use the control in the "Weight Merge" group on the bottom. If we want to apply the segment weighted average image fusion, other than setting up the k_1, k_2, k_3 parameter, we need to set up the alpha value and initial the parameter k_3 as zero when fusing two images together. The alpha and beta values are both needed and can be set up using the slide bar as in the case of the three image fusion. The alpha and beta values can be set up either by using the slide bar control or by using the text edit box on the right. The "Reset" button is used to reset the alpha and beta values to an initial value of 0.33 so that $\alpha = \beta = 1 - \alpha - \beta$, approximately. After setting up the parameters, we can click on the button "Weight Merge" to deploy segmented weighted average image fusion. The button "Weighted Average" is used to simply apply the weighted average fusion algorithm. In that case, only the alpha and beta values take effect, parameterS k_1, k_2, k_3 do not contribute to the algorithm.

The 256x256 window with the gray scale and color coding views on the right column can be activated by double clicking on the area of interest in the center window. The pixels value and coordinates will show up when pointing at the pixel on the 256x256 window. The slider control editor, beneath the window, is used to zoom in and zoom out by scaling the displayed resolution. The button "Save Current View" is used to clip the interested 256x256 area and save it in the JPEG format. The gray scale and color coding views show the pixels' values in a black-gray-white and green-yellow-red scale. Grayscale images, also called monochromatic, have many shades of gray, varying from black at the weakest intensity to white at the strongest.

4.2 Test of image fusion algorithm using elementary images

The above section describes the graphical user interface we developed for image fusion; we further test the pixel-level image fusion algorithm using the elementary images in Figure 4.3. We show the elementary images with characters A, B, and C and fuse them using our proposed approach. Visually, we are able to see that how our approach has segmented and combined them together.

As you can see from the Fig. 4.3 (a) - (c), these 3 input images are JPEG images that consist of characters A, B, and C with red (255, 0, 0), green (0, 255, 0), and blue (0, 0, 255), respectively. Each color image is registered to 1,000 pixels by 1,000 pixels. The objective of using these test images is to make it simple to analyze the effects of the image fusion algorithm while verifying the run time efficiency and computational boundary.

Fig. 4.3(e), Fig. 4.3(f), and Fig. 4.3(g) are zoom in views of the SF fused image with a size of 255 by 255 pixels. They are truncated from the same position, which is the small square frame area, of the resulting image and are used for comparison. It can be observed that the red component repeats the slice 3 times in the horizontal direction while for the green component it is repeated 2 times, and only once for the blue component. Additionally, the interpolation calculates 5 pixels between the 2 existing pixels vertically. It keeps the same aspect ratio with the source image, yet does not reduce the sharpness noticeably. The gray scale image and pseudo-color image provide information from another perspective. The legend is labeled on the right side for the viewer's perusal, as illustrated in Fig. 4.3(f) and Fig. 4.3(g)

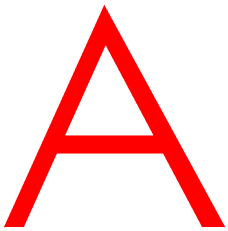

(a) Test Image A

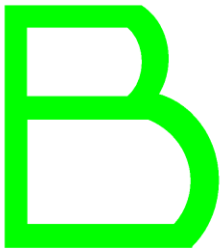

(b) Test Image B

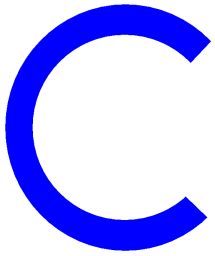

(c) Test Image C

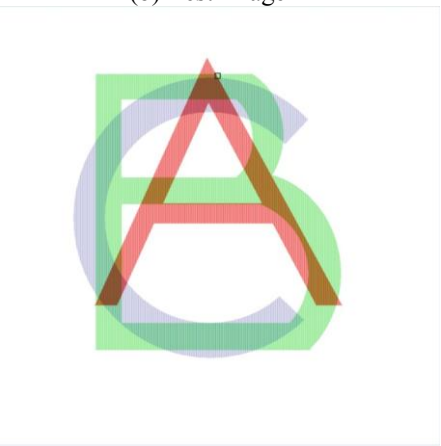

(d) k_1 =3, k_2 = 2, and k_3 =1 SF

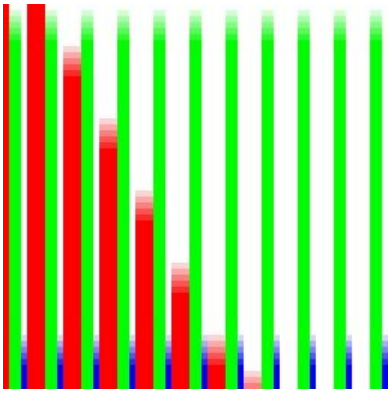

(e) Zoom In View of the Output Image SF

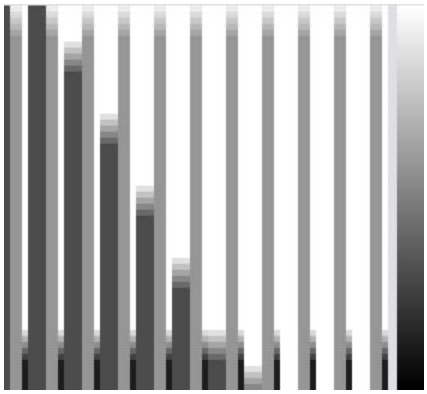

(f) Gray Scale of the Zoom in View SF

Figure 4.3 Test Image and Results of Segmentation-based Fusion and Weighted Average Fusion. Results are shown in the true color mode, gray scale mode, and pseudo-color coding scale mode. The slice width of each component is controlled by its respective parameters. . The gradual change in the vertical direction is generated by the interpolation. . (a) Test Image A, (b) Test Image B, (c) Test Image C, (d) k_1 =3, k_2 = 2, and k_3 =1 SF, (e) Zoom In View of the Output Image SF, (f) Gray Scale of the Zoom in View SF

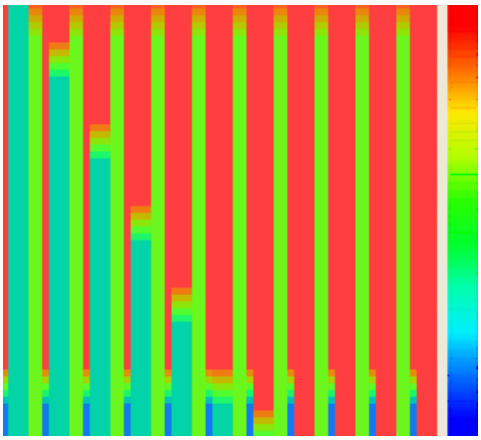

(g) Pseudo-color of the Zoom in View SF

Figure 4.3 (continued) Test Image and Results of Segmentation-based Fusion and Weighted Average Fusion. Results are shown in the true color mode, gray scale mode, and pseudo-color coding scale mode. The slice width of each component is controlled by its respective parameters. The gradual change in the vertical direction is generated by the interpolation. (a) Test Image A, (b) Test Image B, (c) Test Image C, (d) k_1 =3, k_2 = 2, and k_3 =1 SF, (e) Zoom In View of the Output Image SF, (f) Gray Scale of the Zoom in View SF, and (g) Pseudo-color of the Zoom in View SF.

Fig. 4.3(d) shows the fusion results from the SF method with $k_1 = 3, k_2 = 2, k_3 = 1$. The image size is grown from 1,000 by 1,000 pixels to 6,000 by 6,000 pixels. Although the shrunken image size shown in Fig. 2(d) makes the slice and interpolation harder to recognize, one can still notice that the red plane with symbol A is more easily observed than symbols B and C. Additionally, the blue C symbol is harder to perceive than symbols A and B because of the low slice repetitions.

Fig.4.5 (a) shows the results of segment weighted average fusion with size 6,000 pixels by 6,000 pixels, given the initial parameters $k_1 = 1, k_2 = 3, k_3 = 2$, α = 0.37, and β = 0.34 . Because the alpha value is the maximum of $\{\alpha, \beta, 1-\alpha-\beta\}$, the green and blue components are degraded. Only the red component is the "true color", that is to say, the red component has the same intensity value as the original source image. As a result, the green "B" character on the resulting image is more obvious than the other two characters. Compared with the results from SF in Fig.2, it can be seen that the overall image result is grayer than the SF result, which is due to intensity shifting from the weight parameters of $\{\alpha, \beta, 1-\alpha-\beta\}$.

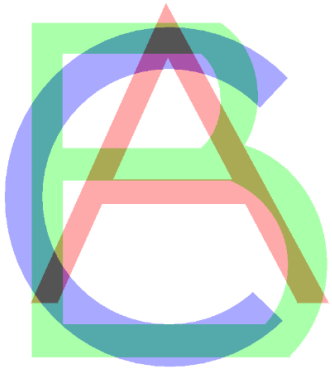

(h) Result of weighted average fusion WA $\alpha = 0.33,\ \beta = 0.33$

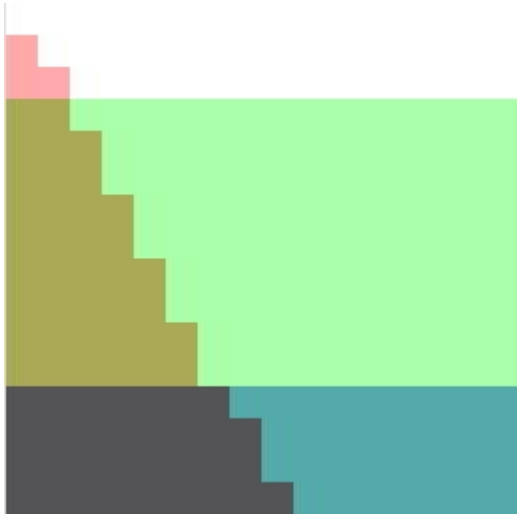

(i) Zoom In View WA, $\alpha = 0.33,\ \beta = 0.33$

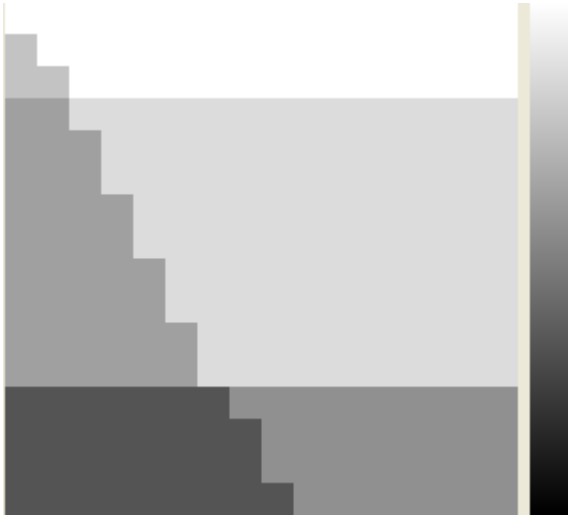

(j) Gray Scale Zoom In View WA, $\alpha = 0.33,\ \beta = 0.33$

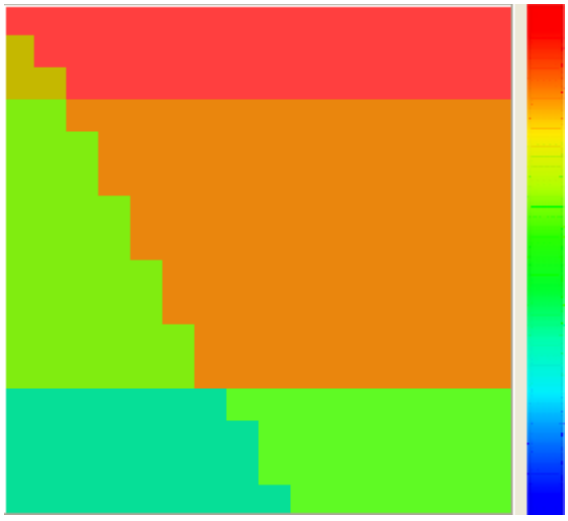

(k) Pseudo-color of the Zoom In View WA, $\alpha = 0.33,\ \beta = 0.33$

Figure 4.4 Test Image and Results of Segmentation-based Fusion and Weighted Average Fusion (continued). Results are shown in the true color mode, gray scale mode, and pseudo-color coding scale mode. (h) Result of weighted average fusion (WA), $\alpha = 0.33,\ \beta = 0.33$, (i) Zoom In View WA, $\alpha = 0.33,\ \beta = 0.33$, (j) Gray Scale Zoom In View WA, $\alpha = 0.33,\ \beta = 0.33$, and (k) Pseudo-color of the Zoom In View WA, $\alpha = 0.33,\ \beta = 0.33$.

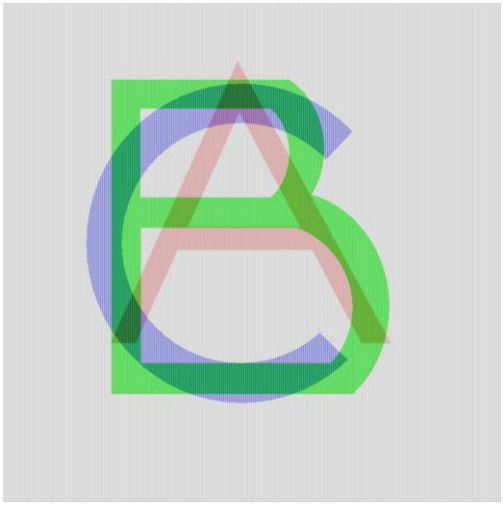

(a) Result of segment weighted average fusion (SWAF) k_1=1, k_2 = 3, k_3 =2 , α = 0.37, β = 0.34

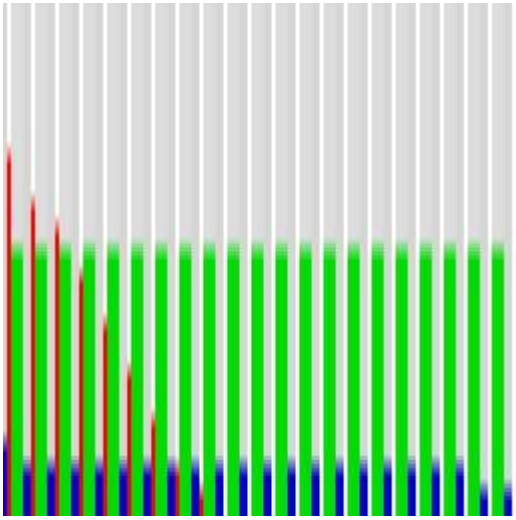

(b)) Zoom in view of SWFA

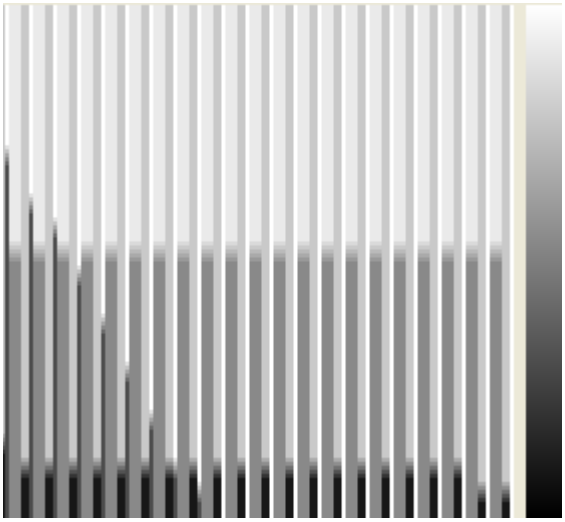

(c) Zoom in gray scale view

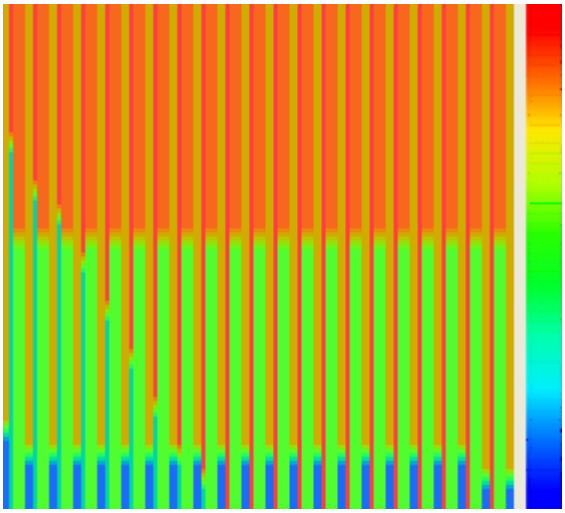

(d) Zoom in pseudo-color view

Figure 4.5 Results of the segment weighted average fusion (SWAF). Results are shown in the true color mode, gray scale mode, and pseudo-color coding scale mode. The slice width of each component is controlled by its respective parameters. The gradual change in the vertical direction is generated by the interpolation. The intensity values of each component are controlled by $\{\alpha, \beta, 1-\alpha-\beta\}$, (a) Result of segment weighted average fusion (SWAF), k_1=1, k_2 = 3, k_3 =2 , α = 0.37, β = 0.34, (b) Zoom in view of SWFA, (c) Zoom in gray scale view, and (d) Zoom in pseudo-color view.

We have tried to illustrate these elementary situations in order to explain the algorithm mechanism at the pixel level. Our approach tries to make the image fusion system guide the user to capture more information and make identification of the object simpler. In the following section, we will continue exploring the algorithm's application with a variety of examples including thermal image and color image fusion, aerial

and satellite image fusion, multi-sensor LMS-Z210 with range image sensor, reflectance image sensor, and CCD color image sensor.

4.3 Test of image fusion algorithm using multi-sensor data integration

There are considerable application areas which utilize image fusion, for example, in the aerial and satellite imaging field, maps, panchromatic images and multispectral images are merged together to provide comprehensive information. In a surveillance system, CCD images, range images, and infrared images are fused together to provide an overview of all weather conditions. In medical imaging, the magnetic resonance image (MRI), computed tomography (CT), and positron emission tomography (PET) are integrated in order to support accurate medical diagnosis and treatment.

4.3.1 Thermal image and color image fusion

As shown in the below figure, gray level and color image fusion schemes are tested for fusing intensified visual and thermal images for scene recognition and perception. With a larger weight applied to the thermal image, the results will represent more information about the thermal image. On the other side, a larger weight to the true color image will result in an image that contains more information from a CCD true color information perspective.

Surveillance and security systems that employ multiple image modalities continue to receive great attention, and it is becoming clear that fusion can significantly improve the overall system performance. Three contributions in our method can apply to surveillance and security system applications. In this section, we provide experiments that indicate that a fused image provides a better representation of the spatial layout of the scene. Therefore, gray level and color image fusion schemes are tested for fusing intensified visual and thermal imagery for global scene recognition and perception. The appropriate use of color information will greatly increase the operator’s situational awareness for a given condition and task.

(a) Face Image from CCD Camera

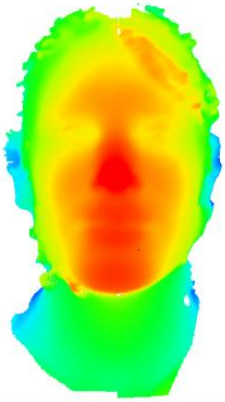

(b) Face Image from Range Sensor

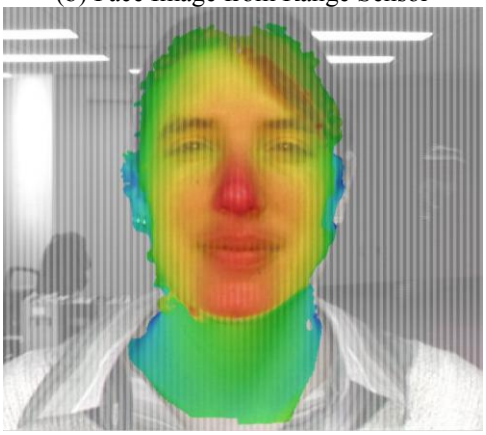

(c) Segmented Fused Image from CCD Camera Image and Range Sensor Image, $k_1 = 1, k_2 = 1$

Figure 4.6 The Test on Human Face Image Fusion from a CCD Camera and Range Sensor. (Original image is from the image database of the Imaging, Robotics and Intelligent Systems (IRIS) Laboratory at the University of Tennessee, Knoxville) (a) Face Image from CCD Camera, (b) Face Image from Range Sensor, and (c) Segmented Fused Image from CCD Camera Image and Range Sensor Image, $k_1 = 1, k_2 = 1$

4.3.2 Aerial and satellite image fusion

In this section, we will discuss tests on aerial and satellite image fusion. It is already known that the image fusion algorithm's performance is application dependent, so for the application of a multi-sensor image fusion system, especially using aerial and satellite image fusion, we will show test results to demonstrate the fusion performance.

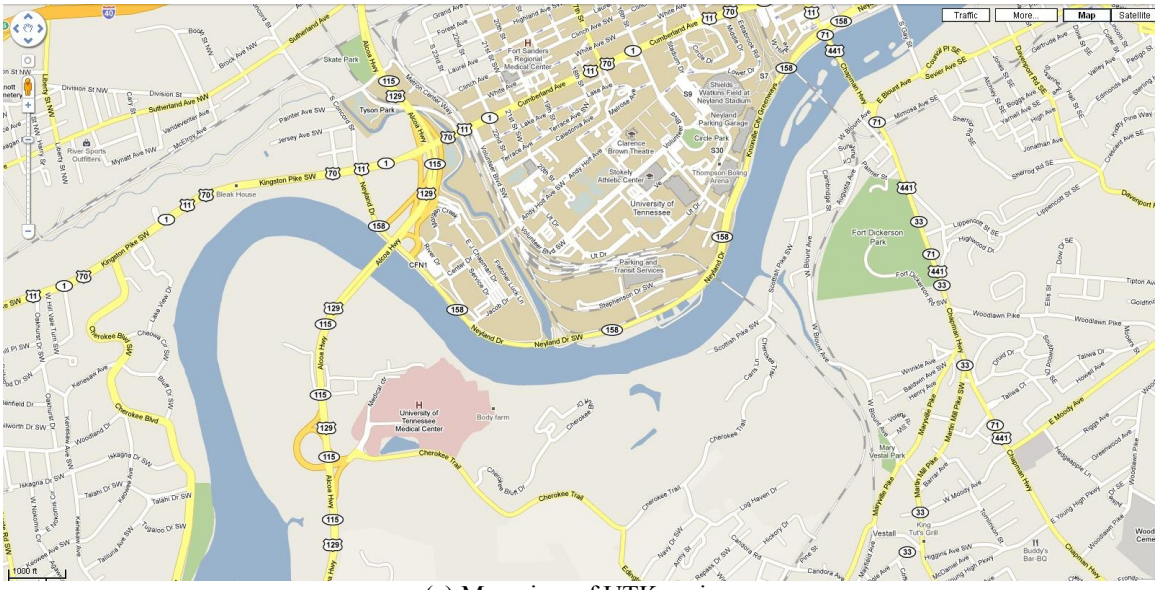

(a) Map view of UTK region

(b) satellite image view

Figure 4.7 Image fusion of aerial and satellite imaging, in the region of Knoxville, TN. (a) Map view of UTK region and (b) satellite image view. Image source: http://maps.google.com.

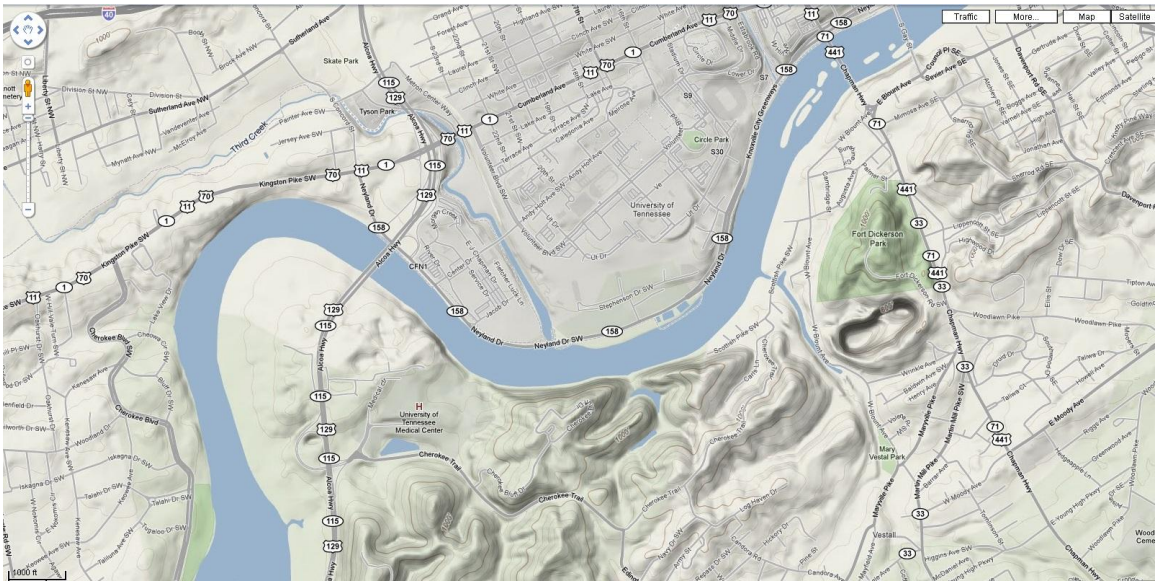

(a) terrain image view

(b) Segment fusion for aerial and satellite image SF result of satellite image $k_1 = 1, k_2 = 2,$ *and* $k_3 = 1$

Figure 4.8 (a) Terrain image of UTK region (source image 3 for fusion) and (b) Segment fusion for aerial and satellite image SF result of satellite image $k_1 = 1, k_2 = 2,$ *and* $k_3 = 1$.

Figure 4.9 Segment fusion for aerial and satellite image. A portion of the zoom in the view is a fused image with parameters, $k_1 = 1, k_2 = 2, k_3 = 1$.

In Fig. 4.7 and Fig. 4.8, we use the images from Google map for aerial and satellite image fusion, 3 source images for the map, satellite, and terrain images are registered. The map shows a visual representation of an area with special highlighting on the road. The satellite image shows the visible colors and detail outline of objects such as the building, forest, river, and lakes. The terrain image provides more relief information. With the help of elevation intensity, it generates three dimensional results. The lightness and darkness shows the elevation change in the mountain, valley, and riverside areas. After the SF image fusion, the result provides more comprehensive information. The legend, road tag, name of region, and elevation is displayed. Although it is not sharp and high defined when you zoom in on the results shown in Fig. 4.9, it can be improved using image enhancement techniques afterward. Still, with a wide range of parameter selections, the fusion provides results with different emphasis on the map, terrain, and satellite images.

4.3.3 Multi-sensor image fusion based on LMS-Z210 system

In addition to the applications we tested in the above section, we would also like to implement some experiments based on multi-sensor systems for security and surveillance. As we know, sensors are widely used to enhance our ability to monitor our surroundings. We will use the LMS-Z210 system to test and evaluate our approach using range sensors, reflectance sensors, and a true color visual camera. However, the sensors used in the real world are not limited to only these sensors, sensors such as infrared cameras

(IR), millimeter wave (MMW) cameras, X-ray imager, and thermal sensors, are also used to provide different types of information.

Our proposed idea to increase the reliability of the fundamental matrix is by generating an uncertainty model in a space-ergodic sense. We excite the random solver with spatially different correspondence data generated by different interest point detectors to generate the ensemble uncertainty samples. Our method then tries to compensate for the deficiencies (uncertainty) in a time-stationary sense with space-ergodicity (and vice versa) with the objective of reducing the total uncertainty of the fundamental matrix.

The multi-sensor image data used here is generated from the Laser Mirror Scanner Z210, and produced by Riegl laser measurement systems. As shown in the below figures, the 3D-terrrestrial laser mirror scanner LMS-Z210 is a surface imaging system based upon accurate distance measurements by means of electro-optical range measurement and a two axis beam scanning mechanism. It provides a unique combination of wide field-of-view, high accuracy, and fast data acquisition. The 3D images are acquired by performing a number of independent laser range measurements in different, but well-defined angular directions. The LMS-Z210 is supported by software for performing scans over a 360 degraded range on the horizontal plane and an 80 degree range on the vertical plane. The laser sensor, which has a maximum laser plus 20,000 points/sec, is able to resolve objects with 80% reflectivity up to 650mm away.

The LMS sensors are designed for surveying tasks, allowing the user to measure the distance to several points along a surface. These sensors are mounted on highly accurate pan tilt units that allow back calculation of the position of the object being measured. They scan a beam along two axes over any field of view. Using a high speed-rotating mirror to direct the laser beam over a precise pattern allows accurate three-dimensional scanning of the surface.

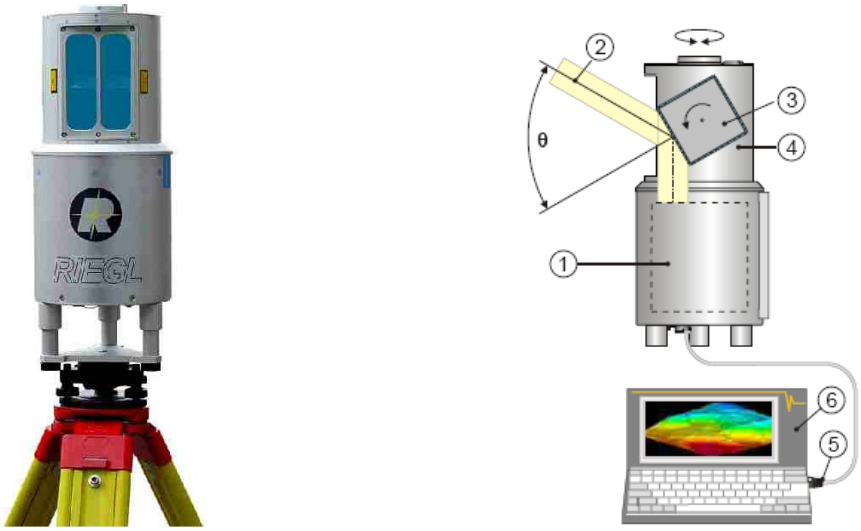

(a) (b)

Figure 4.10 (a) 3D Terrestrial Laser Mirror Scanner System Z210 (b) sketch map of LMS Z210 connected with computer for scanner operation. (1) Range finder electronics, (2) laser beam, (3) polygon, (4) optical head, (5) TCP/IP Ethernet interface, and (6) laptop. Image originally from the Riegl laser measurement systems manual.

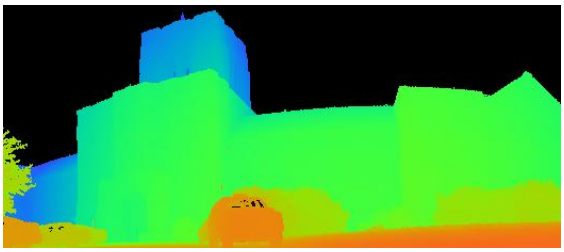

(a) Riegl LMS-Z210 Range Data

(b) Reflectance image of the Ayres building

(c) True color image of the Ayres building

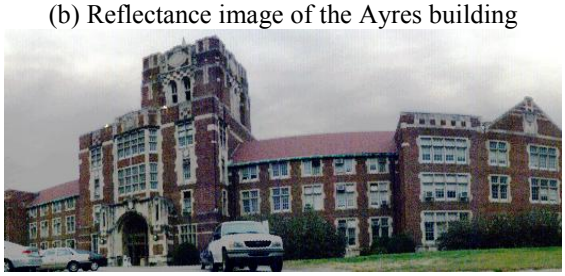

(d) Preprocessed of (c) using histogram equalization

Figure 4.11 Pseudo colored range image of the Ayres building IRIS Lab, University of Tennessee, Knoxville, from (a) Riegl LMS-Z210 Range Data, (b) Reflectance image of Ayres building, (c) True color image of Ayres building, and (d) Preprocessing of (c) using histogram equalization.

We document our experiments in the following paragraphs of this section. In order to show the multi-sensor image fusion system application, we deploy a prototype using the Laser Mirror Scanner Z210 to acquire the outdoor scene data. The LMS Z210 system is capable of capturing data under various situations in terms of brightness and distance. We show the test area chosen for our rigorous evaluation in the above figures. The images above show the Ayres Hall building at the University of Tennessee, Knoxville.

Because of the dark light near the Ayres building, the true color image appeared to be black with low contrast. In order to provide better visual results for the observer, we use the histogram equalization method to preprocess these low contrast images. The histogram equalization method increases the global contrast by effectively disseminating the most frequent intensity values. This method is utilized because it is a fairly straightforward technique and is not computationally intensive. Although the preprocessing introduces a small amount of distortion which produces unrealistic effects, it does improve the contrast and reveal the contour of object. We now can identify the cars, brushwood, and grass in front of the building, the arc shaped gate, and air-conditioners in the windows. In image fusion applications where spatial correlation is more important than the intensity of the signal, the image processed by the histogram equalization method provides better detestability of the objects.

The range sensor data provides meaningful information about the Ayres building by labeling the observed object surface with various colors, with red for the minimum range, green for the moderate range, and blue for the maximum range. With assistance from the range image, we can perceive the "depth" of the respective object by comparing the color with its color scale indicator. However, information such as gray intensity, detailed textile, and edge are not contained in the range data.

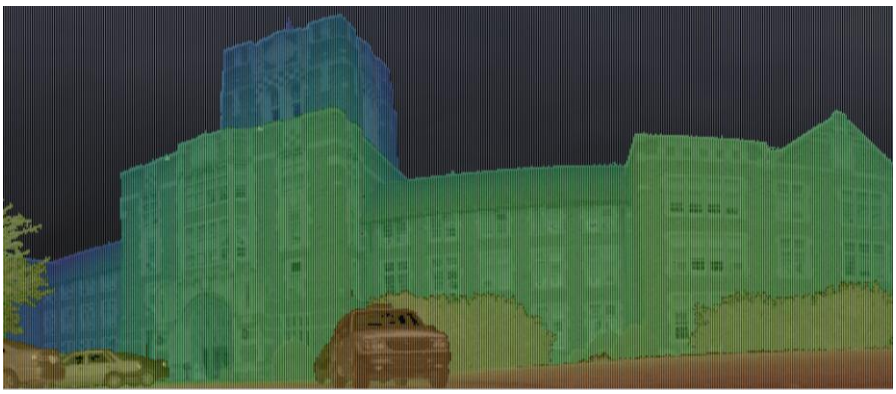

(a) $k_1 = 1, k_2 = 1, k_3 = 1$ Result of segment based fusion (SF) of the Ayres building

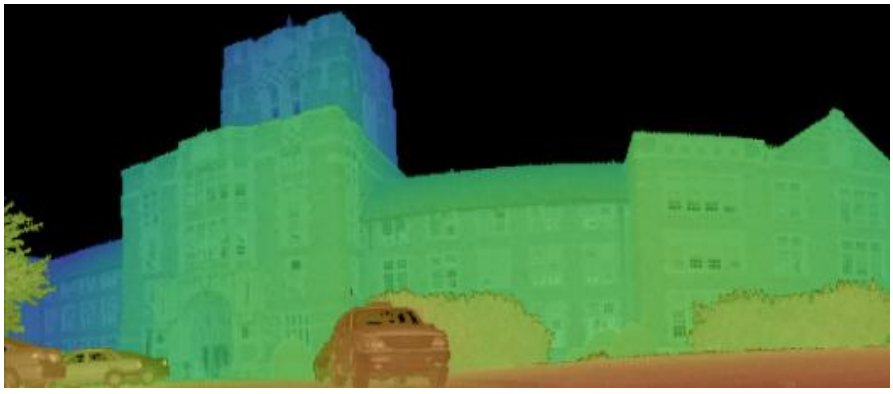

(b) $k_1 = 3, k_2 = 1, k_3 = 1$ Result of segment based fusion (SF) of the Ayres building

(c) $k_1 = 1, k_2 = 1, k_3 = 3$ Result of segment based fusion (SF) of the Ayres building

Figure 4.12 Image fusion data from the multi-sensors data from the Riegl LMS-Z210 system. (a) $k_1 = 1, k_2 = 1, k_3 = 3$, result of segment based fusion (SF) of the Ayres building and (b) Image morphing of the

Ayres building, generated from Fanta morph 0.55 transformation frame from range image to reflectance image $k_1 = 3, k_2 = 1, k_3 = 1$.

Figure 4.11 (b) illustrates the registered reflectance image of the Ayres building. The reflectance image is measured by the power of the reflected beam. Compared with the range data, the reflectance image contains rich textile and edge information. Still, it lacks the true color information of red, green, and blue, and only consists of gray values in the pixels.

Figure 4.11(c) demonstrates the registered true color image from the CCD image sensor. The majority of the surface was too dark to be recognizing because of the shadows. Still, the surface color, pixel values (red, green, and blue), and luminance are unique when compared with the other two images. Figure 4.12(a) indicates that with $k_1 = 3, k_2 = 1, k_3 = 1$ the segment fusion algorithm improves the range data visualization and rationally decreases the content from the reflectance and true color images.

We propose a statistical procedure for uncertainty management when dealing with images from a calibrated camera in pose recovery using the fundamental matrix. We demonstrate results on pose recovery for navigation applications in indoor and outdoor environments. Our method reduces the uncertainty in the convergence of the parameters in the fundamental matrix with the uncertainty of the model itself. The different models generated in the hypothesis-test framework of pose recovery provide statistics for the confidence in the matches while the models generated by different feature detectors provide the statistics for quantifying the uncertainty in the model. By combining both uncertainties, we have formulated a generic scheme using model selection theory that will help us choose methods for reliable estimation of the fundamental matrix while at the same time acting as a performance measure of pose recovery using image features.

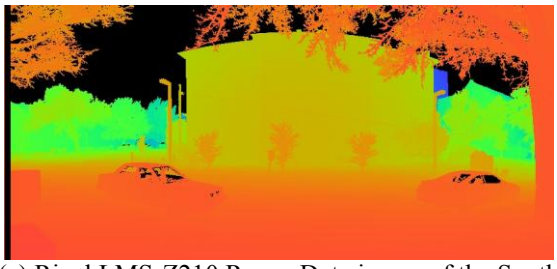

(a) Riegl LMS-Z210 Range Data image of the South College building

(b) Reflectance image of South College building

(c) True color image of South College building

(d) Preprocessed of (c) using histogram equalization

Figure 4.13 Pseudo colored range image of the South College building, from (a) Riegl LMS-Z210 Range Data. (b) Reflectance image of South College building, (c) True color image of South College building, and (d) Preprocessed of (c) using histogram equalization.

Figure 4.14 $k_1 = 1, k_2 = 2,$ *and* $k_3 = 1$ Results of segment based fusion (SF) of the South College building.

The advantage of this type of image fusion is that the image can be viewed properly when the output image is shrunk to an appropriate size, which is usually the same size as the window. By doing this, the discontinuities created by the SWA and SF methods will be concealed. Despite the size of the output image, the algorithm will guide the user into manipulating a wide degree of results within the parameters selected.

We have also used the image data of Franklin Greenwich to illustrate the visual effects of image fusion. From Fig. 4.15, we can see that the range image provides distance information for the guidepost that is nearby, as well as trees and buildings in the distance. Because of the low contrast of the reflectance and true color images, we deploy the histogram equalization method to preprocess them. The preprocessed images are shown in Figs. 4.15(c), and (e), respectively, and are brighter and have a higher contrast than the non-preprocessed images. Note also that the people on the pedestrian walkway and the vehicle on the road are distorted, seemingly shrunk in the horizontal direction. That is because of the LMS system scan image in the horizontal way with a low scanning speed compared with the moving objects. The results of the SF images displayed generate rich information in terms of range information, reflectance information, and the true color of the objects. By evaluating this single image, one can recognize additional data information. A more detailed description about parameter selection for SWF will be discussed in the next chapter.

Below, in Figure 4.17, are illustrations of the results using feature-based image morphing for large-scale urban mapping, utilizing the morphing algorithm. As the source and destination images have shown, they provide similar information despite varying positions and angles of the camera. The morphing results generate the transformation from beginning status to ending status. These two images are captured in the roof of the building in Knoxville's downtown at different time, shown from the sky, sun, cloud, and shadow. Using the Fanta Morph 4, we are able to export a 30-frame sequence. From this sequence, we can perceive not only the position change, but also the time and weather switches. By using this method, we can provide the intermediate images and videos in the scenery such as when a reconnaissance pilot is flying over a geographic region. From this specific application, it can be noted that the similarities of the source and destination images are one of the elements that contribute to a realistic and smooth morphing. Another element is that more control point and accuracy of the control point contributes to a smooth transformation.

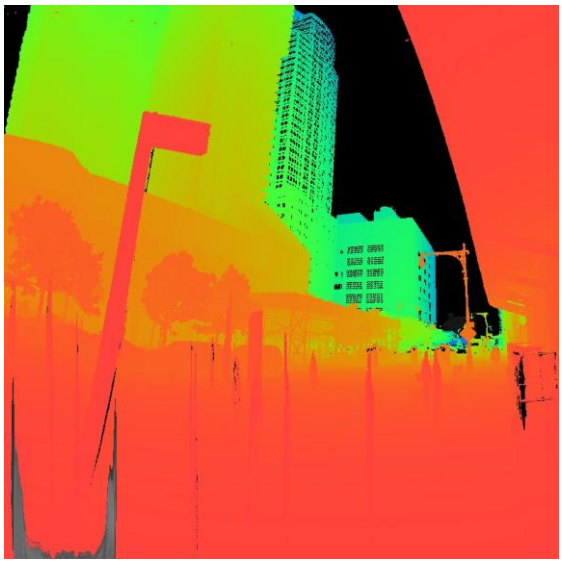

(a) Pseudo colored range image of Franklin Greenwich, from Riegl LMS-Z210 Range Data

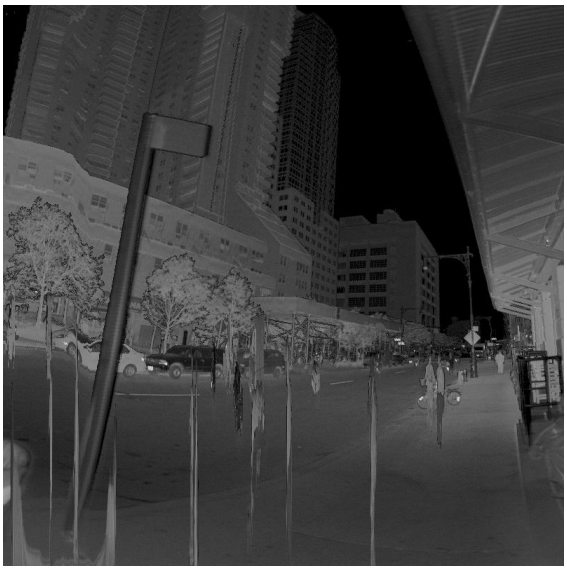

(b) Reflectance image of Franklin Greenwich

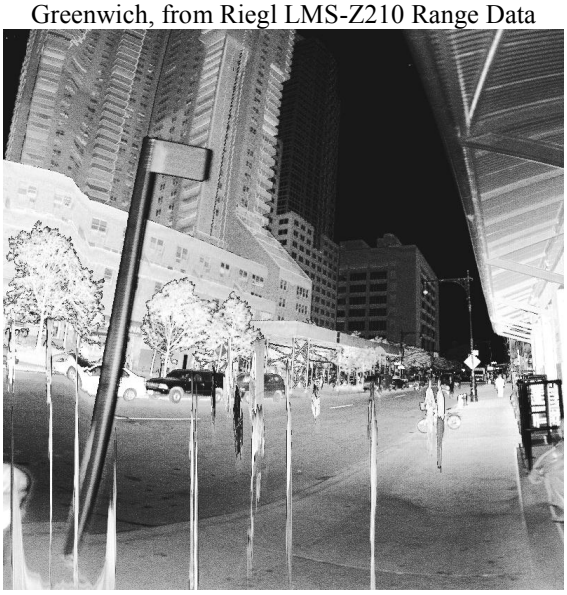

(c) Preprocessed of reflectance image (b) using histogram equalization

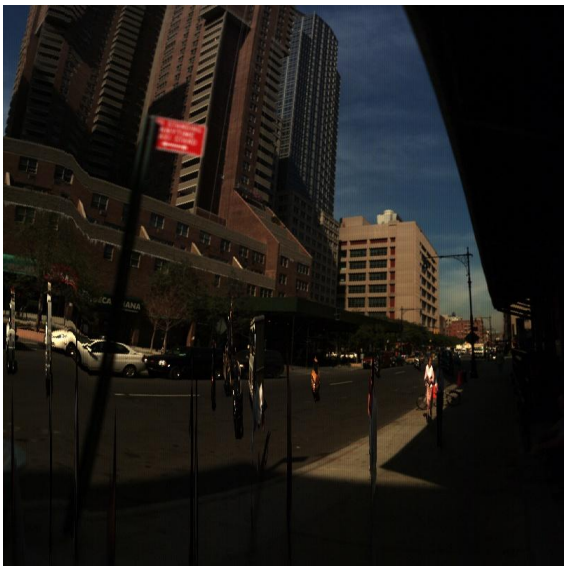

(d) color image of Franklin Greenwich

Figure 4.15 (a) Pseudo colored range image of Franklin Greenwich, from Riegl LMS-Z210 Range Data, (b) Reflectance image of Franklin Greenwich, (c) Preprocessed of reflectance image (b) using histogram equalization, and (d) True color image of Franklin Greenwich.

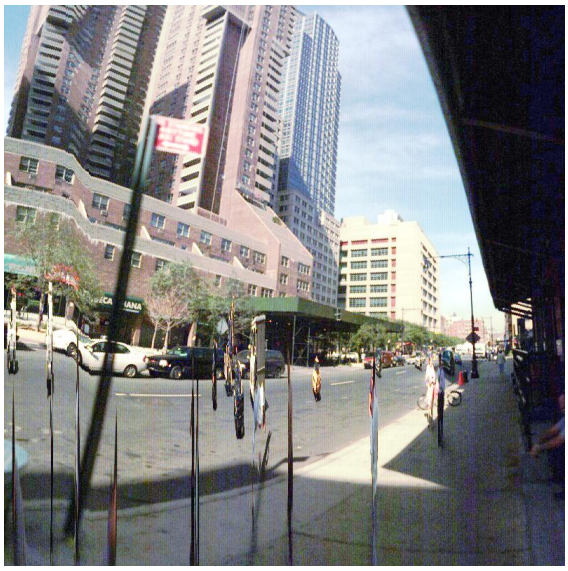

(a) histogram equalization of Fig.4.15 (d)

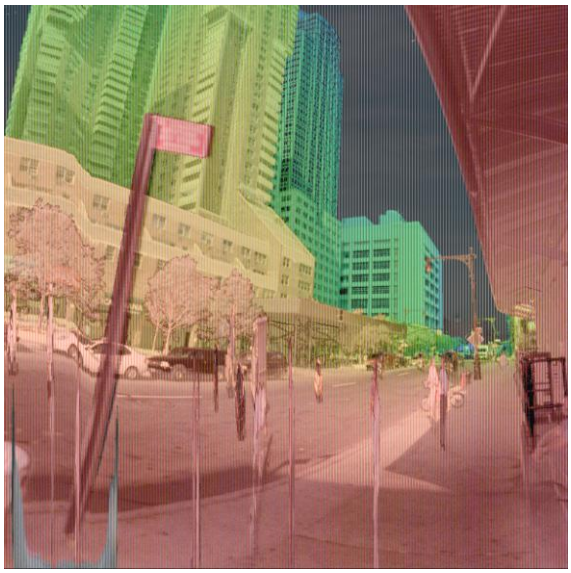

(b) Fusion of Fig.4.15(a) (c) , Fig.4.16 (a) image using SF, $k_1 = 1, k_2 = 1, k_3 = 1$

Figure 4.16 Preprocessed figures of true color image Fig.4.15 (d) using histogram equalization, because of the dark intensity; histogram equalization is utilized to improve the contrast (1). Fusion of Fig.4.15 (a) (c), Fig.4.16 (a) image using SF, $k_1 = 1, k_2 = 1, k_3 = 1$. Comprehensive visual information is achieved (b).

Thus far, we have presented a pixel level image fusion algorithm based on applications of primitive images, thermal and color images, and aerial and satellite image and multi-sensor image fusion systems based on LMS-Z210. Our results provide a wide range of fusion results by selecting a combination of parameters. The approach using image warping further encourages implementation on a well defined sensor position where a low difference between each sensor image is necessary for simulating the fused image in the specific environment. An example of such an urban scenario is provided for surveillance, where the monitoring sensor on the roof of the building should be able to show the transition of two views.

Furthermore, we also note that our method requires additional quantitative criterion for evaluation. Because the visual effect and subjective human feedback do not always provide credible evidence for performance evaluation, we present the mutual information results on handling the data from multi-sensor image fusion systems in the following chapter.

(a) Source image, Sequence image 01

(b) Destination image, Sequence image 30

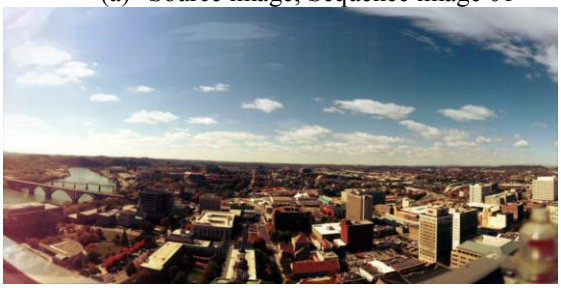

(c) Sequence image 07

(d) Sequence image 15

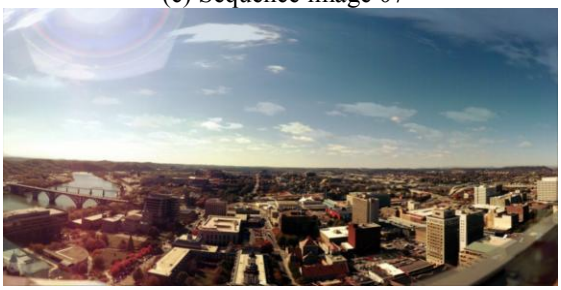

(e) Sequence image 22

Figure 4.17 Deployment for large-scale urban mapping using the feature-based image morphing algorithm: (a) Source image, Sequence image 01, (b) Destination image, Sequence image 30, (c) Sequence image 07, (d) Sequence image 15, and (e) Sequence image 22.

5 Performance Evaluation

In Chapters 3 and 4, we presented several pixel-level image fusion and image morphing algorithms. Experiments of those algorithms were conducted using real world deployment and scenarios. In Chapter 5, we introduce the root mean square error and mutual information methods to further evaluate the performance of the algorithms. Because no benchmark image usually exists for reference, we use mutual information for most of the cases. The experiments showcase potential suggestions for parameter selections using mutual information. Section 5.1 deals with the performance evaluation of the image fusion algorithm, focusing especially on using mutual information methods, which explain the correlated relationship between the mutual information and parameter selection. Section 5.2 documents the deployment of our method for large-scale urban mapping using the feature-based image morphing algorithm.

5.1 Performance evaluation of image fusion

In this section, we demonstrate the quality measure approach for our image fusion algorithm towards its use in a multi-sensor image fusion system. Of these evaluation approaches, there are both objective and subjective evaluations. Researchers occasionally use subjective tests to assess the fused results. However, although subjective tests can sometimes be accurate if performed correctly, they are inconvenient, expensive, and time consuming. Furthermore, it is impossible to use them to continually adjust system parameters in a real time manner. Hence, an objective performance evaluation measure that can accurately predict human perception for a multi-sensor image fusion system would be a helpful method. Image fusion quality measures can be divided into two categories, one type deploys standard quality metrics, such as standard deviation, entropy, and SNR estimation, to extract features from the fused image itself (Zhang et al. 1998); the other type utilizes features of both the fused and source images. Thus, an accurate objective evaluation metric could be used to provide immediate system fusion performance change information and, therefore, to quickly and effectively guide the algorithmic design process of image fusion system parameter optimization.

5.1.1 Root mean square error methods

The evaluation of fusion techniques is a non-trivial task especially as it is often difficult to say which of the two fused images are better without referencing specific tasks. The best approach for assessing the quality of the fused image generally depends on the application domain. In most cases, human observers are the sole end user of the fused image. That is why human perception is perhaps the most important assessment technique.

The evaluation of an image fusion algorithm's performance can first be divided into two categories: one with reference images and one without. The reference image here serves as the ground truth image.

However, most applications do not provide the reference image. The fusion assessment without reference images uses the fused image with the original source images to calculate similarity.

A commonly used reference-based assessment metric is the root mean square error (RMSE) which is defined as follows:

$$RMSE = \sqrt{\sum_{i=1}^{N}\sum_{j=1}^{M}[R(i,j)-F(i,j)]^2} \qquad (5.1)$$

where R(i, j) and F(i, j) are the reference and fused images, respectively, I and J are image dimensions, and N x M is the size of the image. RMSE measures the difference between values that are fused and the actual value. It is an objective evaluation measure requiring a reference image. For certain applications, it is possible to generate an ideal fused image. The ideal fused image is then used as a reference for comparison with the experimental fused results. Still, there are various applications where a reference image is hard, or even impossible, to obtain. Hence, let us consider another evaluation method without using a reference image.

5.1.2 Mutual information methods

The quality of the fused images is of fundamental importance and is usually assessed by a visual analysis which is subjective to the viewers. Among the available methods for assessment, both the mean-square-error (MSE) and signal-to-noise ratio (SNR) are widely accepted because of their simplicity and low computational costs. However, these measurement approaches require a reference image used in conjunction with the resulting image. In this situation, we will introduce other methods without need for a reference image for our application.

Among the variety of existing similarity measures, mutual information (MI) has received substantial attention recently. MI has developed from information theory. It was first developed to set fundamental limits on the performance of communication systems. A general scheme of MI based techniques can be found in the paper published by (Qu et al. 2002). A matrix, which does not require a ground truth image, was also proposed by (Qu et al. 2002) and can be used to evaluate image fusion performance. It essentially computes how much information from each of the source images is transferred to the fused image. In the fields of image processing, MI measures the amount of information that one image contains about another image by looking at its intensity distribution. In discrete random variables case, it is defined as follows:

$$I(A,B) = \sum_{a,b} P_{AB}(a,b)\log\frac{P_{AB}(a,b)}{P_A(a)P_B(b)} \qquad (5.2)$$

where $P_{AB}(a,b)$ is the joint distribution probability and $P_A(a)$ and $P_B(b)$ are the marginal distribution probabilities of A and B, respectively. MI can be described as the reduction of uncertainty (entropy) of one image via knowledge of another image. The mutual information is a measurement for the similarity of image intensity distributions between images A and B. It is a very general similarity measure because it does not rely on any specific relationship between the intensities of the two given images. From its calculation method, we can see that the mutual information reaches its maximum value when images A and B are registered.

Given reference images, the result with a higher value of $I(A,B)$ indicates a better fusion result, due to a better similarity between F and R. Without reference images, we can use the formula below for fusion assessment:

$$M_F(A,B) = I(F,A) + I(F,B) \qquad (5.3)$$

In this equation, $M_F(A,B)$ stand for the total amount of similarity between the fused image F and the source images of A and B. Therefore, a higher value of $M_F(A,B)$ shows that a larger amount of information was preserved in the fused image which indicates better fusion results. If the two images, A and B, are independent, then the mutual information similarity is zero. If the two images, A and B, are identical, all the information of A is shared with B. This performance measurement is used to help human observers make quicker and more accurate decisions. However, it is difficult to find an easy, comprehensive objective performance measure. As Qu (Qu et al. 2002) shows using various outdoor test images, no fusion algorithm always outperforms the other algorithms and that the performance of a fusion algorithm relies primarily on the images of the specific applications.

We use two sets of images to experimentally evaluate the image fusion algorithms. One is the Ayres Building and the other is the South College Building. These are the same images seen in Chapter 4. In order to use the mutual information method to evaluate the images, we expand the source image to be the same size as the fused image. We then choose the parameters shown in Fig. 5.1 to improve the visual effect. The visual result of those images is improved as the mutual information score increased in the Fig. 5.1. From the Table 5.1, we can notice how the individual component value changed as the parameter changes. A higher value of the weight result in a higher mutual information score of the correspondent component.

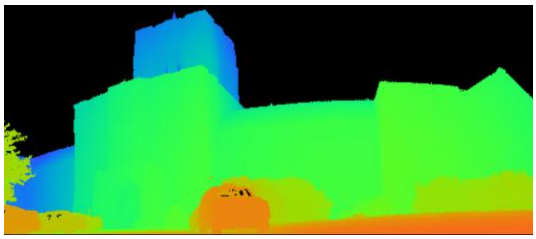

Pseudo colored range image of the Ayres Building

Reflectance image of the Ayres Building

The Ayres Building from CCD camera

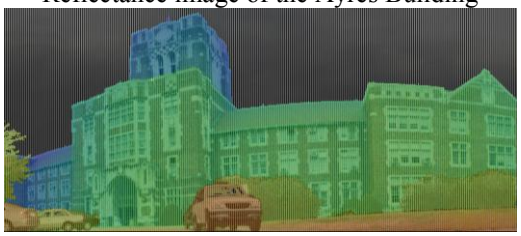

With parameter $k_1 = 1, k_2 = 1, k_3 = 1$ SF MI = 2.94

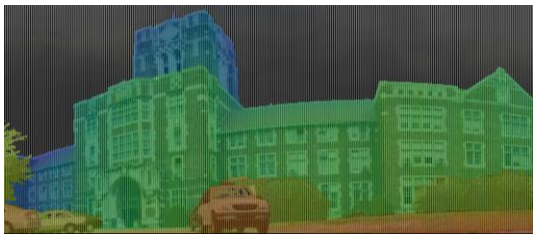

Ayres Building $k_1 = 1, k_2 = 1, k_3 = 1$
Alpha = 0.4 Beta = 0.24 SWAF MI = 2.6707

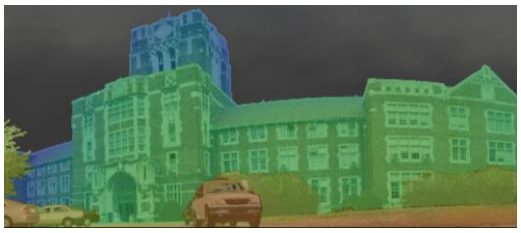

Ayres Building WA MI = 3.6301

Figure 5.1 Image fusion and mutual information results of the Ayres Building.

Fusion Data	I(F,A)	I(F,B)	I(F,C)	$M_F(A,B,C)$
Ayer Building $k_1 = 1, k_2 = 1, k_3 = 1$ SF	1.0248	0.7730	1.1422	2.94
Ayer Building $k_1 = 1, k_2 = 1, k_3 = 1$ SWAF Alpha = 0.4 Beta = 0.24	1.0341	0.6408	0.9957	2.6707
Ayer Building WA	1.1575	0.6055	1.8671	3.6301

Table 5.1 Mutual information results of pixel-level fusion for the Ayres Building images.

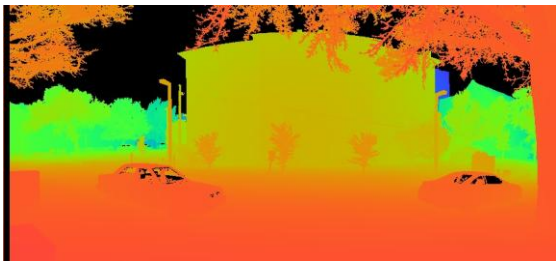

Pseudo colored range image of South College Building

Reflectance image of South College Building

True color image of South College Building

South College Building SF $k_1 = 1, k_2 = 1, k_3 = 1$

South College Building $k_1 = 1, k_2 = 1, k_3 = 1$
Alpha = 0.4 Beta = 0.24 SWAF

South College Building $k_1 = 1, k_2 = 1, k_3 = 1$
Alpha = 0.17 Beta = 0.41 SWAF MI =1.8793

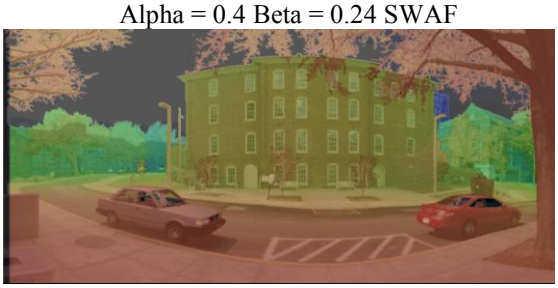

South College Building WA MI = 3.1146

South College Building SF $k_1 = 1, k_2 = 1, k_3 = 2$ MI = 2.5001

Figure 5.2 Image fusion results of the South College Building using SF, WA, and SWAF with various combinations of parameter selection and mutual information (MI).

South College Building $k_1 = 1, k_2 = 1, k_3 = 2$
Alpha = 0.31 Beta = 0.29 SWAF MI = 2.7015

South College Building $k_1 = 1, k_2 = 1, k_3 = 1$ $\alpha = 0.2$
$\beta = 0.3$ SWAF MI = 2.3102

South College Building $k_1 = 1, k_2 = 1, k_3 = 1$ $\alpha = 0.1$
$\beta = 0.2$ SWAF MI = 2.6574

South College Building $k_1 = 1, k_2 = 1, k_3 = 1$ $\alpha = 0.1$
$\beta = 0.3$ SWAF MI = 2.6551

Figure 5.2(continued) Image fusion results of the South College Building using SF, WA, and SWAF with various combinations of parameter selection and mutual information (MI).

Fusion Data	I(F,A)	I(F,B)	I(F,C)	$M_F(A,B,C)$
College building $k_1 = 1, k_2 = 1, k_3 = 1$ SF	0.8256	0.5182	0.5355	1.8793
College building $k_1 = 1, k_2 = 1, k_3 = 1$ Alpha = 0.4 Beta = 0.24 SWAF	0.9746	0.4968	0.5157	1.9871
College building $k_1 = 1, k_2 = 1, k_3 = 1$ Alpha = 0.17 Beta = 0.41 SWAF	0.7753	0.7375	0.8464	2.3592
College building WA	1.2523	0.6111	1.2512	3.1146
College building $k_1 = 1, k_2 = 1, k_3 = 2$ SF	0.7826	0.5818	1.1357	2.5001
College building $k_1 = 1, k_2 = 1, k_3 = 2$ Alpha = 0.31 Beta = 0.29 SWAF	0.7830	0.6110	1.3075	2.7015
College building $k_1 = 1, k_2 = 1, k_3 = 2$ Alpha = 0.35 Beta = 0.29 SWAF	0.7887	0.5688	1.1693	2.5268
College building $k_1 = 1, k_2 = 1, k_3 = 2$ Alpha = 0.33 Beta = 0.29 SWAF	0.7847	0.5834	1.2360	2.6041
College building $k_1 = 1, k_2 = 1, k_3 = 2$ Alpha = 0.32 Beta = 0.3 SWAF	0.7784	0.5970	1.2517	2.6271

Table 5.2 Mutual information results of image fusion for the South College Building

From the mutual information results, note that there are significant differences when the parameters changes. For the use of alternating control for an imaging system, the algorithms we proposed provide large degrees of freedom and a low computational cost. However, in order to produce a single comprehensive image with maximized mutual information, an appropriate parameter selection is still necessary. As the figures above show, with a higher value of k_i, then the alpha and beta will increase the mutual information value. Based on these experiments, WA methods appear to outperform the other methods. On the other hand, there is no best solution for each kind of application to guarantee the highest mutual information score. Based on using a specific application, though, the user needs to choose the specific method with the appropriate parameters in order to produce optimized fusion performance.

Fig. 5.3 demonstrates the mutual information results using SWAF for the South College Building's image set, with parameters of k_1=1, k_2=1, and k_3=1. The parameter's alpha has a range from 0.1 to 0.8 and the beta has a range from 0.1 to 0.8. The mutual information results range from 1.8 to 2.7. Considering the dependency relationship of $\alpha+\beta+\gamma=1$, the alpha and beta are the only two parts that play a role to control the fusion result in this experiment. The data in the triangular area $\{\alpha>0,\beta>0,\alpha+\beta\le 1\}$ is the valid test results from our test. Additionally, the values in the upper left region are not drawn as they are not applicable to our test. The mesh grid result is processed with a two-dimensional cubic interpolation. The color map legend is shown on the right side and ranges from blue to red. It passes through cyan, yellow, and orange, representing the maximum of 2.6574 to the minimum of 1.8224. It also shows the corresponding color for the mutual information value along the z axis. As shown in this figure, the maximum mutual information (dark red) region lies on the "ridge" of the left most area, which has an alpha of [0.05, 0.15], a beta of [0.25, 0.35], and a gamma of [0.5, 0.7]. The minimum mutual information (dark blue) region lies on the "canyon" of the center area, which has an alpha of [0.3, 0.5] and a beta of [0.2, 0.4].

As we can see in Fig. 5.4, the mutual information results with the parameter selection α,β,γ does generate a ridge similar to the ridge of the data of the South College Building. As with the previous example, the triangular area in the upper-left region is not drawn out since the value is not applicable in this situation. Depending on the specific image set, the maximum value and the "optimized" parameter selection is different. For this example, the mutual information result is comparably smaller, 2.2636 compared with 2.6551. The maximum mutual information region is located in alpha [0.05, 0.1], beta [0.7, 0.8], and gamma [0.1, 0. 25], shown as the dark red region.

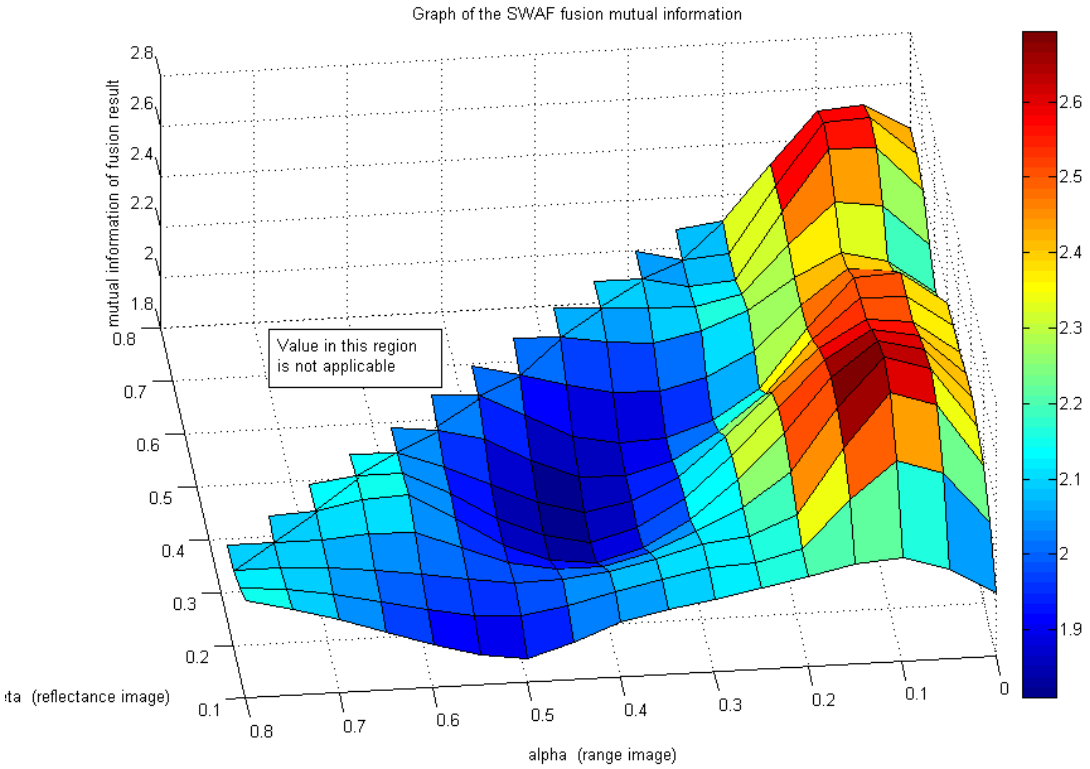

Figure 5.3 Graph of the Segmented Weighted Average Fusion mutual information results. Source images are the South Collage Building, with parameters of $k_1 = 1, k_2 = 1, k_3 = 1$. The parameters' alphas have a range from 0 to 0.8 and a beta range from 0 to 0.8. The mutual information result ranges from 1.8 to 2.8. As shown in this figure, the maximum mutual information region is alpha [0.1, 0.2], beta [0.2, 0.4], and gamma [0.5, 0.7].

Still, there are many criteria for fusion performance evaluation. In this work, we simply illustrate the evaluation result based on mutual information since it provides a reasonable calculation without the use of a reference image. That is not to say that the mutual information method is the best evaluation criterion for all fusion applications. On the other hand, the source image also affects the mutual information result. If several of the source images for the fusion have color, shape, and texture similarities, the mutual information might increase when compared with cases where all the source images have significant differences. For now, the mutual information measurement only serves as a quantitative method to assist users with their judgment and for comparison purposes.

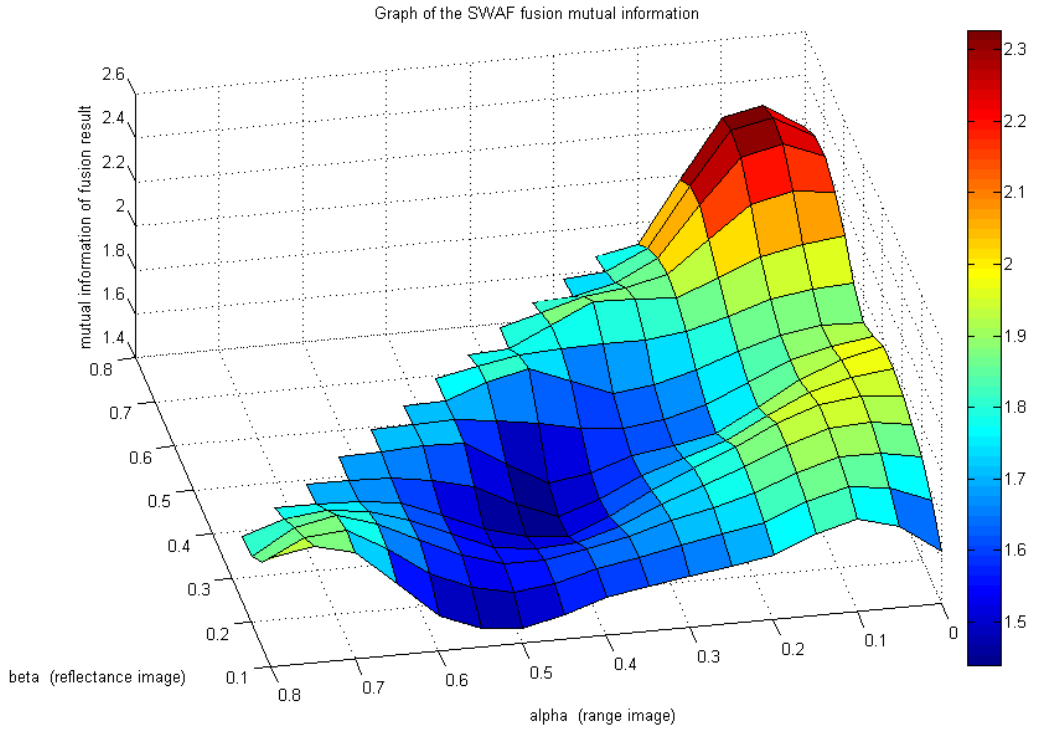

Figure 5.4 Graph of the Segmented Weighted Average Fusion mutual information results. Source images are the Franklin Greenwich shown in Figure 4.14. $k_1 = 1, k_2 = 1, k_3 = 1$, with a parameter alpha range from 0 to 0.8 and a beta range from 0 to 0.8. The mutual information result ranges from 1.4 to 2.4. As shown in this figure, the maximum mutual information region is alpha [0.05, 0.1], beta [0.7, 0.8], and gamma [0.1, 0. 25].

We have experimented on the data using a LMS-210 multi-sensor system. The LMS-210 is mounted on the front of the South College Building to acquire the necessary data. We deployed one measurement - mutual information, because there is no ground truth image for comparison. Mutual information shows the information that X and Y share. The mutual information results using SWAF illustrate the relationship between the sum mutual information and the parameter selection. Although it is different from case to case given different source images, it still provides suggestions on how to choose a parameter combination to improve the mutual information. Next we test the run time performance of SF using two different computer configurations.

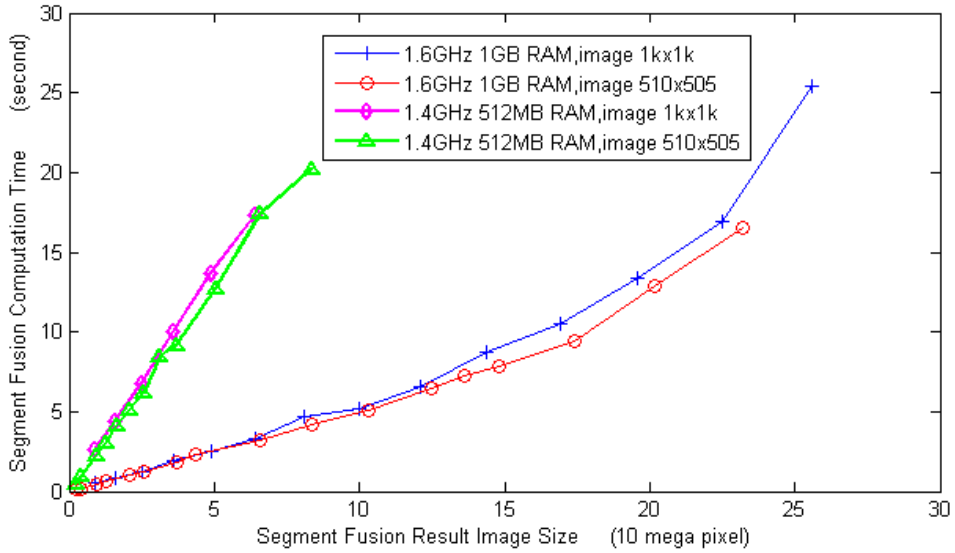

Figure 5.5 Segment Fusion Algorithm Computation Time verse Output Image Size. Considering that the megapixel image has a resolution size with 10^6 pixel and the giga-pixel image has a resolution size with 10^9 pixel, the performance of image fusion provides a satisfactory result. The computation time has a linear relationship with the image size and the speed of the computer's hardware.

In order to evaluate the performance of the algorithm, the computation times of SF are measured. By inserting the clock function between the algorithm codes in our implementation, we are able to compute the C++ run time. As you can see from Fig. 5.4, the performance of segment fusion on the computer with 1G RAM is considerably better than that on the computer with only 512 RAM. The computer with 512 RAM takes four times as long as the computer with 1G RAM takes to generate the same-sized image. For the size of an output image with 50 mega-pixels, the computation time grows from 2.47 sec to 12.61 sec. The color or gray-scale test images produce no significant differences on computation performance given the same computer and neither does the test image size. The size of the output image has a linear relationship with computation time. Normally, the size of the output image, CPU, display adapter, and RAM are the main criteria affecting the performance of the algorithm. Due to the size of the image data, the output functions' long run time is unavoidable. The output image size limit for effective computation is approximately 240 megapixels for the computer with 1G RAM. If the output image's size is beyond the limit, a warning of "out of memory" or the computer not responding will result. Still, this is helpful to know given a high performance computer.

5.2 Performance evaluation of image morphing

In this section, we will illustrate the results of image warping for fusion purposes. The performance is evaluated using multiple sets of images with different sizes ranging from 1.2 mega pixels to 36 mega pixels, a various number of control points ranging from 0 to 50, and a variety of exported data types. For our purpose of moving toward a multi-sensor fusion system, these features and characteristics represent the basic requirement for system performance consideration. Using the same computer configuration, a 1.6GHz

CPU and 1G RAM, we test the image warping performance using the Fanta Morph 4 software. The layout of the Abrosoft Fanta Morph image morphing software is shown in the following figure. In this test, we use the default settings to export the data file. The Animated Graphics Interchange Format (GIF) exports the data with 15 frames/s, while Flash Movie exports with 12 frames/s and JPEG quality at 75. (Please note that the GIF quality is lower because GIF only supports 256 colors). The upper left and upper right windows are for the source and destination images respectively, while the lower window is for the image morphing preview. The green dot on the two upper windows shows the position of the control point. When the user places the cursor on the green dot of one image, the corresponding control point of the other will be automatically highlighted. Regarding the software, it has several features such as:

- Morph 2 to unlimited images Application. Preview and Play in real time. Export morph animation to Image Sequence, AVI, Flash, Animated GIF, EXE, and Screen Saver.

- Fanta Morph uses a rendering engine which makes use of OpenGL hardware acceleration. OpenGL is an industrial graphics standard and is supported by most modern video cards.

- If your video card supports this feature, morph speed can be very fast, even reaching hundreds of frames per second, but, if your video card is old, morph speed may be under 15 frames per second. In this case, updating your video card is recommended.

- For our test computer, with a 1.6GHz CPU and 1G RAM, with an ATI Radeon 1300 video card, the limitation of the image size is between 6,000x6,000 pixels and 7,000x7,000 pixels. If the test images' size is beyond the limitation, the preview window is completely black and so is the resulting movie.

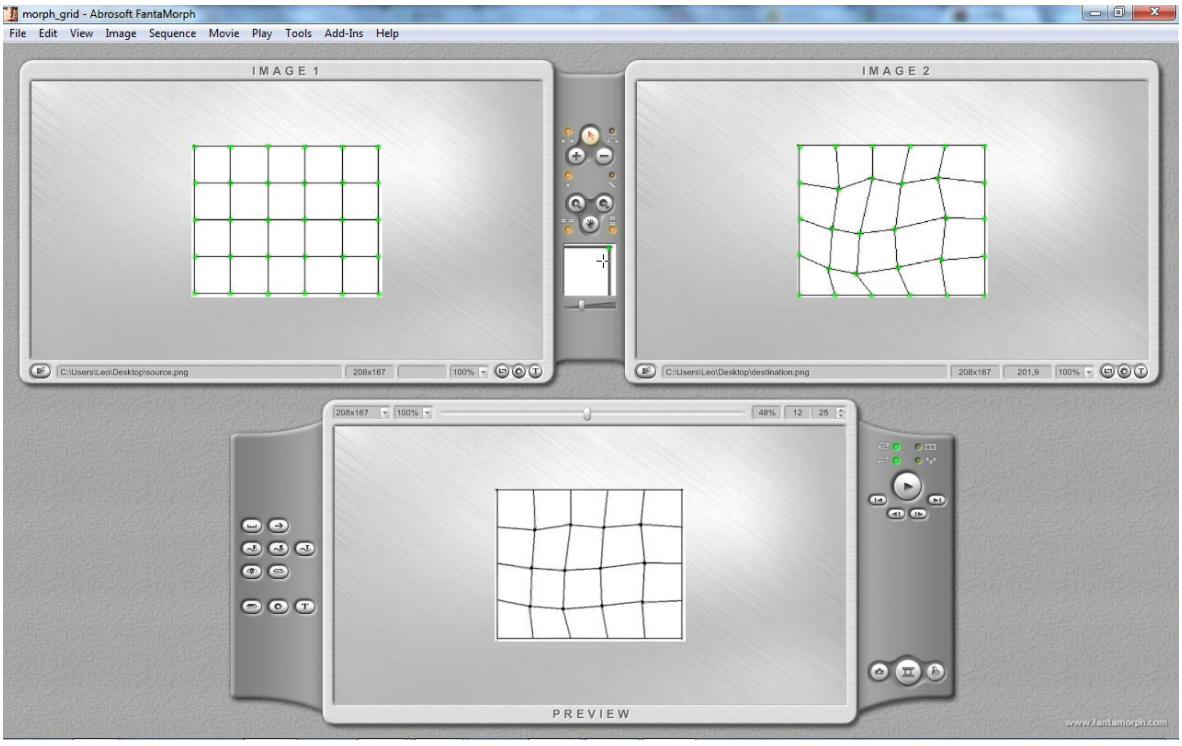

Figure 5.5 Layout of Abrosoft Fanta Morph image morphing software. The upper left and upper right windows are for the source and destination images respectively, and the lower window is for the image morphing preview. The green dot on the two upper windows shows the position of the control point. When the user places the cursor on the green dot of one image, the corresponding control point of the other will be automatically highlighted.

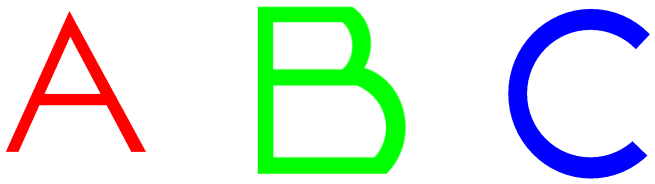

Figure 5.6 Test images for image fusion. The size of the image varies from 3,000x3,000 pixels to 6,000x6,000 pixels. With these primitive shape images, multiple control points and various data type are considered for performance evaluation.

State num	Image size	Control point num	Data type	Time (min)	Data size (MB)	Content
2	3000x3000	10	GIF	4	8.8	B->C
2	6000x6000	21	GIF	22	27	A->B
2	6000x6000	21	Flash movie	8	28	A->B
2	6000x6000	34	GIF	28	35	A->B
2	6000x6000	34	Flash movie	10	31	A->B
2	6000x6000	50	GIF	40	35	A->B
2	6000x6000	50	Flash movie	11	32	A->B
4	6000x6000	0	GIF	64	81	A-B-C-A
4	6000x6000	0	Flash movie	28	87	A-B-C-A
9	1200x1000	10	GIF	6	54	Face
9	1200x1000	10	Flash movie	1.5	11	Face

Table 5.3 Performance results of image morphing regarding image size, control point number, exported format type, computation time, and data size.

Above is the test image we used to evaluate the image morphing algorithm performance in terms of control point number, image size, data format type, computation time, and output data size. The test results and test images are shown in later figures.

From the figures above, we can see that the data type shows that to export a GIF image usually requires a longer processing time when compared with the processing time of a flash movie. For the case of two 6,000x6,000 images, the control point varies from 21 to 50, and morphing time increases from 8 minutes to 11 minutes. The runtime of image morphing is proportional to the number of lines and pixels, as well as being proportional to the size of the image. Besides, before performance runtime, feature specification is still a time-consuming aspect of morphing. Although it depends on the specific image, the number needed for feature specification may vary; all images require the feature precisely placed in the source and destination images. Generally, the more feature specification that is used (especially along the transformed feature contour), the smoother a morphing result it will generate. When we compare the mesh warping with feature-based image morphing, the speed of mesh warping is the better of the two methods. The low computational cost comes from the localized mesh computational influence, and polynomial (bilinear, biquadrates, and bi-cubic) interpolation.

6 Conclusions

This thesis work is motivated by the potential and promise of image fusion technologies in the multi-sensor image fusion system and applications. We studied different image fusion techniques and documented their theory mechanisms along with several of their applications. We have evaluated and demonstrated applications of multiple multi-sensor system solutions including thermal image and true color image fusion, aerial and satellite image fusion, multi-sensor image fusion based on LMS-Z210 system, and large-scale urban mapping using feature based image warping. Our approach is easy to deploy, lending itself to easier application to various multi-camera imaging visualization.

6.1 Dissertation key points

How to combine the relevant information from an image of a scene into a single highly informative image is the major concern of image fusion. Image fusion techniques have shown great progress towards this goal in recent years. This paper reviewed several of these applications and evaluated their performance. The proposed fusion algorithms allow images from different sensors integrated with a manual option to reach a more informative image for human-visual and automated recognition proposes. Of all the different types of image fusion algorithms, the pixel-based and spatial-based fusion algorithms are the most straightforward approaches with the lowest computational costs. Other approaches such as the nonlinear method and multi-scale-decomposition-based fusion method have respective advantages in certain areas. Both the quantitative and qualitative assessment approaches are used to determine which fusion algorithm is the most appropriate for an application. They also help the user by providing additional technical evidence for the user's decision-making process.

Despite recent technical progress, image fusion has not yet reached the stage where it can be reliably and massively applied to a broad range of applications. One way to apply image fusion widely to industry and engineering is to develop more robust fusion algorithms and related hardware devices for real-time practical use. A combination of image fusion techniques at all levels (i.e. pixel-level, feature-level, and decision-level) will likely improve the quality of fused images and thus lead to improved decision-making. For now, future work will place an emphasis on computing and merging images automatically without distortions.

Our proposed SWAF algorithm generates image fusion results with a low computational cost. It can be applied to fields where short computational time is demanded. By using mutual information criteria, we can provide guidance for the parameter selection for the SWAF algorithm. The adaptive image fusion algorithm can be designed with help from this evaluation measurement.

Our works here provide an image morphing algorithm to compare the results. When using the scenario of the same object with the registered image, the image morphing can generate images that simulate the image fusion result. Given appropriate parameters, the mutual information of SWAF methods can be maximized. On the other hand, inappropriate parameters will result in images with an obvious slice effect and a low mutual information score. Our proposed SWAF algorithm generates image fusion results with a low computational cost. It can be applied to fields where short computational time is demanded.

6.2 Future directions

The fusion theory is inspired by information theoretic concepts with strong foundations in concepts of information complexity. For future improvements in image fusion, the development of hardware along with additional sophisticated software will allow the implementation of algorithms and techniques that require large data volumes and time intensive computations. For example, the involvement of expert systems in a Geographic information system (GIS) can support the integration and evaluation of fused data.

Another aspect in future development and improvement is how to estimate and evaluate the quality of a fused image. As we have discussed in the previous chapter, depending on the applications, some fusion system might not have a perfect ground truth reference image for objective evaluation. Therefore, access methods without reference image are important for our concern in multi-camera imaging system.

In the field of multi-camera image fusion, the evaluation of the achieved results becomes relatively complex because of the different sources of data that are involved. Occasionally, the lack of simultaneously acquired multi-sensory data hinders the successful implementation of image fusion. The registration is also important for a multi-camera imaging system, because the resolution and sensor placement would contribute different factors.

Other points for future works include, but are not limited to, using mutual information criterion; we can provide guidance for the parameter selection for the SWAF algorithm. The adaptive image fusion algorithm can be designed with help from this evaluation measurement. More experiments about the mutual information and parameter selection need to be conducted to help decide the maximum mutual information region.

References

(Abidi, 1992) M.A. Abidi and R.C. Gonzalez, "Data fusion in robotics and machine intelligence," *Academic Press Professional*, Inc, 1992.

(Adam, 2001) A. Adam, E. Rivlin and I. Shimshoni, "ROR: Rejection of outliers by rotations," *IEEE Transactions on Pattern Analysis and Machine Intelligence*, Vol. 23, No. 1, pp. 78-84, 2001.

(Toet, 2002) A. Toet, Detection of dim point targets in cluttered maritime backgrounds through multisensor image fusion, In: W.R. Watkins, D. Clement & W.R. Reynolds (Ed.), Targets and Backgrounds: Characterization and Representation VIII, pp. 118-129, The International Society for Optical Engineering, Bellingham, WA, 2002.

(FIR) [online]. Available: http://www.flir.com/thermography/americas/us/ The FLIR systems infrared cameras, 2009

(HE) [online]. Available: http://www.hehighroad.org

(COLI) [online]. Available: www.coli.uni-saarland.de/groups/MC/lab.html

(FSR) [online]. Available: http://www.imgfsr.com

(RSL) [online]. Available: disi.unitn.it/rslab/

(ABL) [online]. Available: www.ablesw.com/3d-doctor/reslice.html

(DGT) [online]. Available:http://www.digitalglobe.com/

(IFS) The Image Fusion Server. Available from: http://www.imagefusion.org/

(LHG) Lehigh fusion test examples. Available from: http://www.ece.lehigh.edu/SPCRL/

(Geosage) http://www.geosage.com/highview/imagefusion.html , mapping our land more clearly and colorfully for better analysis and visualization

(Nandhakumar, 1998) Nandhakumar and J.K. Aggarwal, Integrated analysis of thermal and visual images for scene interpretation, IEEE Transactions on Pattern Analysis and Machine Intelligence 10 (4) 469–481, 1998.

(Blum et al., 2006) R.S. Blum, Z. Liu (Eds.), Multi-Sensor Image Fusion and Its Applications (special series on Signal Processing and Communications), Taylor and Francis, CRC Press, 2006.

(Smith, 2005) M.I. Smith, J.P. Heather, Review of image fusion technology in 2005, in: Proceedings on Defense and Security Symposium, Orlando, FL, March 28–April 1, 2005.

(Zeng et al., 2006) J.Zeng, A.Sayedelahl, T.Gilmore, and M.Chouikha, Review of Image Fusion Algorithms for Unconstructed Outdoor Scenes, Department of Electrical and Computer Engineering, Howard University, Washington, DC 20059, 2006.

(Zhang, 2002) C.Zhang, A New Automatic Approach for Effectively Fusing Landsat 7 images as well as IKONOS Images. IEEE/IGARSS '02, Toronto, Canada, June 24-28, 2002

(Shapiro, 1982) L.G.Shapiro, Organization of relational models in: International Conference on Pattern Recognition, pp. 360-365, 1982.

(Williams, 1999) M. L. Williams, R.C. Wilson, E.R. Hancock, Deterministic search for relational graph matching, Pattern Recognition 32, 1255-1516, 1999.

(Zhang, 2004) Y.Zhang and R.Wang, "Multi-resolution and multi-spectral image fusion for urban object extraction". International Society for Photogrammetry and Remote Sensing, XXth ISPRS Congress, 2004.

(Piella et al., 2002) G.Piella and H.Heijmans, "Multiresolution Image Fusion Guided By A Multimodal Segmentation", Proceedings of ACIV 2002, Ghent, Belgium, September 9-11, 2002

(Unser 1999) M.Unser: Splines – A Perfect Fit for Signal and Image Processing, IEEE Signal Processing Magazine, November, pp. 22-38, 1999.

(Keys 1981) R.G. Keys: Cubic Convolution Interpolation for Digital Image Processing, IEEE Transactions on Acoustics, Speech, and Signal Processing, Vol. ASSP-29, No. 6, December pp.1153-1160, 1981.

(Luo, 1995) R.C, Luo, Michael G.Kay, Multisensor Integration and Fusion for Intelligent Machines and Systems, Published by Intellect Books, ISBN 0893918636. P154-159, 1995.

(Mitianoudis , 2007) N.Mitianoudis, Tania, Stathaki, Pixel-based and Region-based Image Fusion Schemes using ICA bases. Information Fusion 8 131-142, 2007.

(Piella, 2003) G.Piella, A General Framework for Multiresolution Image Fusion: from Pixels to Regions. Information Fusion 4 (2003) 259-280, 2003.

(Rockinger et al., 1998) O.Rockinger and T.Fechner, "Pixel-Level Image Fusion: The Case of Image Sequences". in SPIE Proceedings, vol. 3374, pp. 378-388, 1998.

(Lewis et al., 2007) J. Lewis and J.Robert. et al. "Pixel- and Region-based Image Fusion with Complex Wavelets". Information Fusion 8 (2007) 119-130, 2007.

(Qu et al., 2002) G. Qu, D. Zhang, and P. Yan, Information Measure for Performance of Image Fusion, Electronic Letters 38 (7) 313 – 315, 2002.

(Zitova et al., 2003) B.Zitova, and J.Flusser. "Image Registration Methods: A Survey" Department of Image Processing, Institute of Information Theory and Automation, Academy of Sciences of the Czech Republic, 2003.

(Zeng et al., 2006) J.Zeng and A.Sayedelahl, et al. "Review of Image Fusion Algorithms for Unconstrained Outdoor Scenes". Department of Electrical and Computer Engineering, Howard University, Washington, DC 20059, ICSP 2006 Processings, 2006.

(Sadidy et al., 2005) J.Sadidy, P.Firouzabadi, and A.Entezari. "The Use of Radarsat and Landsat Image Fusion Algorithms and Different Supervised Classification Methods to Improve Landuse Map Accuracy", Department of Geography, Tarbiat Moallem Sabzevar University 2005.

(Wan et al., 2003) R.Wan and M.Li, "An Overview of Medical Image Registration", Fifth International Conference on Computational Intelligence and Multimedia Application (ICCIMA'03), 2003.

(Maintz et al., 1998) A.Maintz and M. Viergever. "A survey of medical image registration : Medical Image Analysis", Volume: 2, Issue: 1, pp. 1-36, March, 1998

(Baboulaz et al., 2007) L. Baboulaz and P.L. Dragotti, "Beyond Vision with New Image Super-Resolution Algorithms", 9th Great British Research Show for Early-Stage Researchers, SET for Europe, House of Commons, Westminster, London, UK, March 2007.

(Van Ouwerkerk 2006) J.D. Van Ouwerkerk, "Image super-resolution survey", Image and Vision Computing 24 (2006) 1039-1052.

(Nikolov et al., 1999) S.G.Nikolov, D.R.Bull, C.N. Canagrarjah, M.Halliwell and P.N.T. Wells, „Image fusion using a 3-d wavelet transform', in Proc. 7th International conference on Image Processing and Its Applications, 1999,pp. 259-280.

(Scheunders et al., 2001) P.Scheunders and S. De Backer, Multispectral image fusion and merging using multiscale fundamental forms, Proc. IEEE International Conference on Image Processing, 2001.

(Chan et al., 2003) L.Chan, S. Der and N. M. Nasrabadi. "Dualband FLIR fusion for automatic target recognition", Information Fusion, 4, 35-45, 2003

.

(Rajan et al., 2002) D.Rajan and S.Chaudhuri. "Data fusion techniques forsuper-resolution imaging", Information Fusion, 3, 25-38, 2002.

(Zhang et al., 1999) Z.Zhang and R.S. Blum, " A Categrorization of Multiscaledecomposition- based Image Fusion Schemes with a Performance Study for a Digital Camera Application", Proceedings of the IEEE Vol. 87, No. 8, Aug. 1999, pp. 1315-1326.

(Katartzis et al., 2006) A.Katartzis and M.Petrou "Current trends in super-resolution image reconstruction" Communication and Signal Processing Group, Department of Electrical and Electronic Engineering,Imperial College, London, UK, 2006

(Aiazzi et al., 2006) B.Aiazzi, S.Baronti and M.Selva "Image fusion through multi-resolution oversampled decompositions" Institueof Applied Physics „Nello Carrara' of the National Research Council, Florence, Italy 2006

(Aiazzi et al., 2003) B.Aiazzi, L.Alparone, S.Baronti, I.Pippi, M.Selva "Generalised lappacian pyramid-based fusion of MS+P image data with spectral distortion minimisation" Institute of applied physics, Florence, Italy 2003

(Clevers et al., 2008) Jan G.P.W Clevers and Raul Zurita-Milla "Multi-sensor and multi-resolution image fusion using the linear mixing model" Wageningen University, Centre of Geo-Information, Wageningen, The Netherlands, 2008.

(Mitianoudis et al., 2007) N.Mitianoudis and T. Stathaki "Image fusion schemes using ICA bases" Communications and Signal Processing Group, Imperial College London, London, UK 2007

(Achim et al., 2006) A.Achim, A.Loza, D. Bull and N.Canagarajah "Statistical modeling for wavelet-domain image fusion" Department of Electrical and Electronic Engineering, University of Bristol, Bristol, UK. 2006

(Otazu 2005) X.Otazu "Theory and implementation of image fusion methods based on the a trous algorithm" Computer Vision Center, Universitat Autonoma de Barcelona, Barcelona, Spain, 2005

(Beyerer et al., 2007) J.Beyerer, M.Heizmann, J.Sander and I.Gheta "Bayesian methods for image fusion" Fraunhofer-Institut fur Informatioins- and Datenverarbeitung IITB, Karlsruhe, Germany, 2007

(Schechner et al., 2007) Y.Schechner and S. K.Nayer "Multidimensional fusion by image fusion" Department of Computer Science, Columbia University, New York, USA 2007

(Garzelli et al., 2006) A.Garzelli, L.Capobianco and F. Nencini "Fusion of multispectral and panchromatic images as an optimization problem" Department of Information Engineering, University of Siena, Siena, Italy, 2006

(Oudre et al., 2007) L.Oudre, T. Stathaki and N.Mitianoudis "Image fusion using optimization of statistical measurements" Imperial College London, UK. 2007

(Giannarou et al., 2003) S. Giannarou and T.Stathaki "Fusion of edge maps using statistical approaches" Communication and Signal Processing Group, Imperial College London, London, UK. 2003

(Mitianoudis et al 2007) N.Mitianoudis and T.Stathaki "Enhancement of multiple sensor images using joint image fusion and blind restoration" Communication and Signal Processing Group, Imperial College London, London, UK.2007

(Looney et al., 2007) D.Looney and D.P.Mandic "Empirical mode decomposition for simultaneous image enhancement and fusion" Imperial College London, UK, 2007

(Li et al., 2005) S.Li and B.Yang "Region-based multi-focus image fusion" College of Electrical and Information Engineering, Hunan University, China, 2005

(Morabito et al., 2008) F.C.Morabito, G.Simone and M.Cacciola "Image fusion techniques for non-destructive testing and remote sensing application" University Mediterranea of Reggio Calabria, Faculty of Engineering, Dimet, Italy 2008

(Pradham et al., 2006) P.Pradham, N.H.Younan and R.L. King "Concepts of image fusion in remote sensing applications" Department of Electrical and Computer Engineering, Mississippi State University, 2006

(Xydeas et al., 2006) C.Xydeas and V.Petrovic "Pixel-level image fusion metrics" Imaging Science and Biomedical Engineering, University of Manchester, Oxford Road, Manchester, UK 2006

(Petrovic et al., 2007) V.Petrovic and T.Cootes "Objectively adaptive image fusion" Imaging Science and Biomedical Engineering, University of Manchester, Oxford Road, Manchester, UK 2007

(Wang et al., 2005) Q.Wang, Y.Shen and J. Jin "Performance evaluation of image fusion techniques" Department of Control Science and Engineering, Harbin Institute of Technology, China 2005

(Meng et al., 2006) M. Meng, and L.Liu "Sketching image morphing using moving least squares" Department of Mathematics, Zhejiang University, China 2006

(Wolberg 1998) G.Wolberg "Image morphing: a survey" Department of Computer Science, City College of New York, New York, NY 1998

(Oswal et al., 1998) P.K.Oswal and P.Y. Govindaraju "Image morphing: a comparative study" Department of Electrical and Computer Engineering, Clemson University, Clemson 1998

(Zhang et al., 1998) Z.Zhang and R.S.Blum. "On estimation the quality of noisy images" Proceedings of ICASSP, 2897-2900, 1998

(Beier et al., 1992)T.Beier and S.Neely. "Feature-based image metamorphosis" In Computer Graphics, 26(2): 35-42, New York, NY, July, Proceedings of SIGGRAPH '92 1992..

(Pohl et al., 1998) C.Pohl and J.L.Van Genderren "Multisensor image fusion in remote sensing: concepts, methods and applications" INT.J.REMOTE SENSING, 1998, vol. 19, No. 5, 823-854.

(Smith et al., 2005) M.Smith and J. Heather, "Review of image fusion technology" in 2005, www.waterfallsolutions.co.uk, 2005

(Wang et al., 2003) H.Wang, Z.Jing and J.Li "An image fusion approach based on discrete wavelet frame", Institute of Aerospace Information and Control, Shanghai Jiao Tong University. 2003.

Vita

Sicong Zheng is an researcher with wide interests in science and engineering. He received his Bachelor's degree in Electronics Engineering from the Beijing Normal University in 2007, a Master's degree in Computer Engineering from the University of Tennessee, Knoxville in 2010 respectively. Though he has pursued degrees in computer engineering with research focus on image processing and pattern recognition, he astutely follows the literature on cognitive psychology fascinated by the human mind, reads physics to learn about natural philosophy, investigates creative problem solving for the design of future innovations and studies statistical data analysis for surviving in the present. As an engineer, he motivates himself to be an innovator, believes in bearing the pain of being a pioneer to enjoy the pleasure of being one and enjoys his time exploring ideas and solutions from unseen out-of-the-box perspectives.